Università di Roma La Sapienza

Neutron Detection Techniques and their applications

Antonino Pietropaolo

ENEA

Dipartimento di Fusione e Tecnologie per la Sicurezza Nucleare

antonino.pietropaolo@enea.it

1935

1994

Discovery of the neutron
1932

James Chadwick

Clifford G. Shull
"for the development

of the neutron diffraction technique"

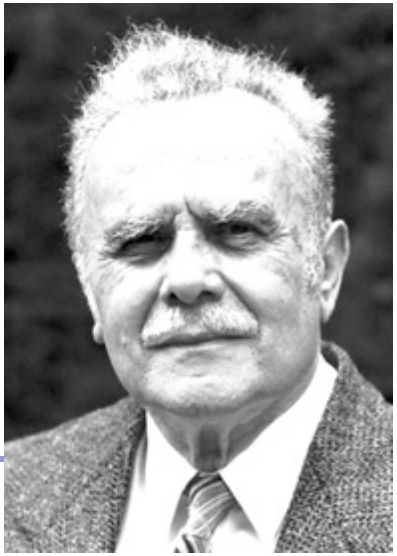

Bertram N. Brokhouse
"for the development
of neutron spectroscopy"

Nomenclature

Category	Energy [meV]	Temperature [K]	λ [Å]
Ultra-cold	< 0.1	< 1	< 30
Cold	0.1 – 10	1 – 120	30 – 3
Thermal	10 – 100	120 – 1000	3 – 1
Hot	100 – 500	1000 – 6000	1 – 0.4
Epithermal	> 500	> 6000	> 0.4

Neutron detectors

- What does it mean detecting a neutron ?
  - A measurable elctric signal has to be produced
  - It is not possible to detect directly slow neutrons

- Nuclear reactions needed to convert neutrons in charged secondary particles.

- Then typical charged particle detectors can be used:
  - Gaseous proportional counters & ionization chambers
  - Scintillation detectors
  - Semiconductors detectors

Nuclear reactions for neutron detection

- $n + {}^{3}He \rightarrow {}^{3}H + {}^{1}H + 0.764$ MeV
- $n + {}^{6}Li \rightarrow {}^{4}He + {}^{3}H + 4.79$ MeV
- $n + {}^{10}B \rightarrow {}^{7}Li^{*} + {}^{4}He \rightarrow {}^{7}Li + {}^{4}He + 0.48$ MeV γ +2.3 MeV (93%)
  $\rightarrow {}^{7}Li + {}^{4}He$ +2.8 MeV (7%)
- $n + {}^{155}Gd \rightarrow Gd^{*} \rightarrow \gamma$-ray spectrum $\rightarrow$ conversion electron spectrum
- $n + {}^{157}Gd \rightarrow Gd^{*} \rightarrow \gamma$-ray spectrum $\rightarrow$ conversion electron spectrum
- $n + {}^{235}U \rightarrow$ fission fragments + ~160 MeV
- $n + {}^{239}Pu \rightarrow$ fission fragments + ~160 MeV

Gaseous detectors

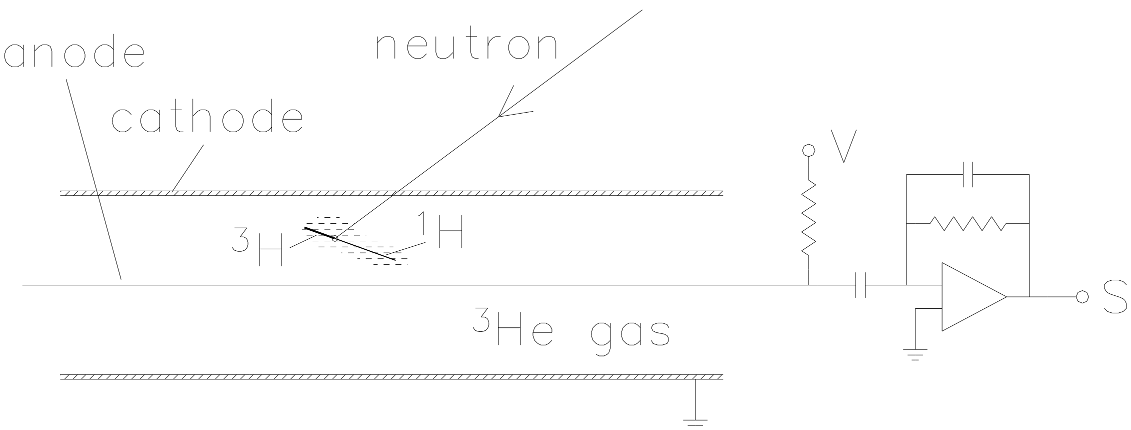

$$n + {}^3\text{He} \rightarrow {}^3\text{H} + {}^1\text{H} + 0.76\,\text{MeV}$$

$$\sigma = 5333\frac{\lambda}{1.8}\ \text{b}$$

~25,000 ions + electrons produces per absorbed neutron (~4×10^{-15} coulomb)

Operational principle

- Ionization
  - E- drift towards the anode producing a chrage pulse

- Proportional regime
  - If DV is sufficiently high the e- - gas collisions produce local ionization and thus e- cascade:

    - Amplification with Gauin up to 10^3

BF_3 detector

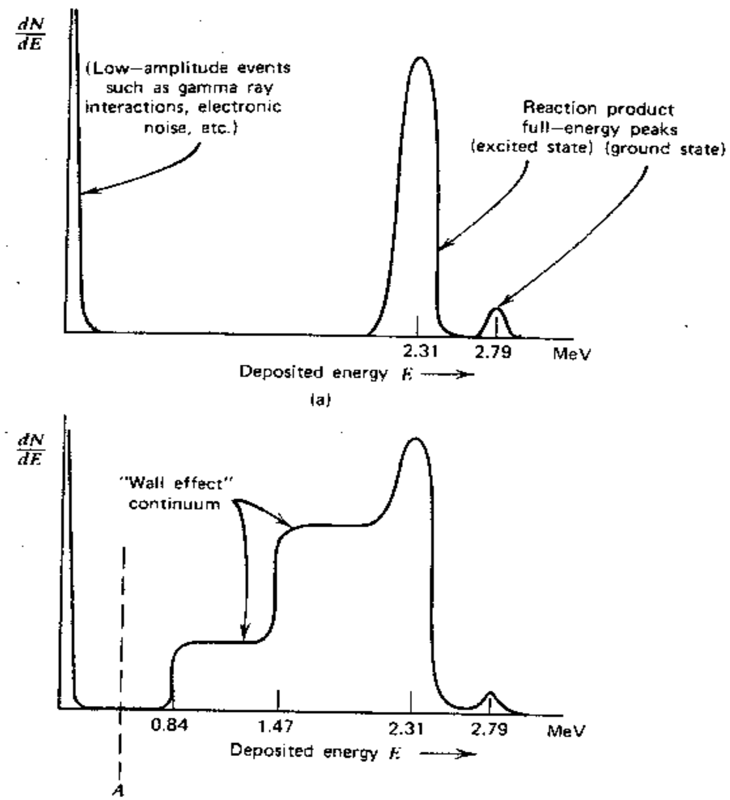

- For large BF_3 detectors the secondaries are completely absorbed *(full energy peaks)*

- In small BF_3 si ha la presenza di discontinuità *("wall effect")*

Fission Counters

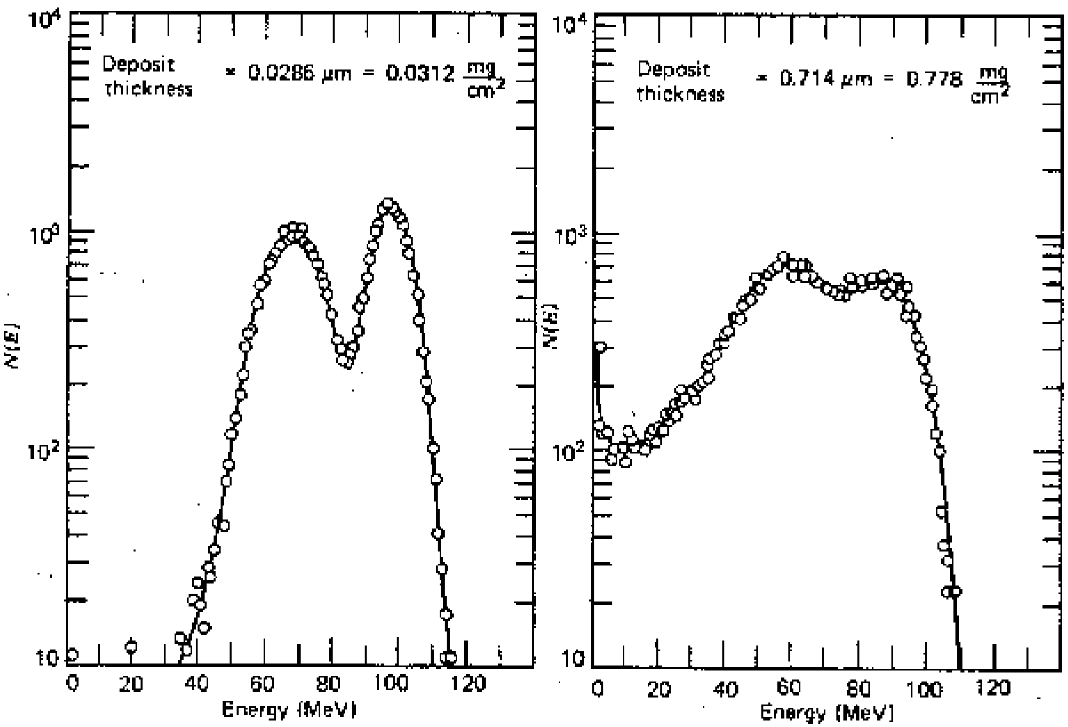

With large thickness of fissile material deposition the fission fragments may lose a significant fraction of their energy in the material itself thus releasing less energy into the detector

The fission reaction

FIGURE 1: Three nuclear reations: one using naturally fissile U_{235} and two which breed fissile materials from U_{238} and Th_{232}.

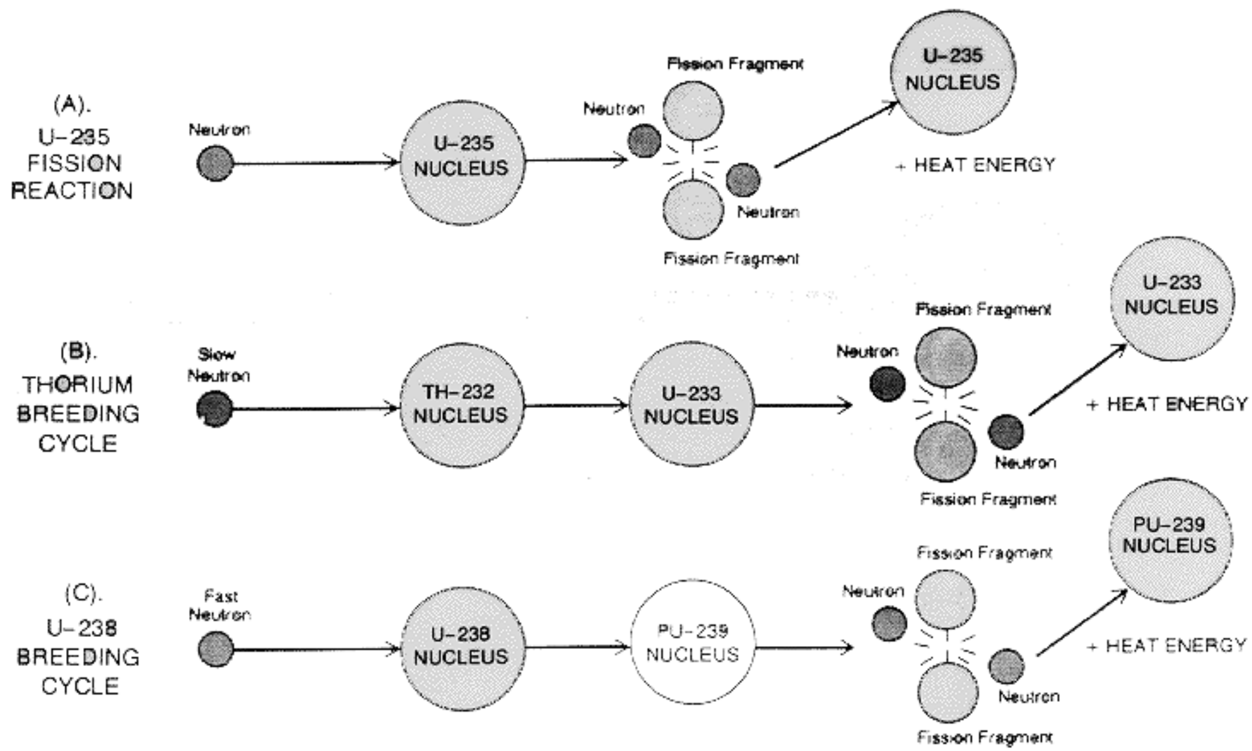

Fission cross sections

Thermal neutron region

Fast neutron region

MAPS Detector Bank

Scintillation detectors

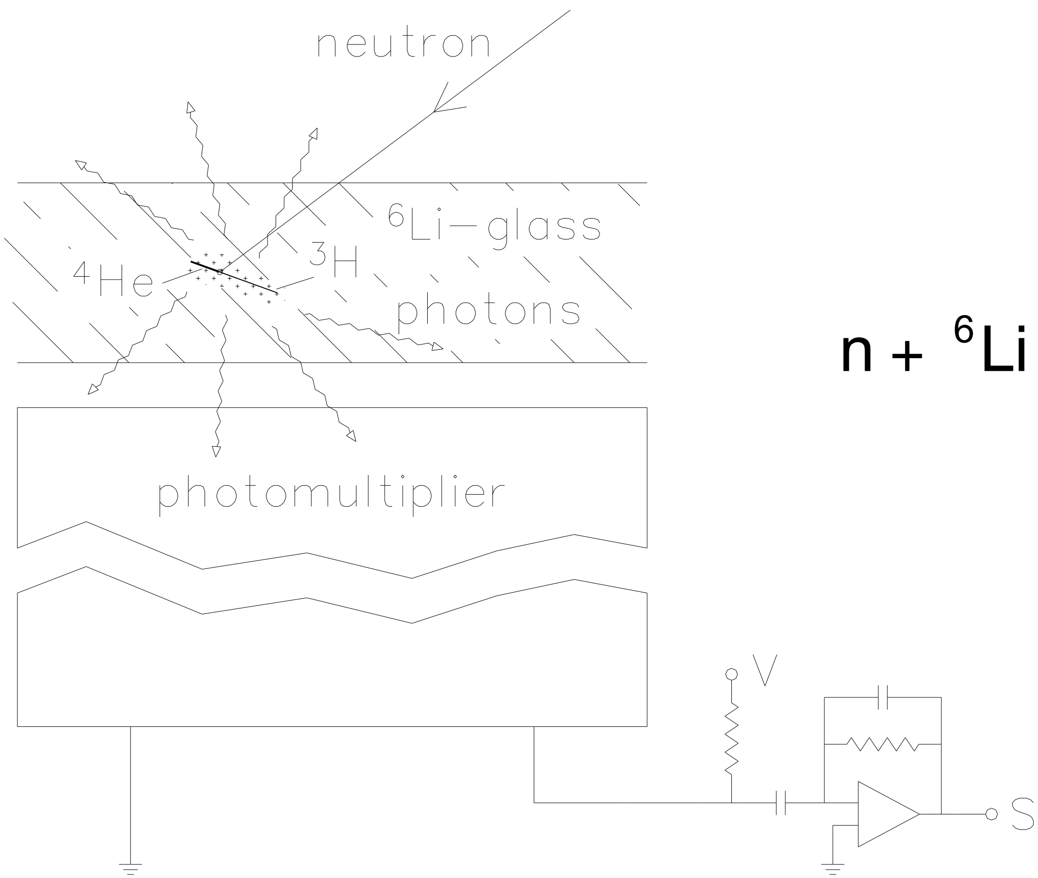

$$n + {}^6\mathrm{Li} \rightarrow {}^4\mathrm{He} + {}^3\mathrm{H} + 4.79\ \mathrm{MeV}$$

$$\sigma = 940 \frac{\lambda}{1.8}\ \mathrm{barns}$$

A few types of scintillation detectors

Material	^{6}Li density of atoms (cm^{-3})	Scintillation efficiency	Scintillation photon λ (nm)	Yield photons/ neutron
Li glass (Ce)	1.75×10^{22}	0.45 %	395 nm	~7,000
LiI (Eu)	1.83×10^{22}	2.8 %	470	~51,000
ZnS (Ag) - LiF	1.18×10^{22}	9.2 %	450	~160,000

GEM Detector Module

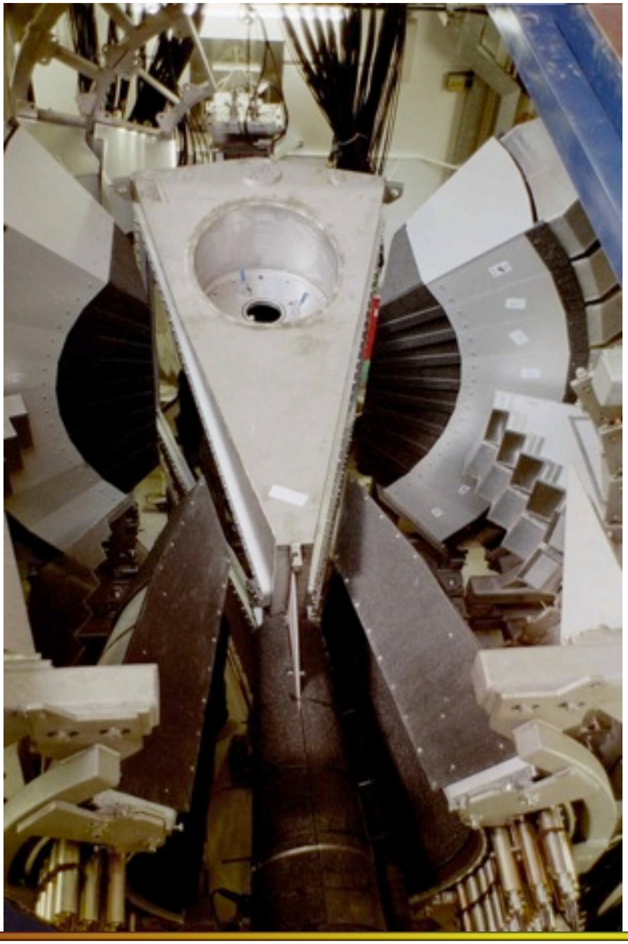

Semiconductors detectors

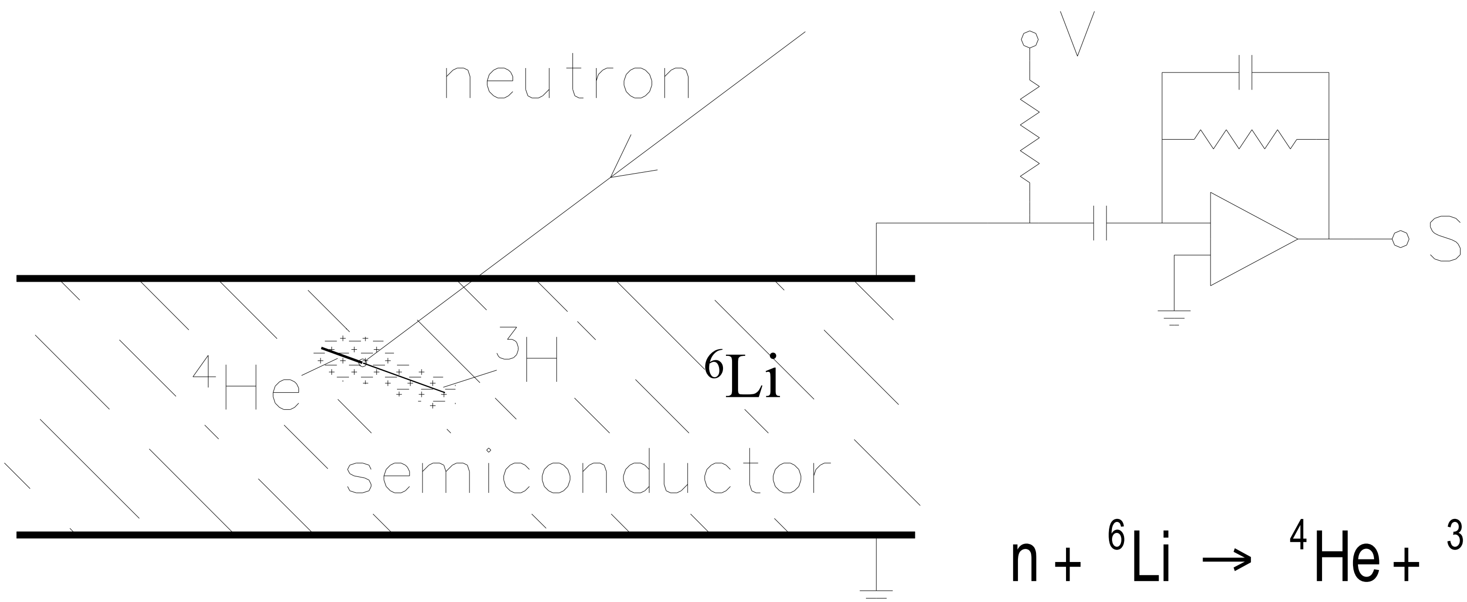

$$n + {}^{6}Li \rightarrow {}^{4}He + {}^{3}H + 4.79\,MeV$$

$$\sigma = 940 \frac{\lambda}{1.8} \text{barns}$$

Operational principle

- ~1,500,000 e - h produced per neutron (~2.4×10^{-13} coulomb)
  - This signal may be read directly without further amplification

  But

  - Semiconductor detectors do not contain a sufficient number of ansorbing nuclei so to provide a good efficiency
  - An absorbing layer can be used onto the semiconductor surface

An example

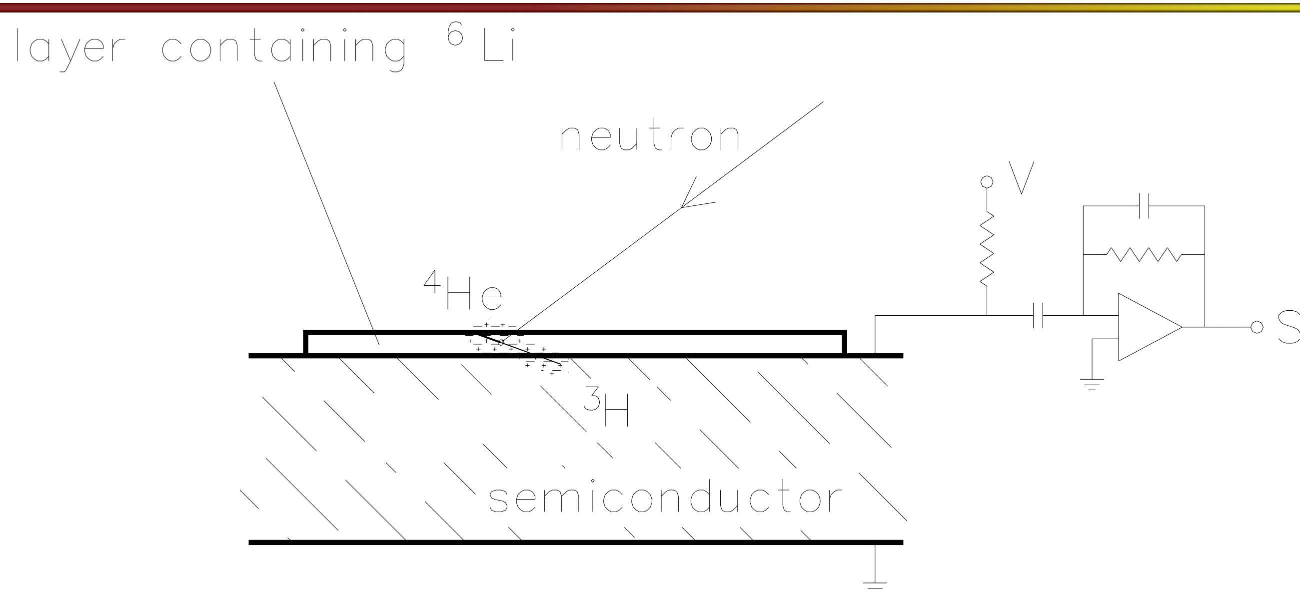

- The layer has to be thin (a few microns) in order to allow the secodaries to escape:
  - Low efficiency
- Some of the energy is not released into the detector
  - Pulse height discrimination is not good

Detection efficiency

- Complete expression: $\varepsilon = 1 - e^{-N\sigma(E)t}$
- Approximate expression for low efficiencies: $\varepsilon \approx N\sigma t$
- where:

σ = absorption cross section

N = density of absorbing centers

t = thickness

$N = 2.7\times10^{19}\ \mathrm{cm}^{-3}\cdot\mathrm{atm}^{-1}$ for a gas

For a 1 cm thickness of ^{3}He at 1 atm and for λ=1.8 Å

$\varepsilon = 0.13$

Pulse height discrimination

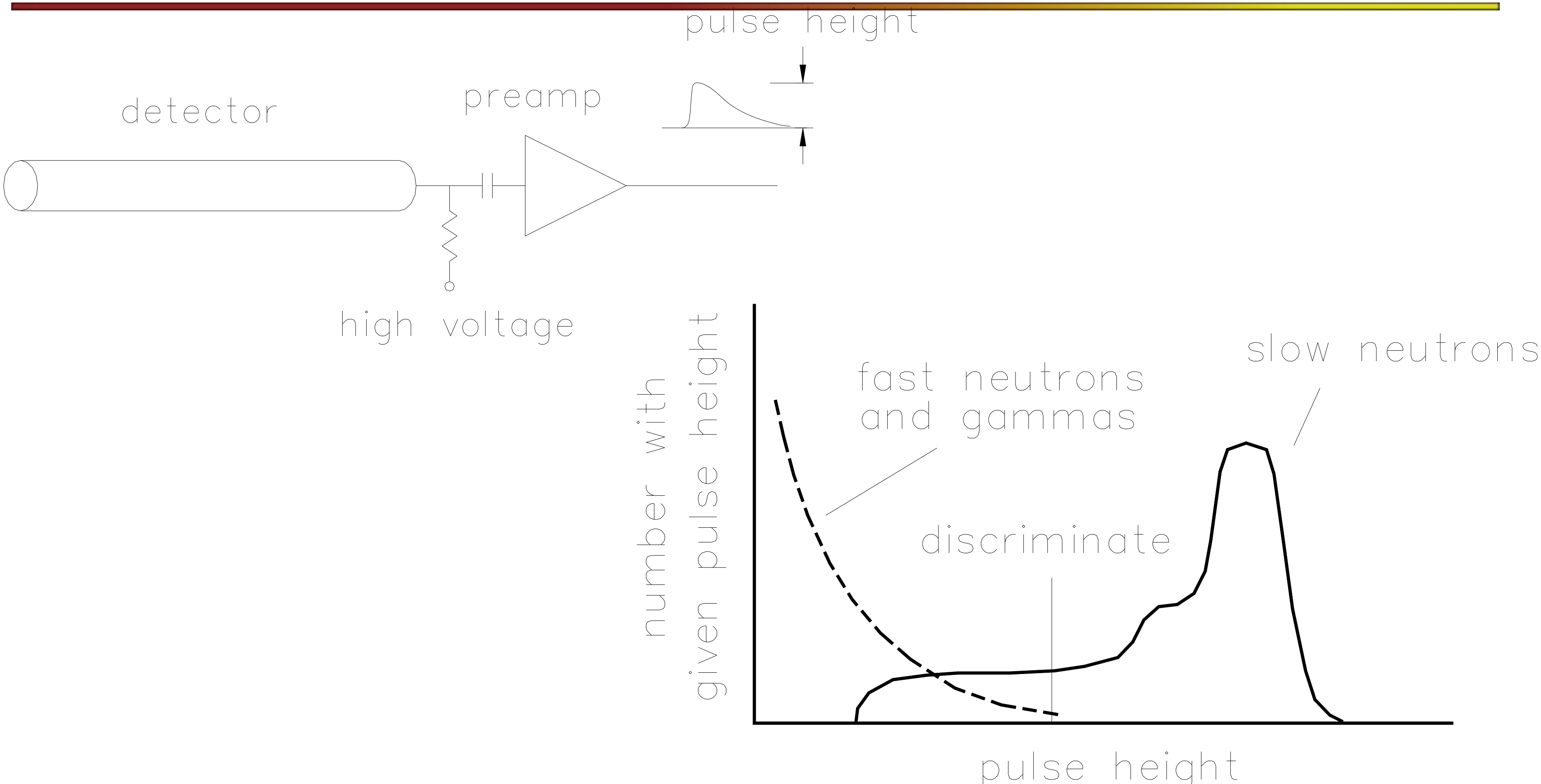

Operation principle

- A discrimination threshold may be used to reject the unwanted events (fast neutrons, gamma, electronic noise)
- Pulse Height discrimination is useful to enhance the signal-to-background ratio.
- Discrimination capability is an important characteristic in choosing a detector (^{3}He gaseous detectors are good to this aim)

Multi Wire Proportional Counters

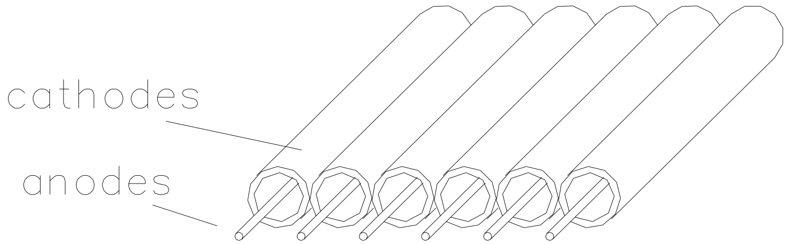

- Detectors array

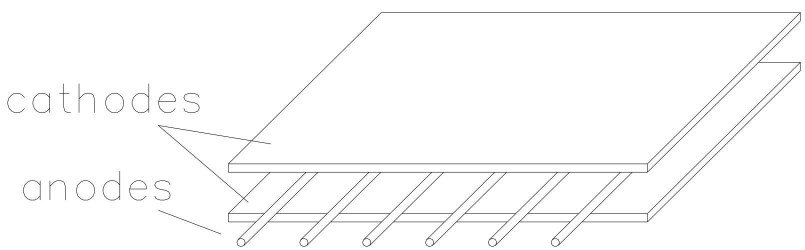

MWPC operation principle

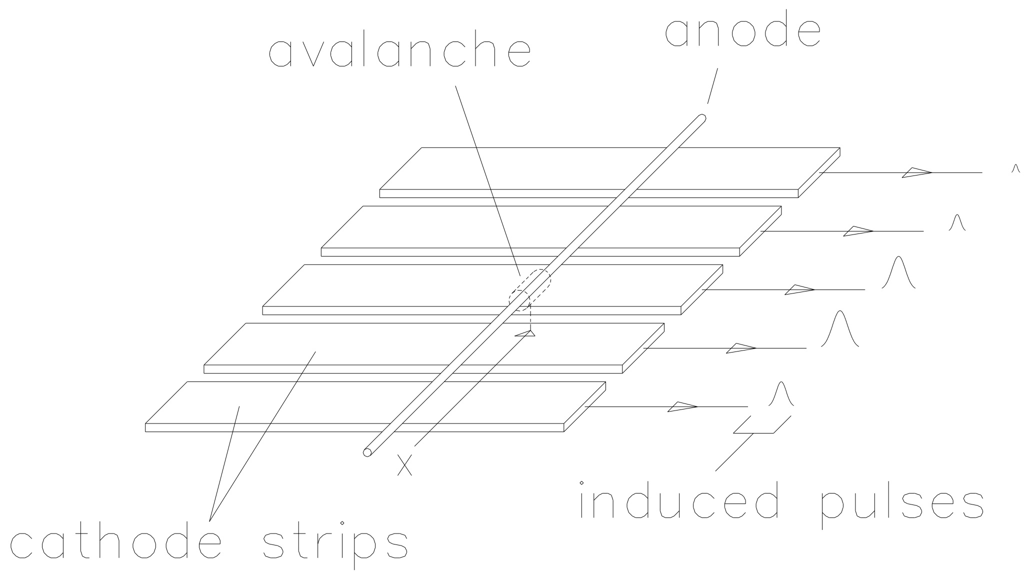

- By segmenting the cathode a 2D readout is achieved and thus the (x,y) position determination

Resistive encoding of a MWPC

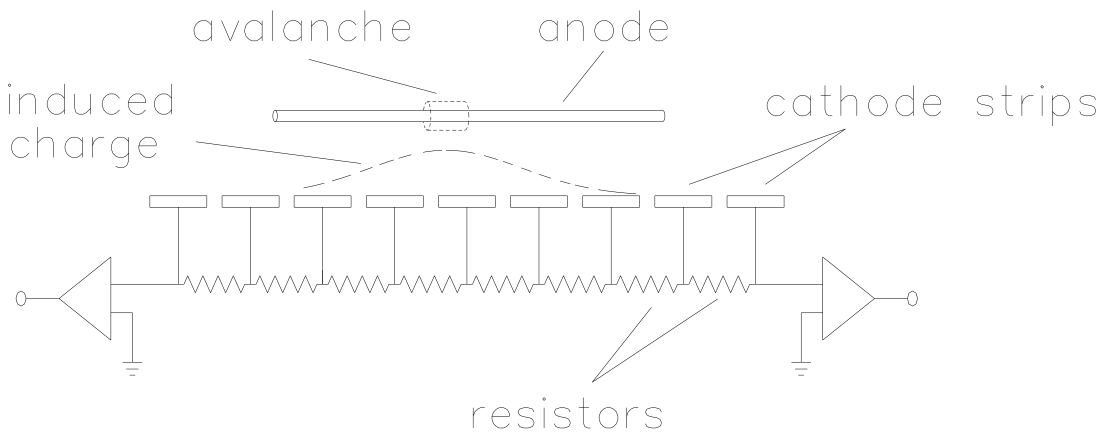

- Instead of a single ctahode strip readout, the strips can be resistively coupled (cheap but slow)

- The event position is determined by the fraction of the charge that reach each side of the resistive chain (charge-division encoding).

- The event position can be also determined from the time of arrival of the pulse at the two edge of the resistive net (rise-time encoding)

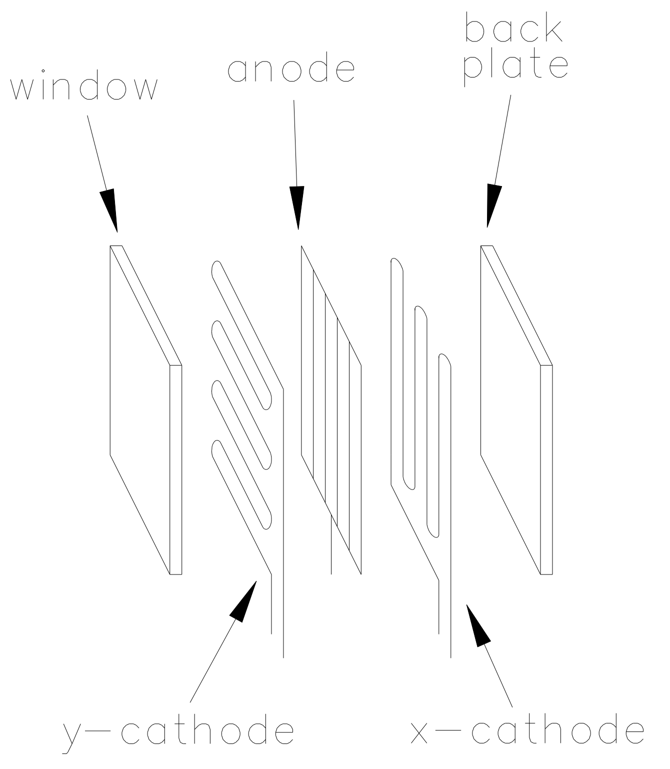

Micro-Strip gas counters

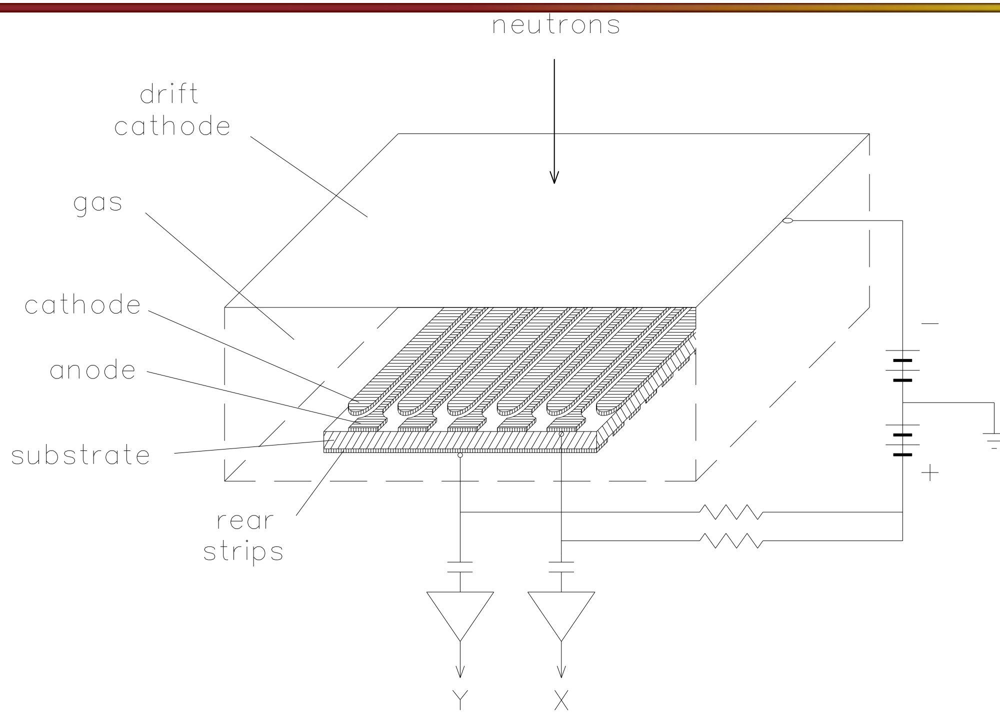

- The electrodes are made by means of lithographic techniques
  - Small structures – high spatial resolution – charge localization and fast recovery time

Crossed-Fiber scintillator

- dimensions: 25 cm x 25 cm
- thickness: 2 mm
- Number of fibers: 48 per ogni asse
- Spatial resolution: < 5 mm
- Shaping time: 300 nsec
- Count rate capability: ~ 1 MHz
- Time resolution: 1 μsec

16 elements prototype

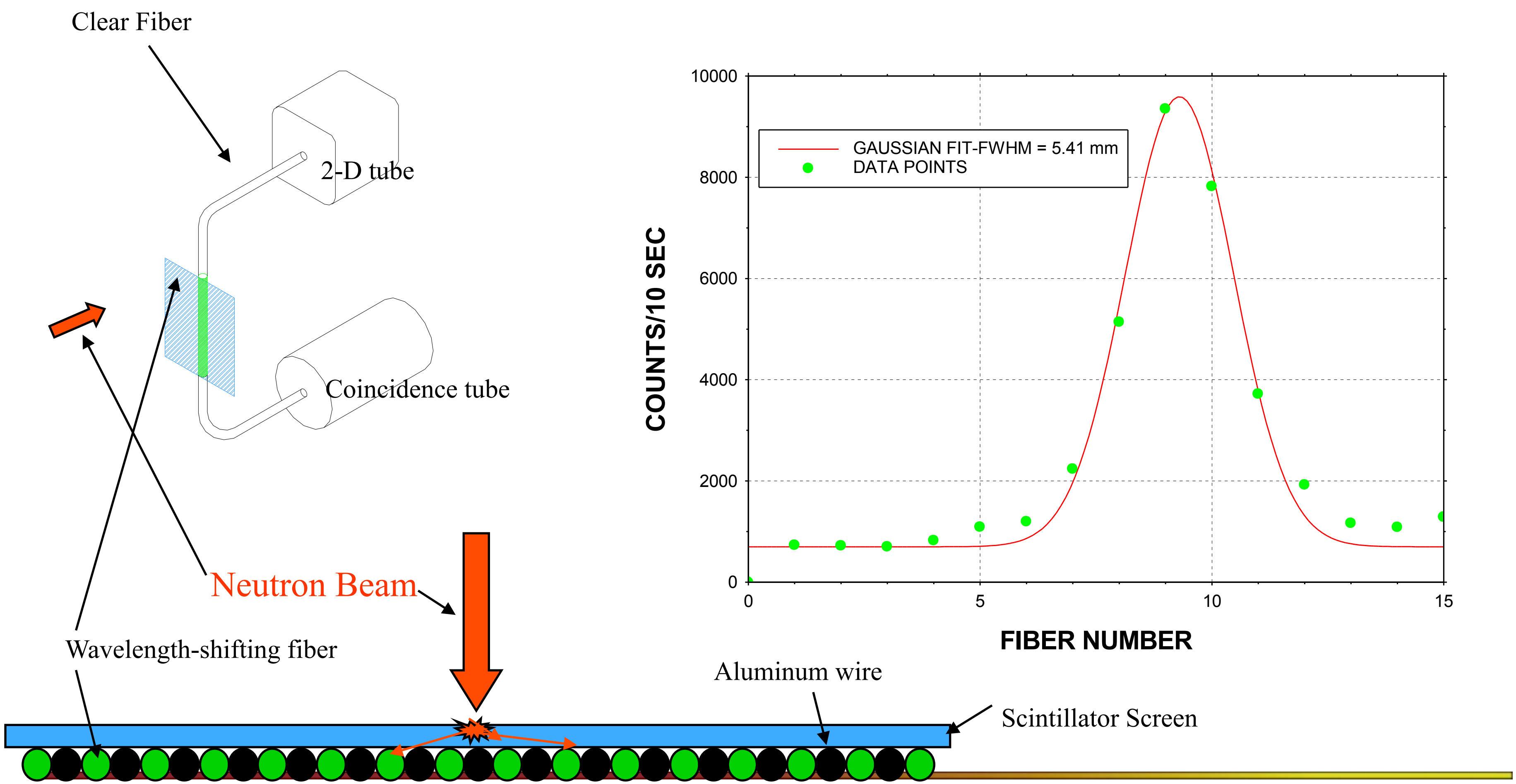

Operation principle of a Crossed-Fiber Position-Sensitive scintillator

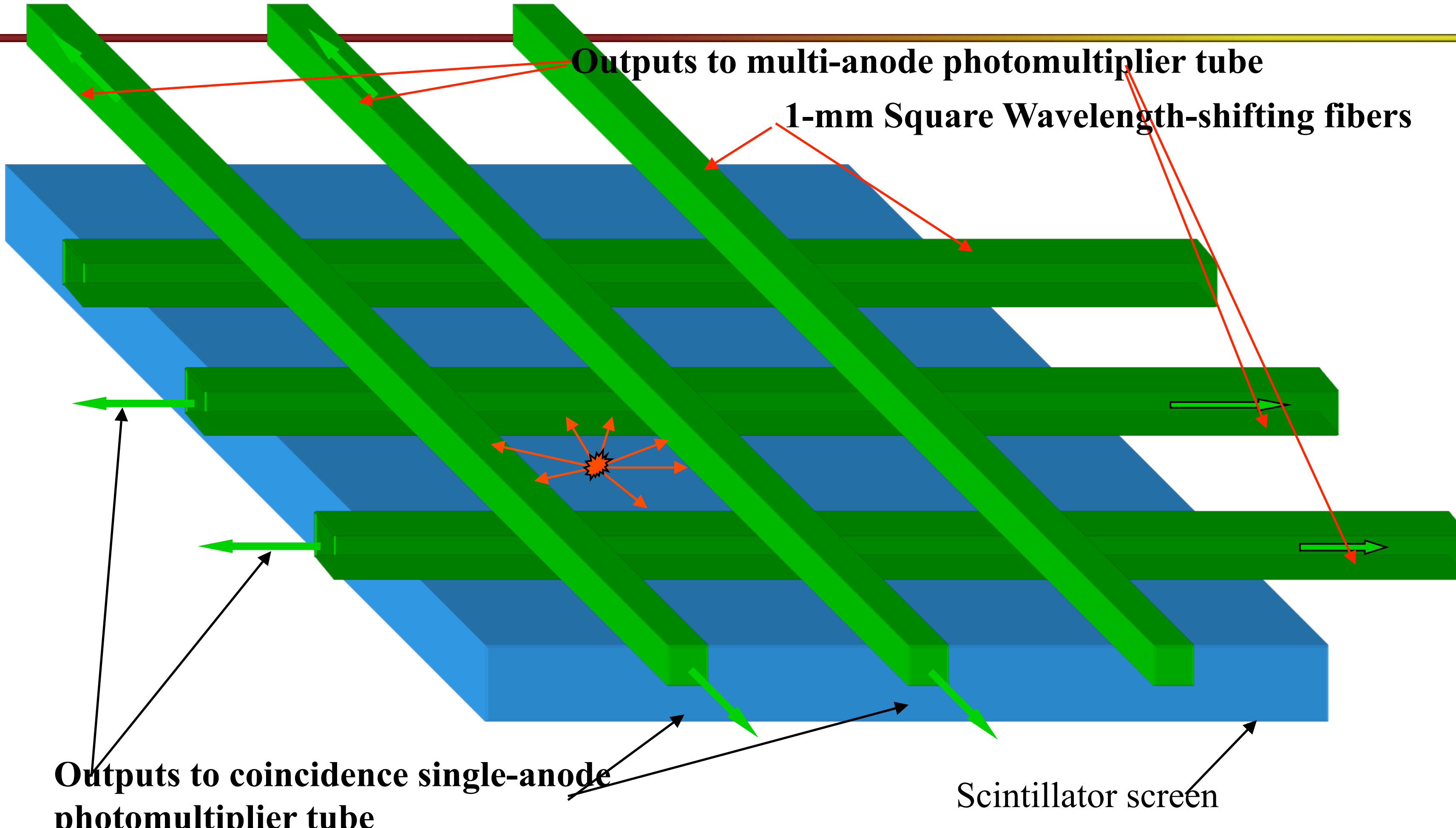

Neutron scattering off a Ge crystal neasured by a Crossed-Fiber detector

- Normalized diffusion forma Ge crystal (1 cm height)
- $E_n \sim 0.056$ eV
- Detector at 50 cm from the sample

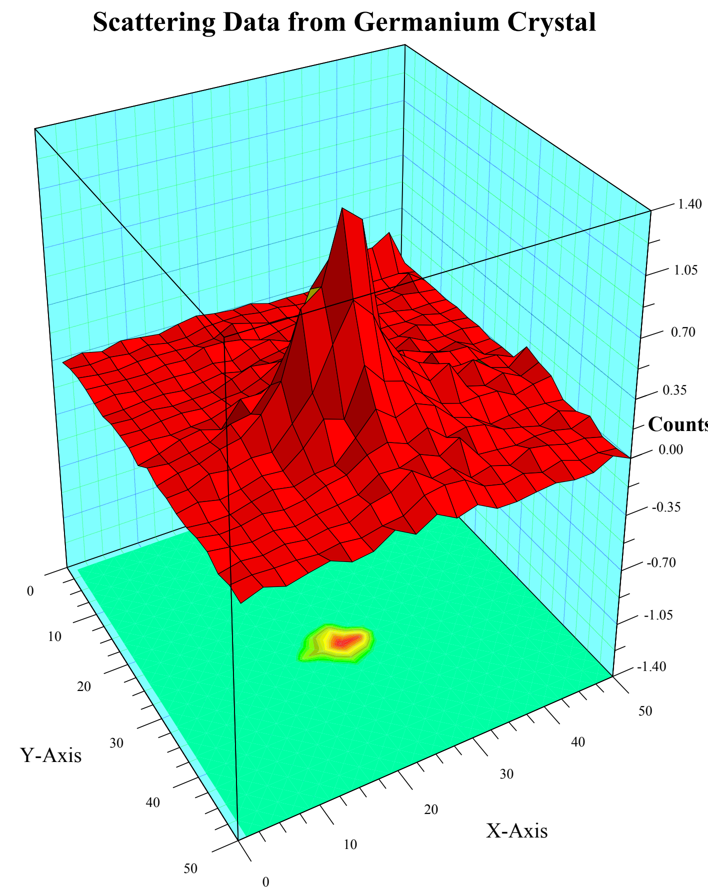

A close view to a Crossed-Fiber

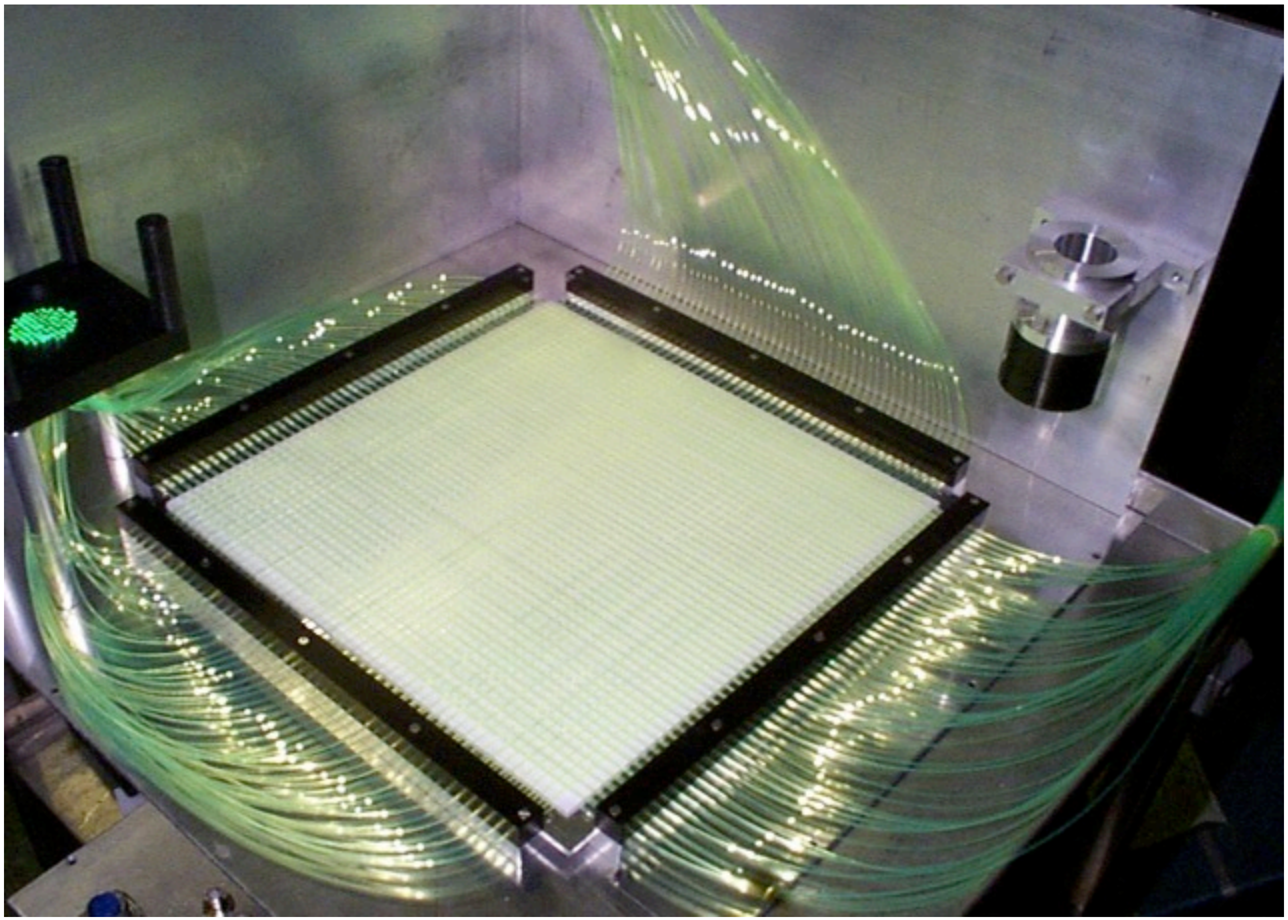

Where atoms are

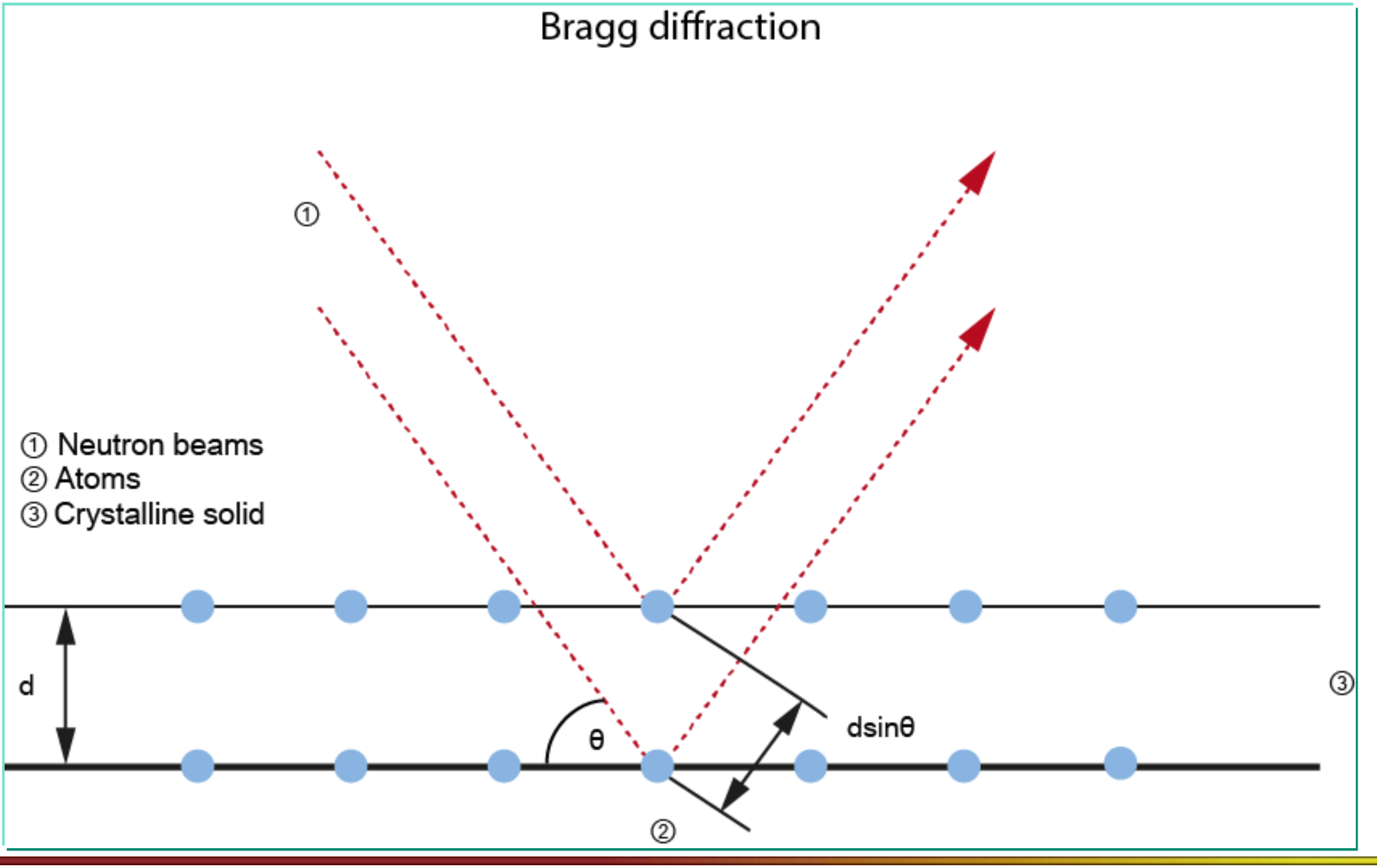

Diffraction

Diffraction pattern

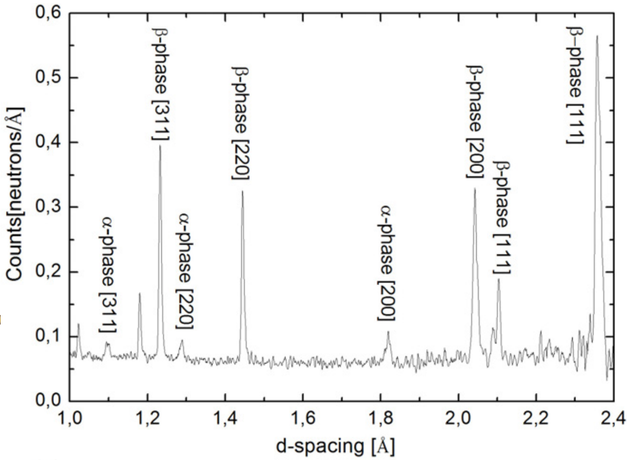

Cultural heritages

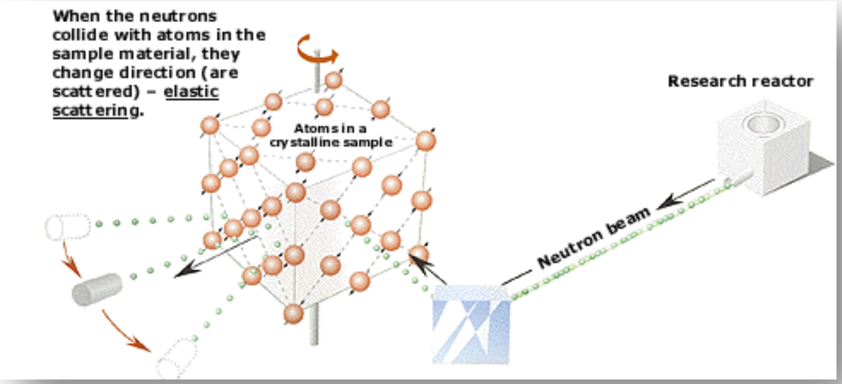

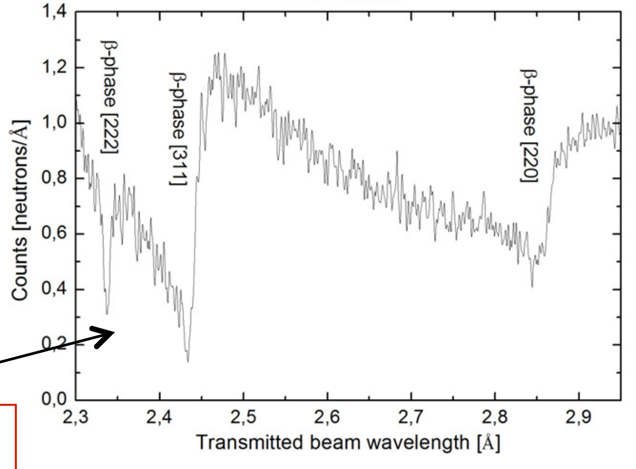

Bragg edges

Rietveld refinement

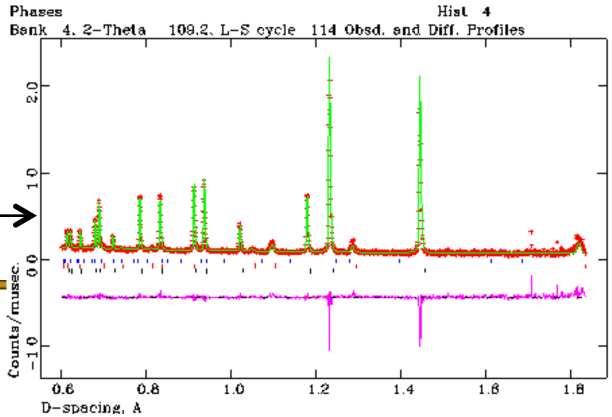

Magnetic neutron scattering
μ_n- σ_n interaction

Solid state physics

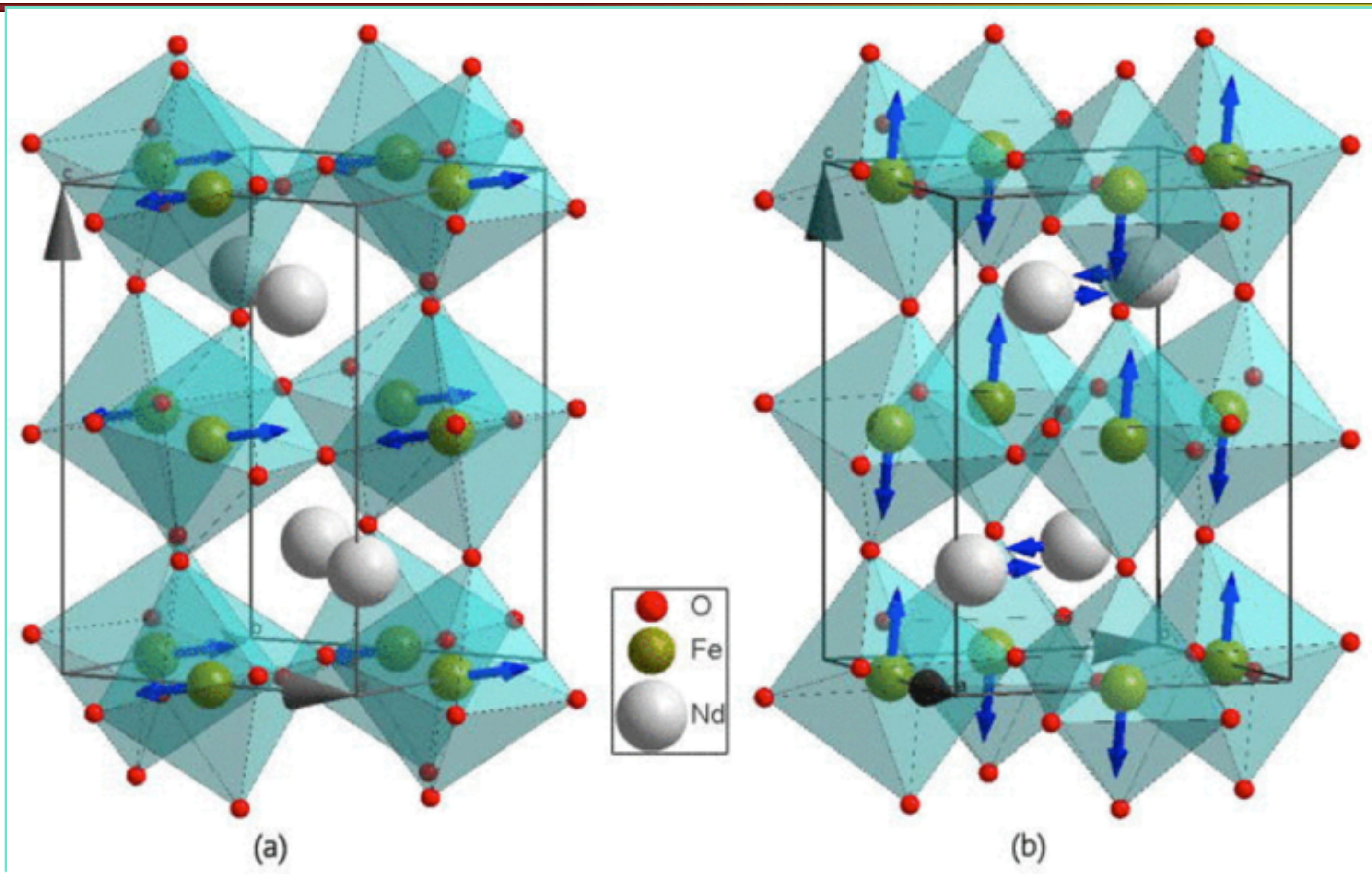

Crystal and magnetic structures of $NdFeO_3$

Fast neutron detection

- Lethargy
- Spherical dosimeters
- The "*Long Counter*"
- "*Li-glass*" scintillators
- ^{3}He proportional counters
- *"Proton Recoil Telescope"*
- Activation threshold targets

Lethargy

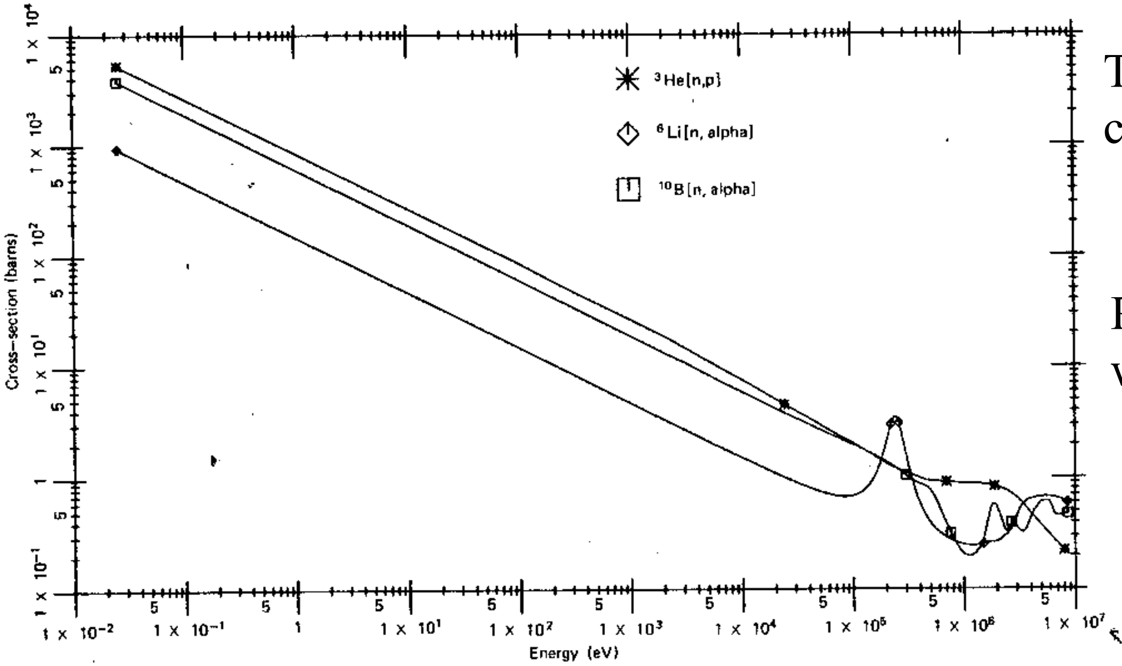

Figure 14.1 Cross section versus neutron energy for some reactions of interest in neutron detection.

The charge particel production corss section is proportional to $1/v_n$

Possible solution: Moderation with hydrogenated materials

$$\xi = 1 + \frac{(A-1)^2}{2A} \ln \frac{A-1}{A+1}$$

$$n = \frac{1}{\xi} \ln \frac{E_0}{E_f}$$

By moderating, the energy distribution function shifts towards lower energies

Spherical dosimeters

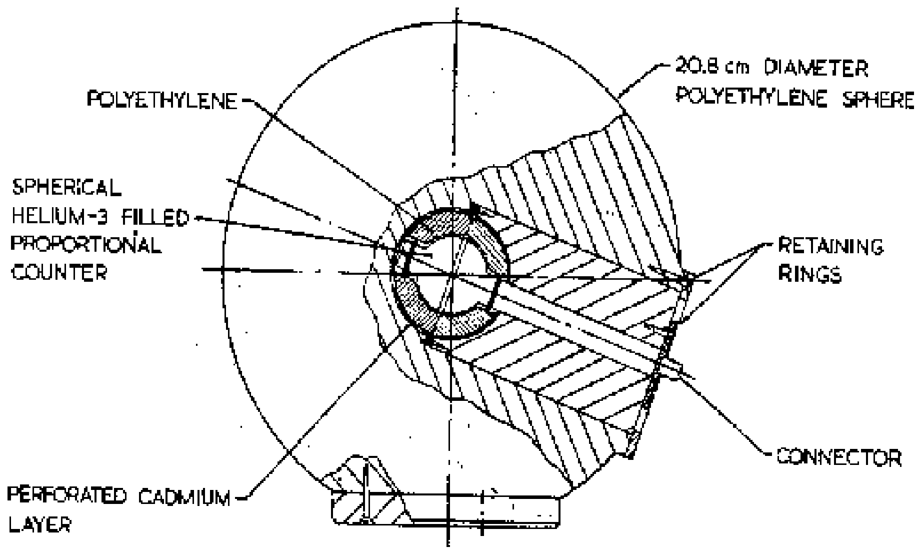

Figure 15.5 A spherical neutron dosimeter based on a ^{3}He neutron detector. (From Leake.[14])

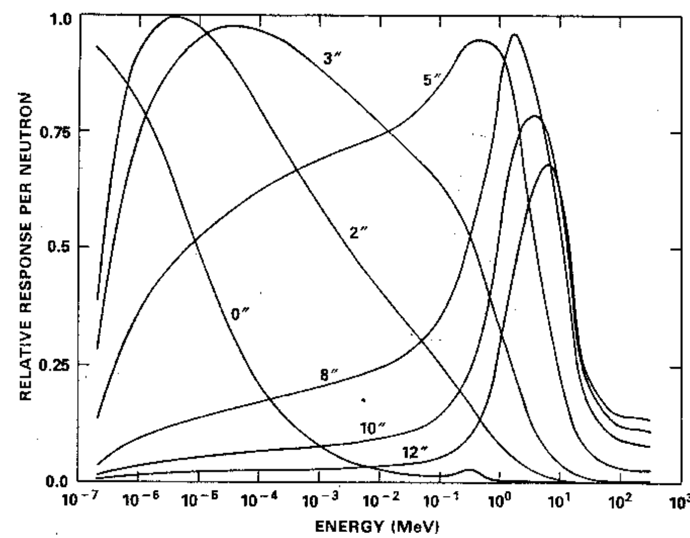

Figure 15.2 The energy dependence of the relative detection efficiencies of Bonner sphere neutron detectors of various diameters up to 12 inches. (From Johnson et al.[2])

The “*Long Counter*”

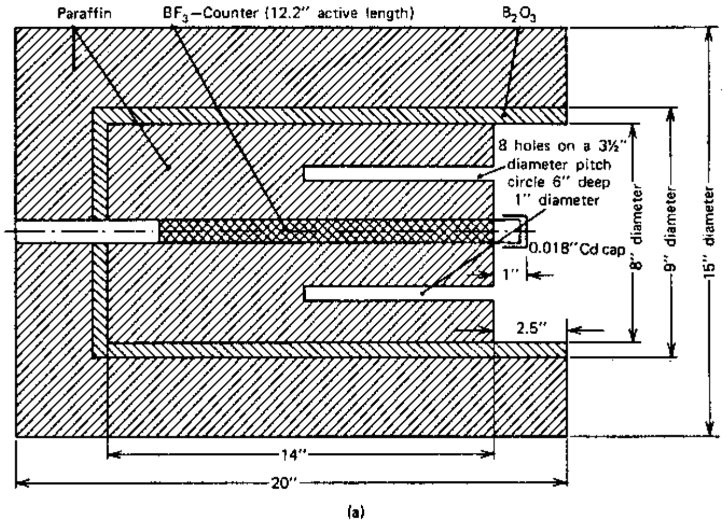

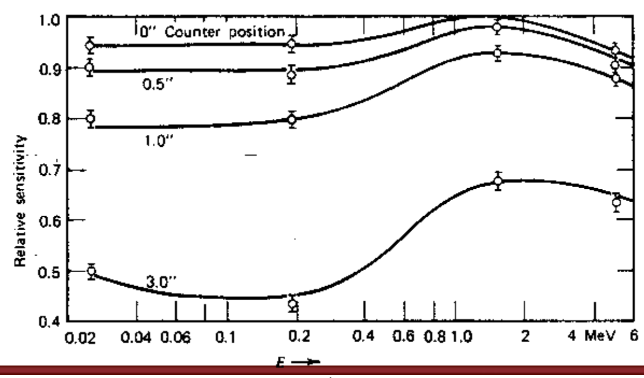

This detector is characterized by a response function that, in a wide interval, is independent of neutron energy

(“flat response detector”)

^{6}*Li-glass* scintillators

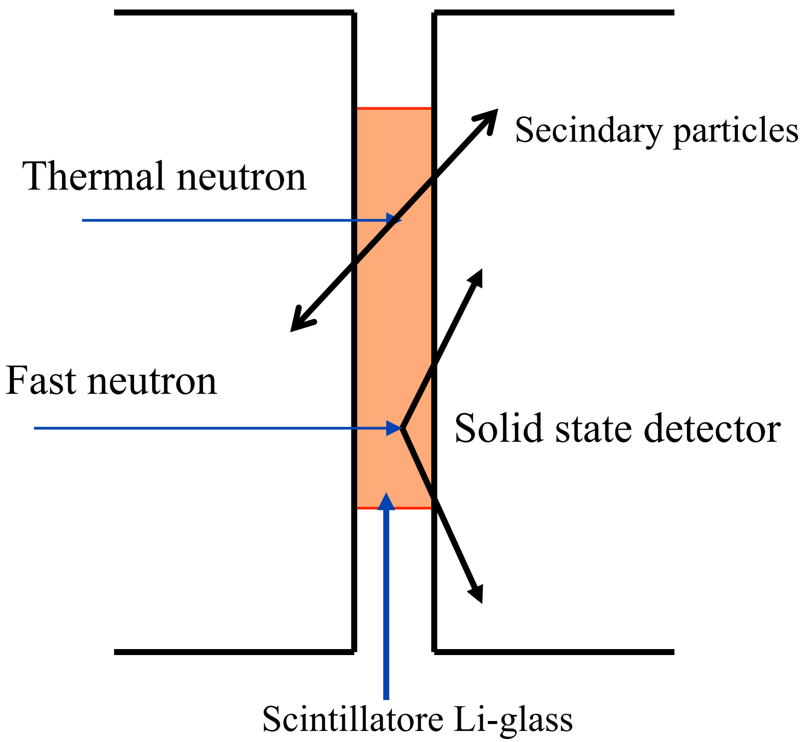

The use of coincidence produces a lowering in the efficiency with increasing neutron energy ($E_n \geq$ Q-value of the reaction)

Some characteristics

	NE902	NE905	NE908	NE912
D (gr/cm^3)	2.6	2.48	2.674	2.55
n	1.58	1.55	1.57	1.55
$T_{fusione}$ (°C)	1200	1200	1200	1200
λ_{max} (nm)	395	395	395	397
Light emission (rel.antracene)	22-34%	20-30%	20%	25%
Decay time (ns)	75	100	75	75
Arr. ^{6}Li	95%	95%	95%	95%
Activity α (/min)	100-200	100-200	100-200	10
$\Delta E/E$	13-22 %	15-28 %	20-30 %	20-30 %

^{3}He proportional counters

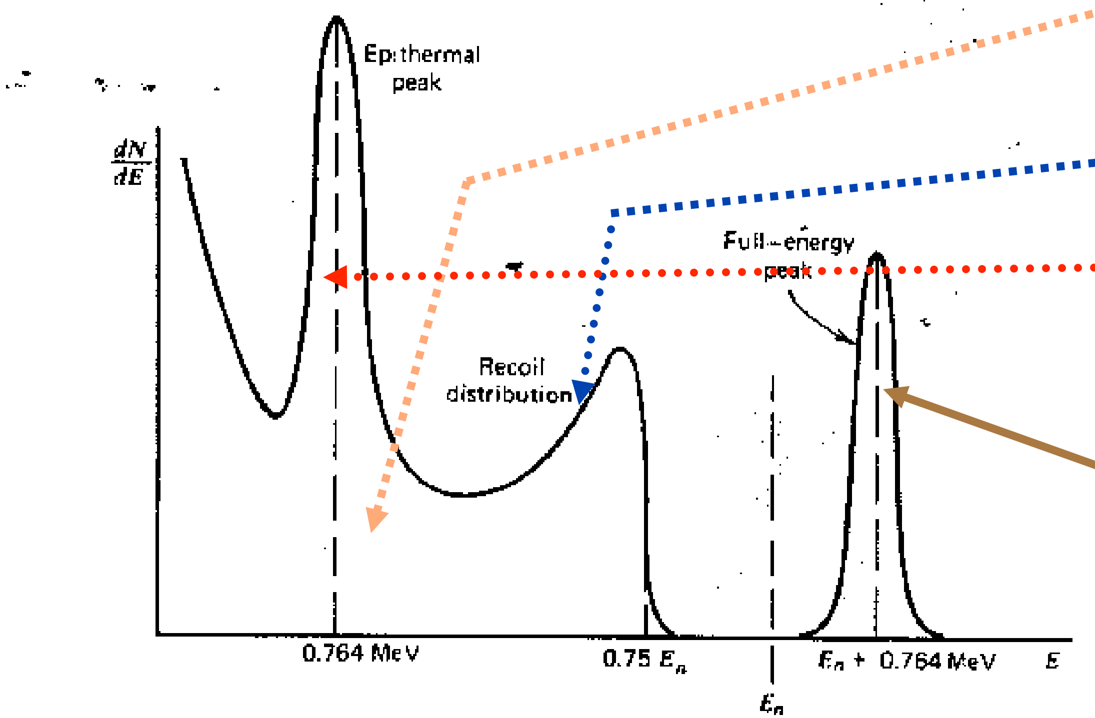

Figure 15.11 Differential energy spectrum of charged particles expected from fast neutrons incident on a ^{3}He detector.

Elastic scettering continuum

With a peak at **0,75 E_n** (cinematica)

e

Peak at the **Q-value** dovuto a interazioni di neutroni moderati

Peak due to (n,p) reactions induced by fast incident neutrons

Proton Recoil Telescope

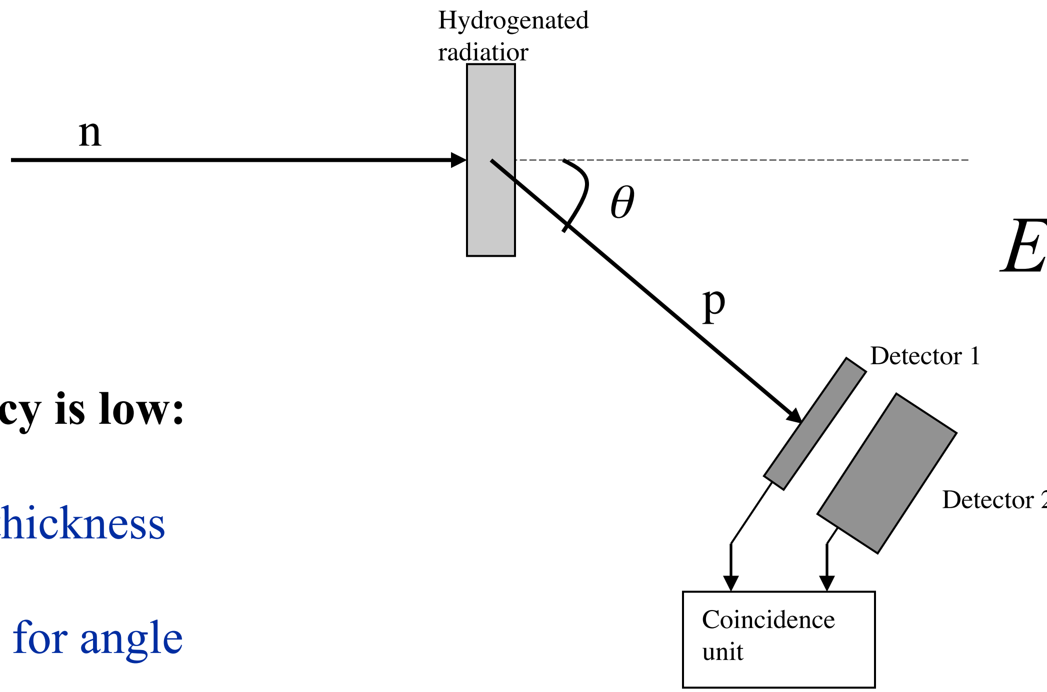

$$E_p = E_n \cos^2 \vartheta$$

Efficiency is low:

- small radiator thickness
- small detectors for angle determination

Thin Foil Magnetic Proton Recoil Neutron Spectrometer MPRu at JET

Fusion technology

MPR conceived for 14 MeV neutrons

MPRu also for 2.5 MeV neutrons measurments

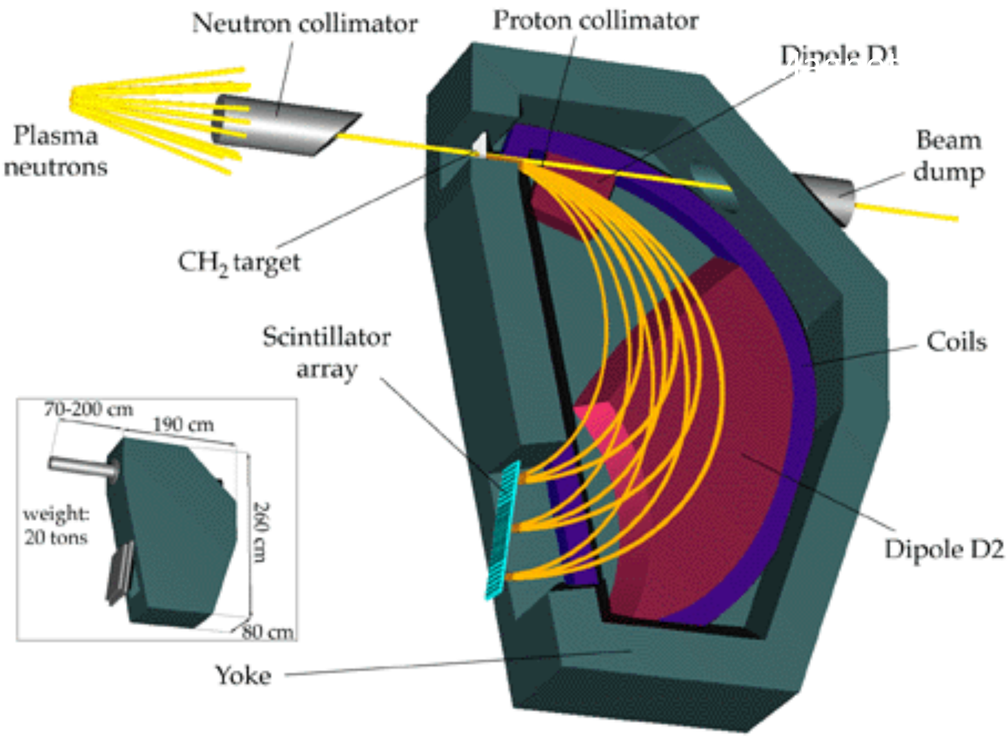

A. Sundén, at al, NIM A610 (2009)682

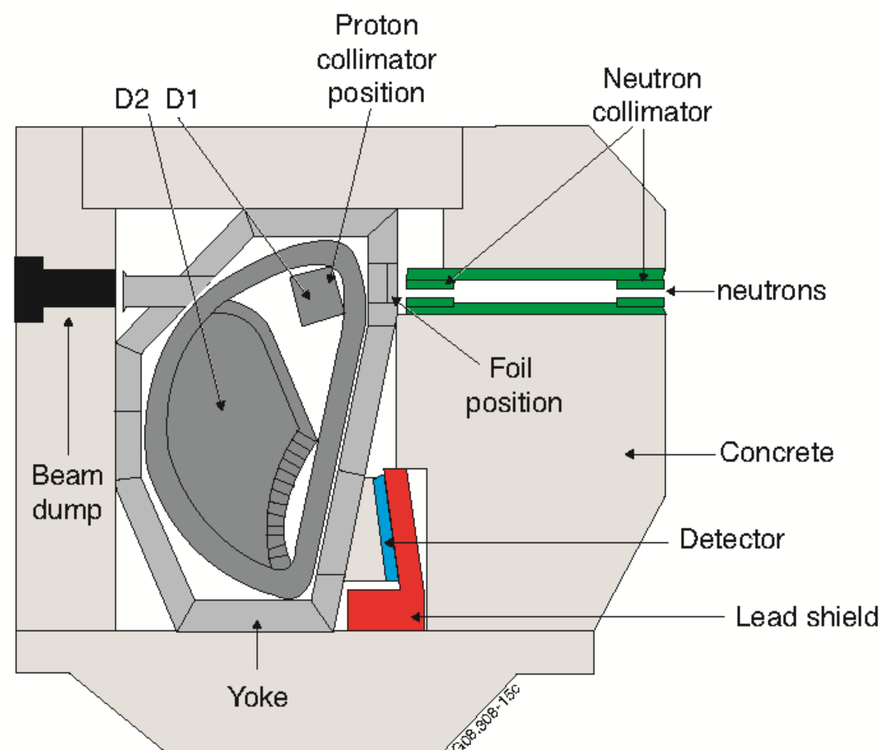

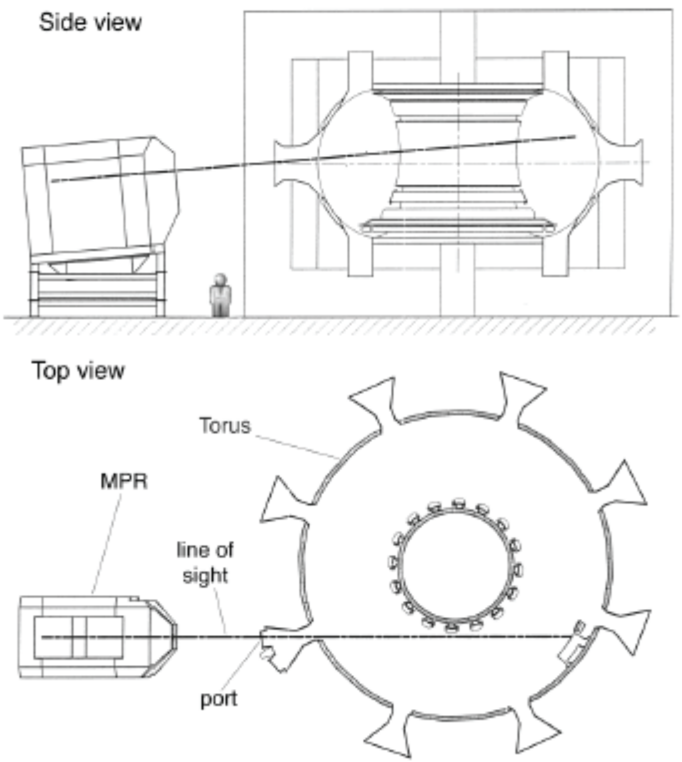

Illustration of the semi-tangential Line Of Sight (LOS) of the MPRu.

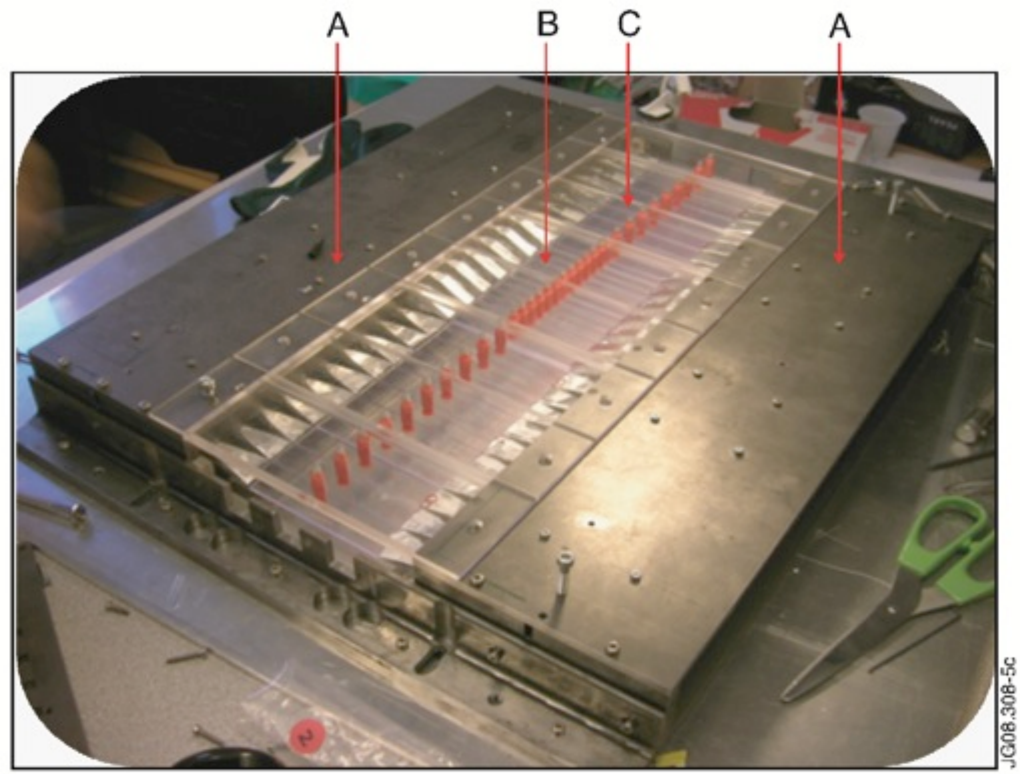

Overview of detector mechanics, with the PMTs mounted inside their magnetic shield boxes (A).
The plastic roof (B) and the fibre guides pieces (C) are also visible

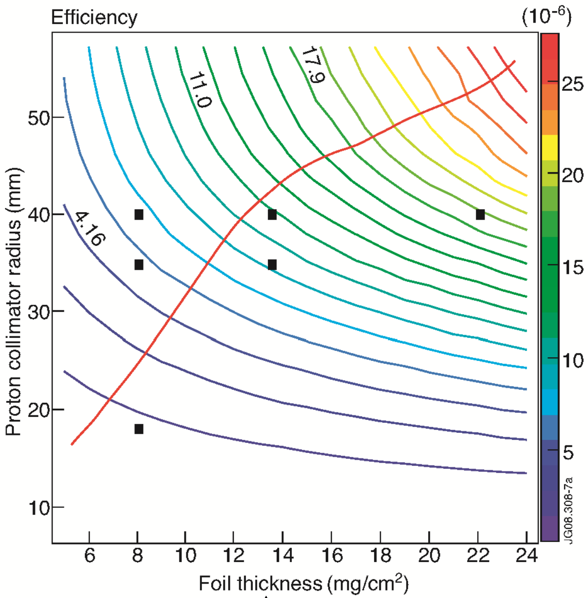

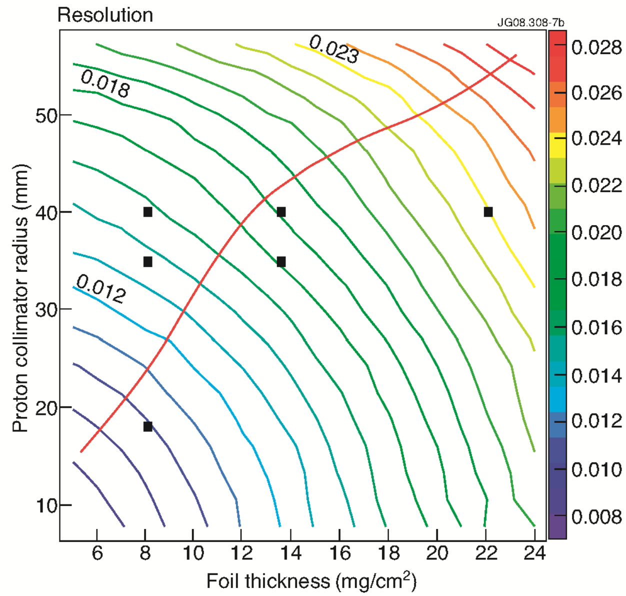

Resolution (σ/En) of the MPRu as a function of proton collimator radius and foil thickness.

14 MeV case

Black squares in the figures refer to the possible MPRu settings for the proton collimator and the foil target.

2.5 MeV case

14 MeV case

The efficiency of the MPRu as a function of proton collimator radius and foil thickness.

2.5 MeV case

Black squares in the figures refer to the possible MPRu settings for the proton collimator and the foil target.

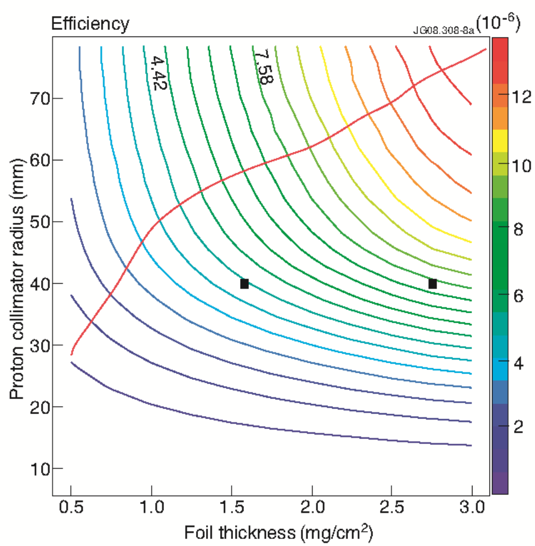

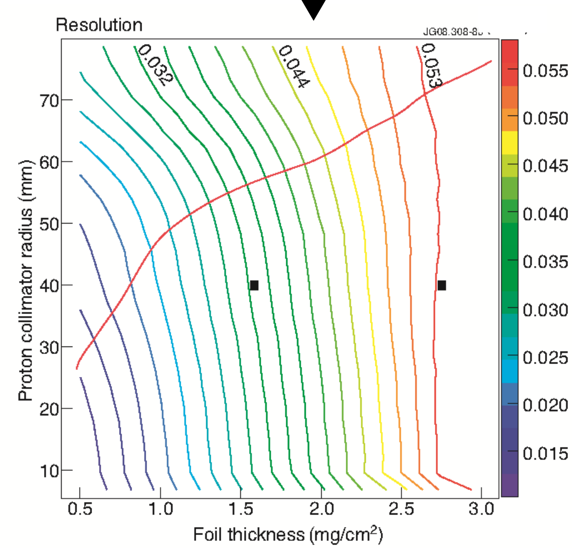

Activation threshold technique

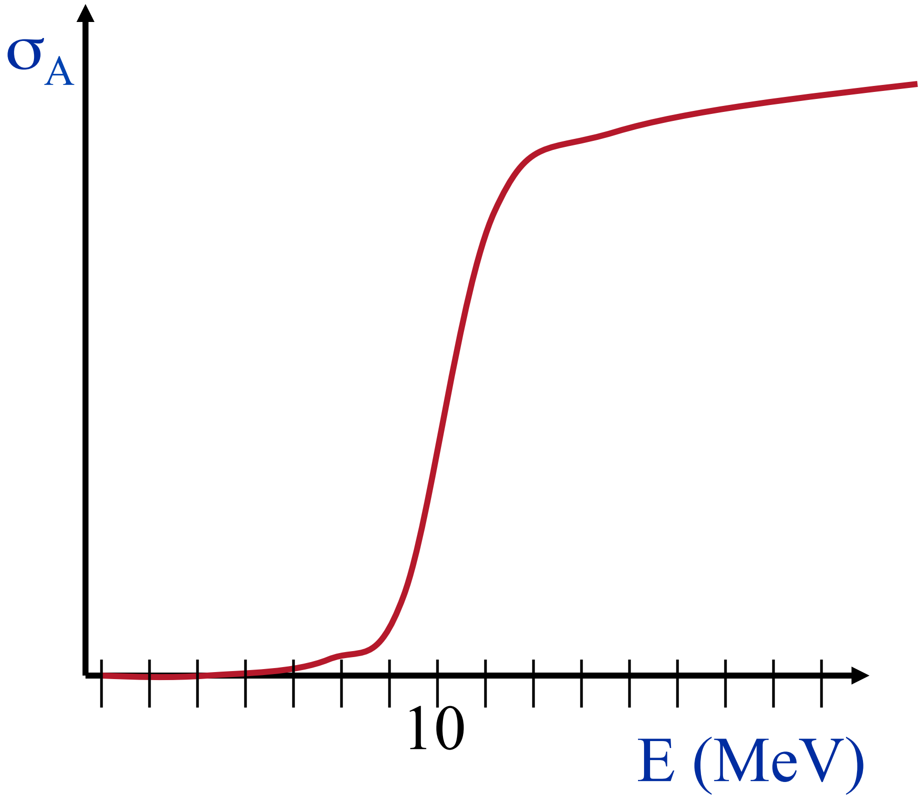

A target of a proper material is irradiated with a neutron beam and after an irradiation time Δt is removed from the beam and the induced activity is measured

Some examples

Material	Reaction	Ab.Is.(%)	H.L	Eγ	Treshold (MeV)
F	$^{19}F(n,2n)^{18}F$	100	109.7min	0.511	11.6
Mg	$^{24}Mg(n,p)^{24}Na$	78.7	15.0 h	1.368	6.0
Al	$^{27}Al(n,\alpha)^{24}Na$	100	15.0 h	1.368	4.9
Fe	$^{56}Fe(n,p)^{56}Mn$	91.7	2.56 h	0.84	4.9
Co	$^{59}Co(n,\alpha)^{56}Mn$	100	2.56 h	0.84	5.2
Ni	$^{58}Ni(n,2n)^{57}Ni$	67.9	36.0 h	1.37	13.0
Cu	$^{65}Cu(n,2n)^{64}Cu$	69.1	9.8 min	0.511	11.9
Zn	$^{64}Zn(n,p)^{64}Cu$	48.8	12.7 h	0.511	2.0
In	$^{115}In(n,n')^{126}In$	95.7	4.5 h	0.335	0.5
I	$^{127}I(n,2n)^{126}I$	100	13.0 d	0.667	9.3

Neutron spectra of different sources

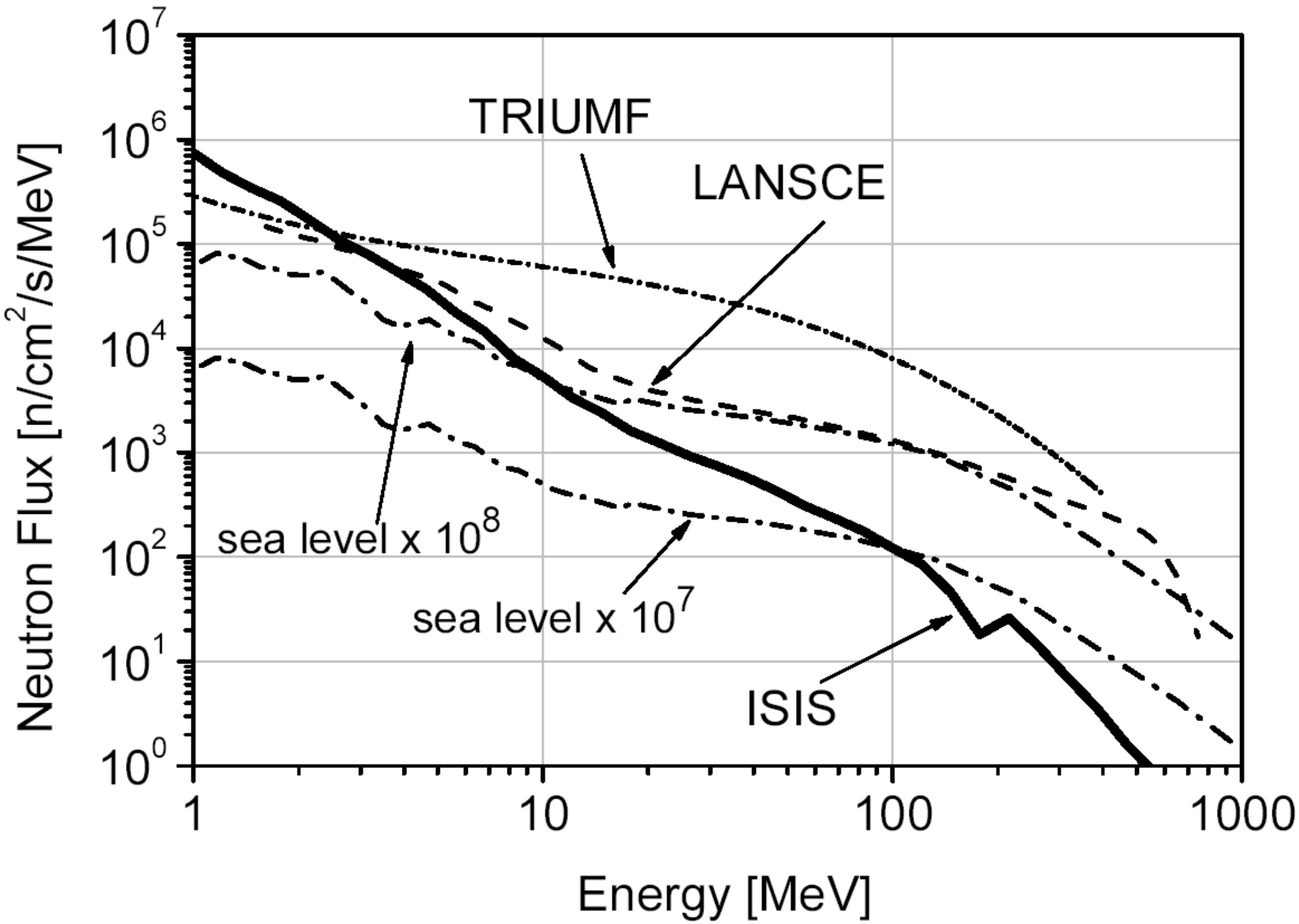

Metodo delle targhette a soglia di attivazione

Epithermal neutrons

- Pulsed sources

- Condensed matter applications

- Spectrometers

- Detection methods

The ISIS pulsed neutron source

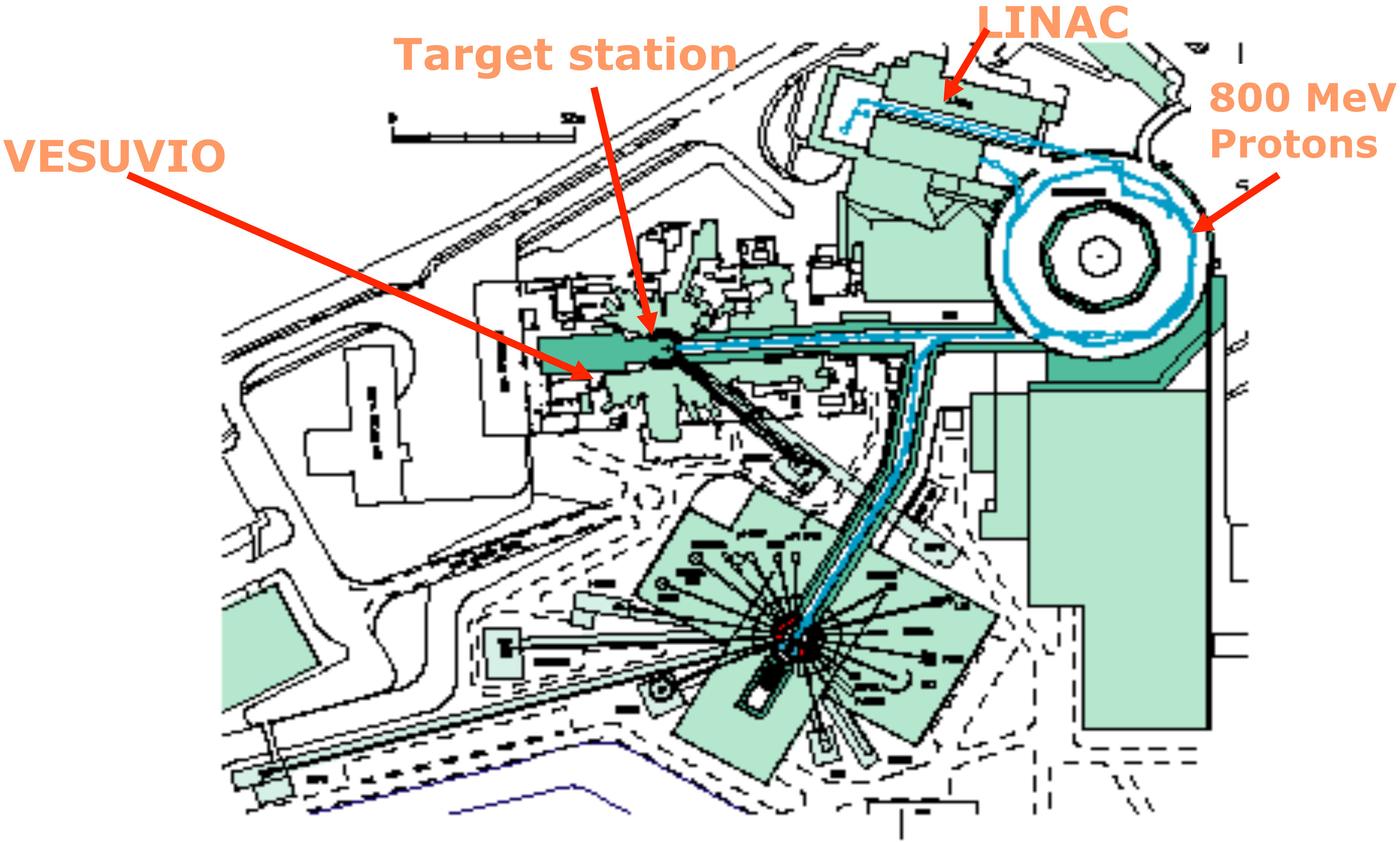

ori
ori)

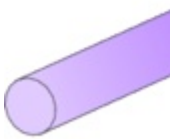

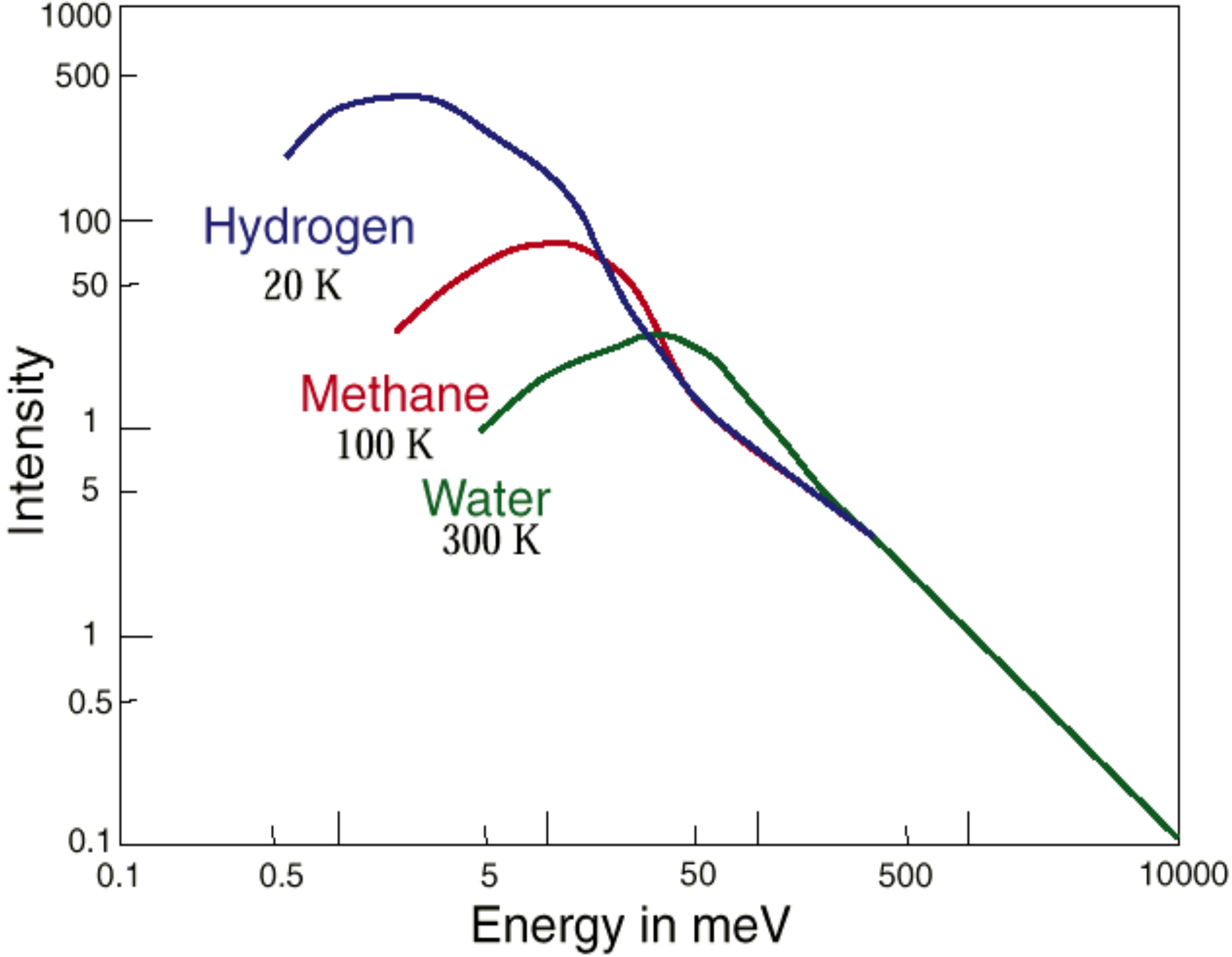

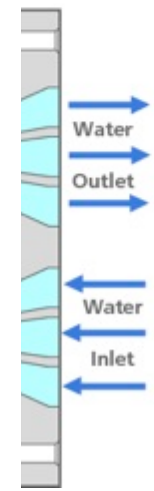

Il rif
riman
in que
ne

Caratterisitche principali della sorgente ISIS

All beam in synchrotron extracted in one turn

β = v/c = 0.84, 163 m circumference → revolution time = 0.65 μs

4 μC ÷ 0.65 μs → 6 A circulating current

Extracted pulse ~0.3 μs long (double peak proton pulse)

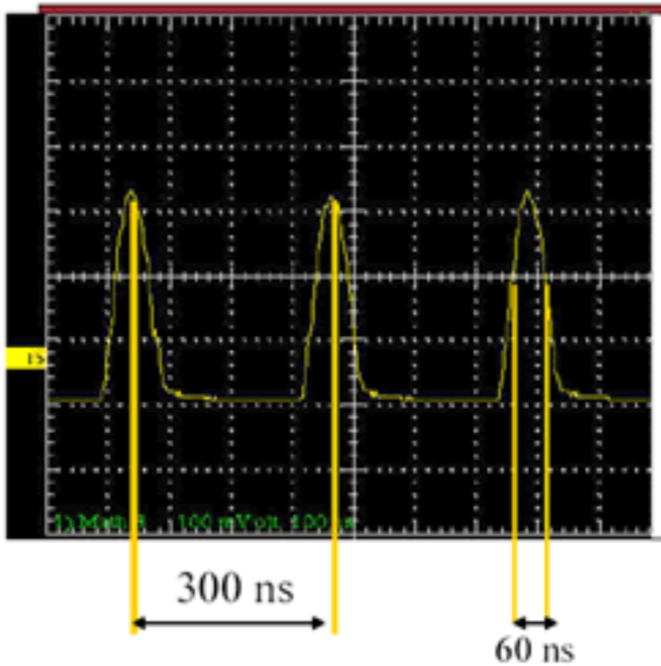

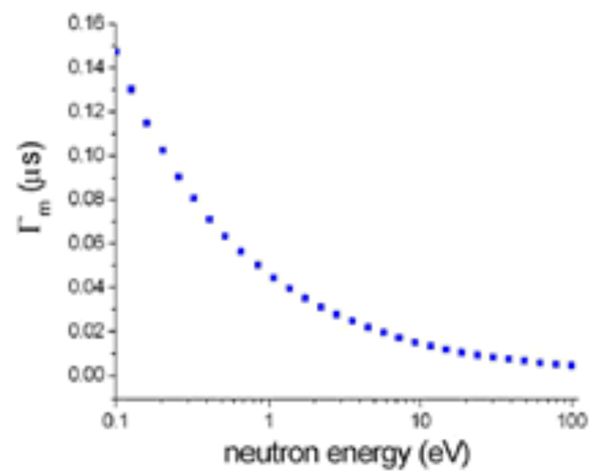

$$\Delta t = \sqrt{\Gamma_m^2 + \Gamma_{acc}^2}$$

The Time of flight technique

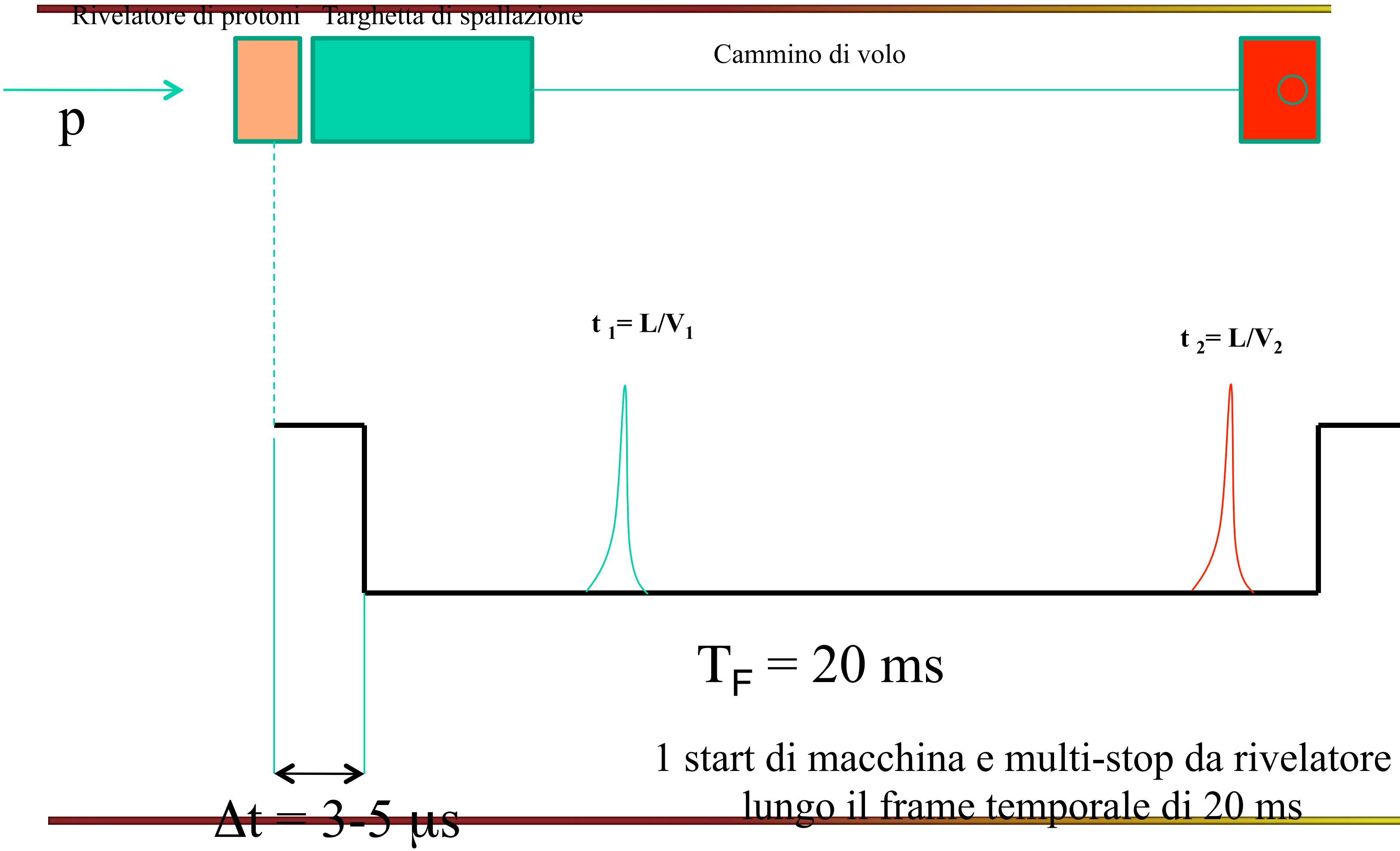

1 start di macchina e multi-stop da rivelatore lungo il frame temporale di 20 ms

Background sources

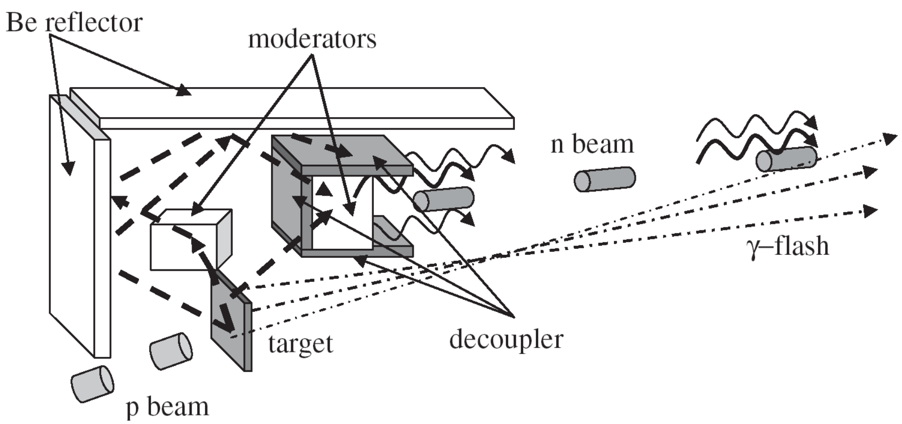

Fig. 2. Schematic of the target station: the flux of neutrons produced in the spallation reactions impinging on the moderator is enhanced by the use of the Be reflector. The pulsed neutron beams from the moderator travel together with γ-ray beams produced in the decoupler and into the moderator.

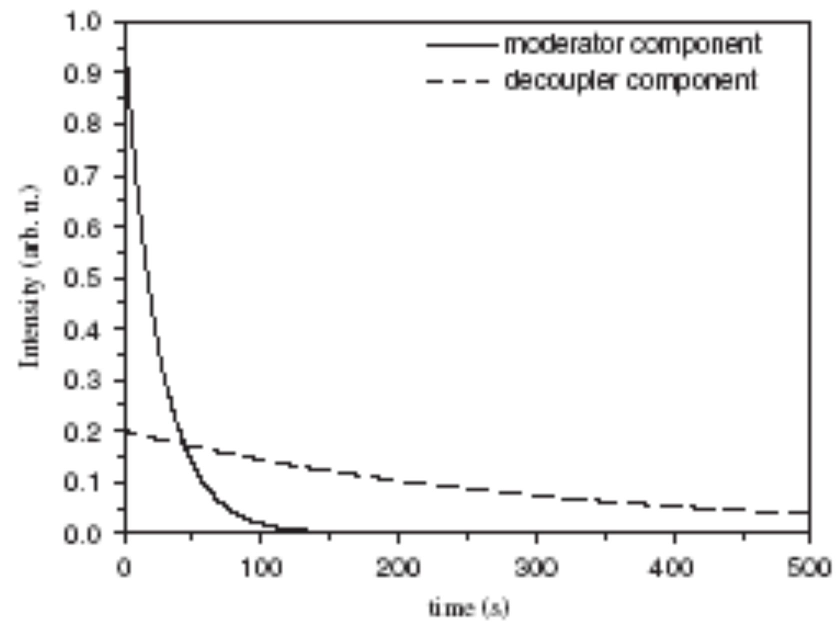

Fig. 6. Plot of $B_1(t)$ and $B_2(t)$ in Eq. (3). The amplitude of the moderator component is normalized to 1, while the amplitude of the decoupler component is chosen as a fraction of the first one.

Direct geometry spectrometers

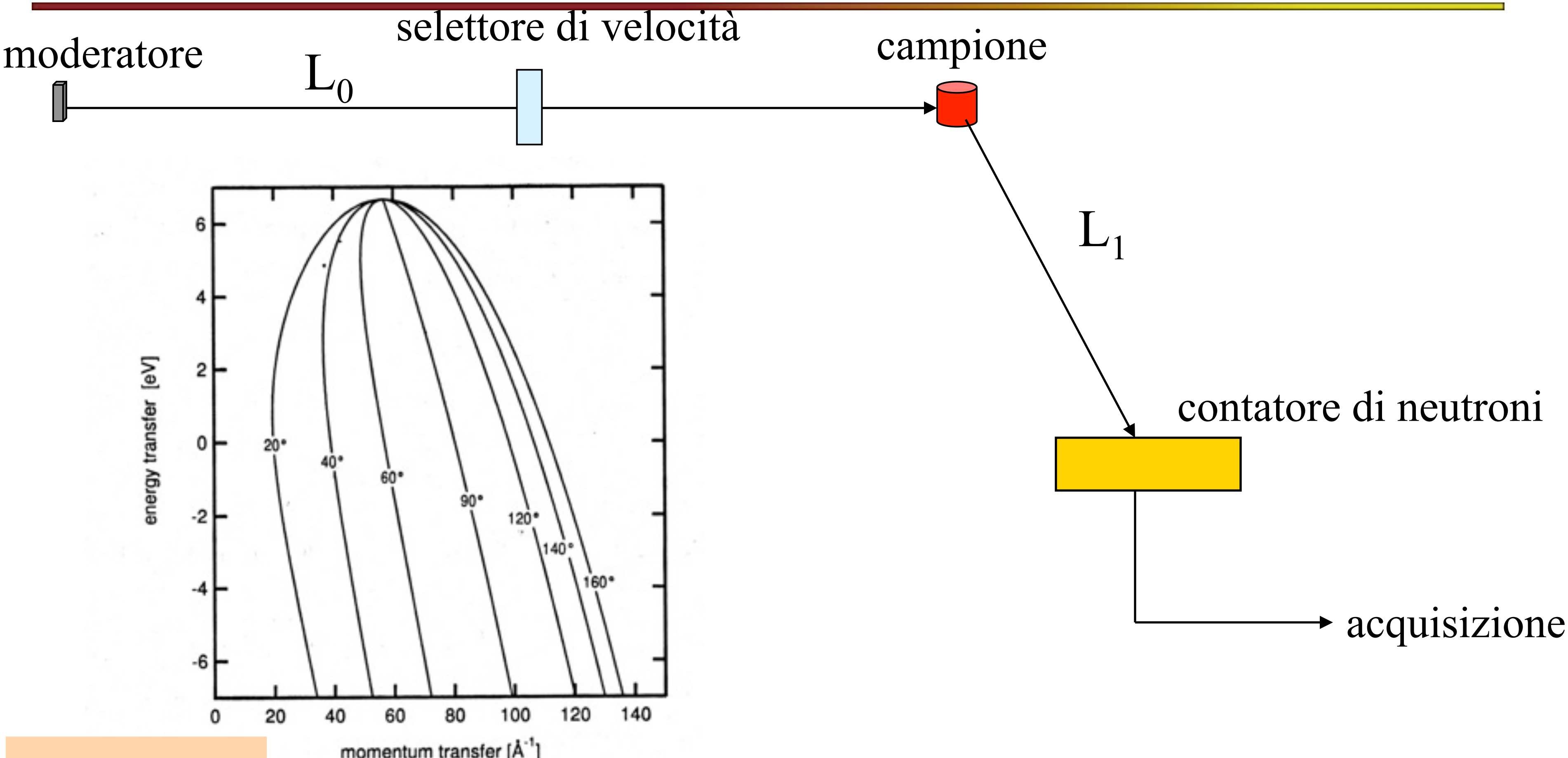

$E_0 = 6.67$ eV

Inverse geometry spectrometers

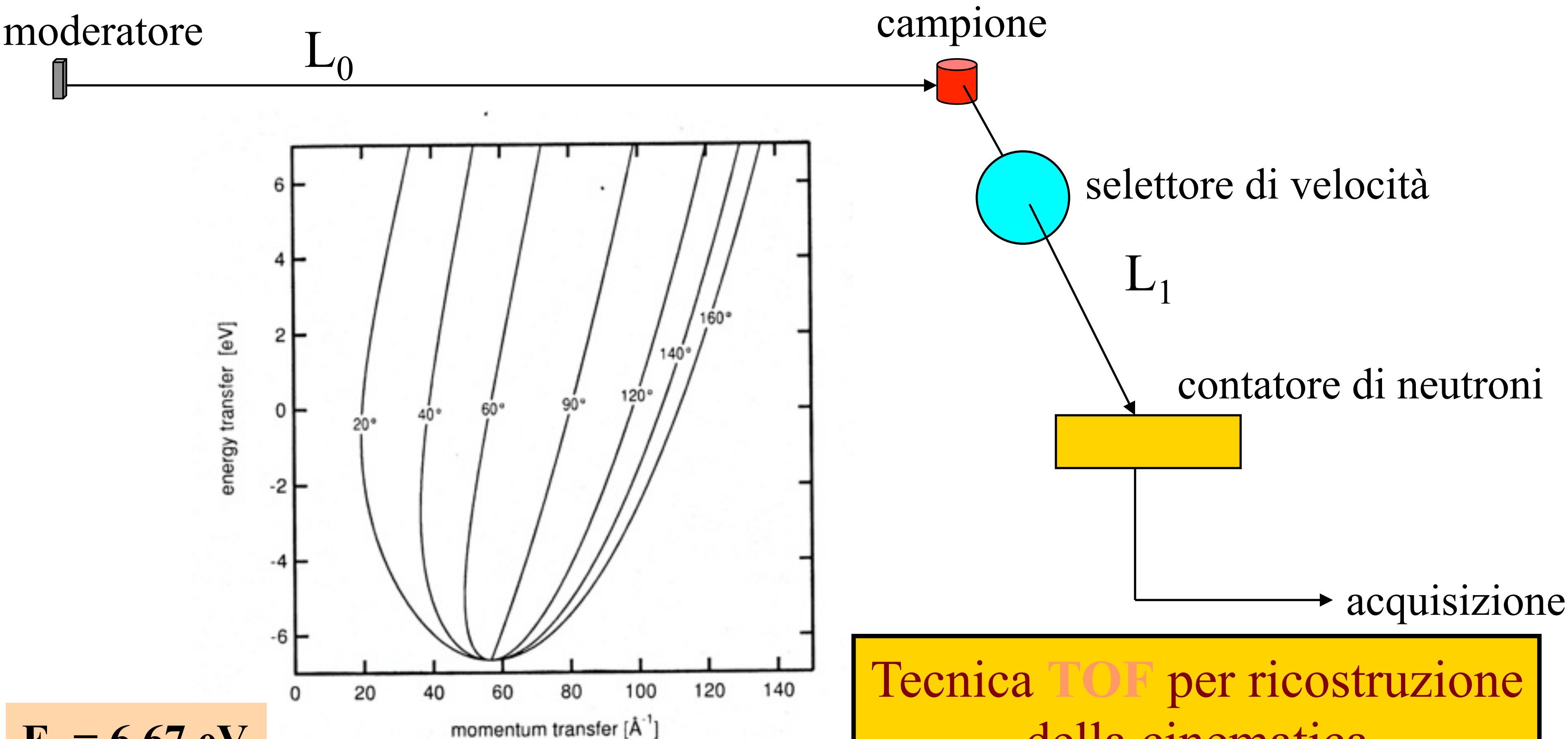

$E_1 = 6.67$ eV

Tecnica TOF per ricostruzione della cinematica

Spettrometri a geometria inversa

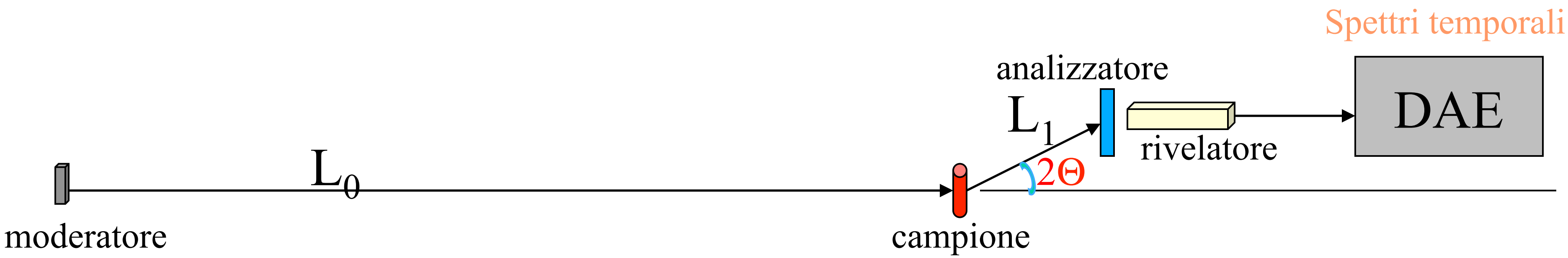

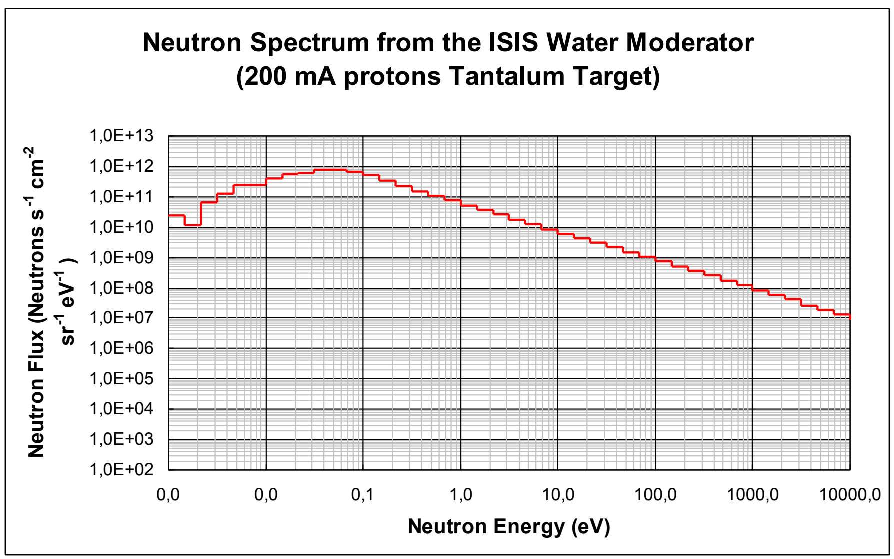

The Resonance Filter Spectrometer configuration

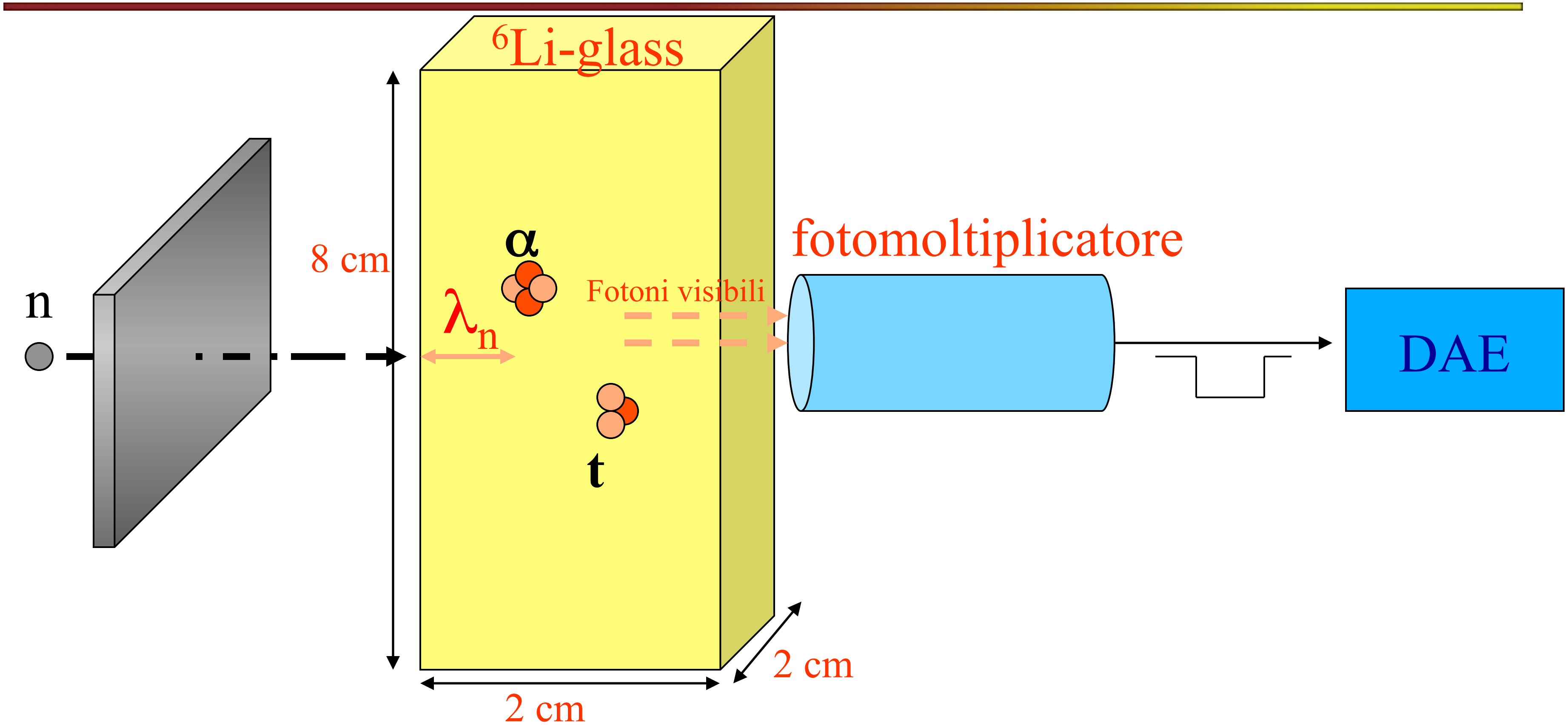

The Resonance Detector Spectrometer configuration

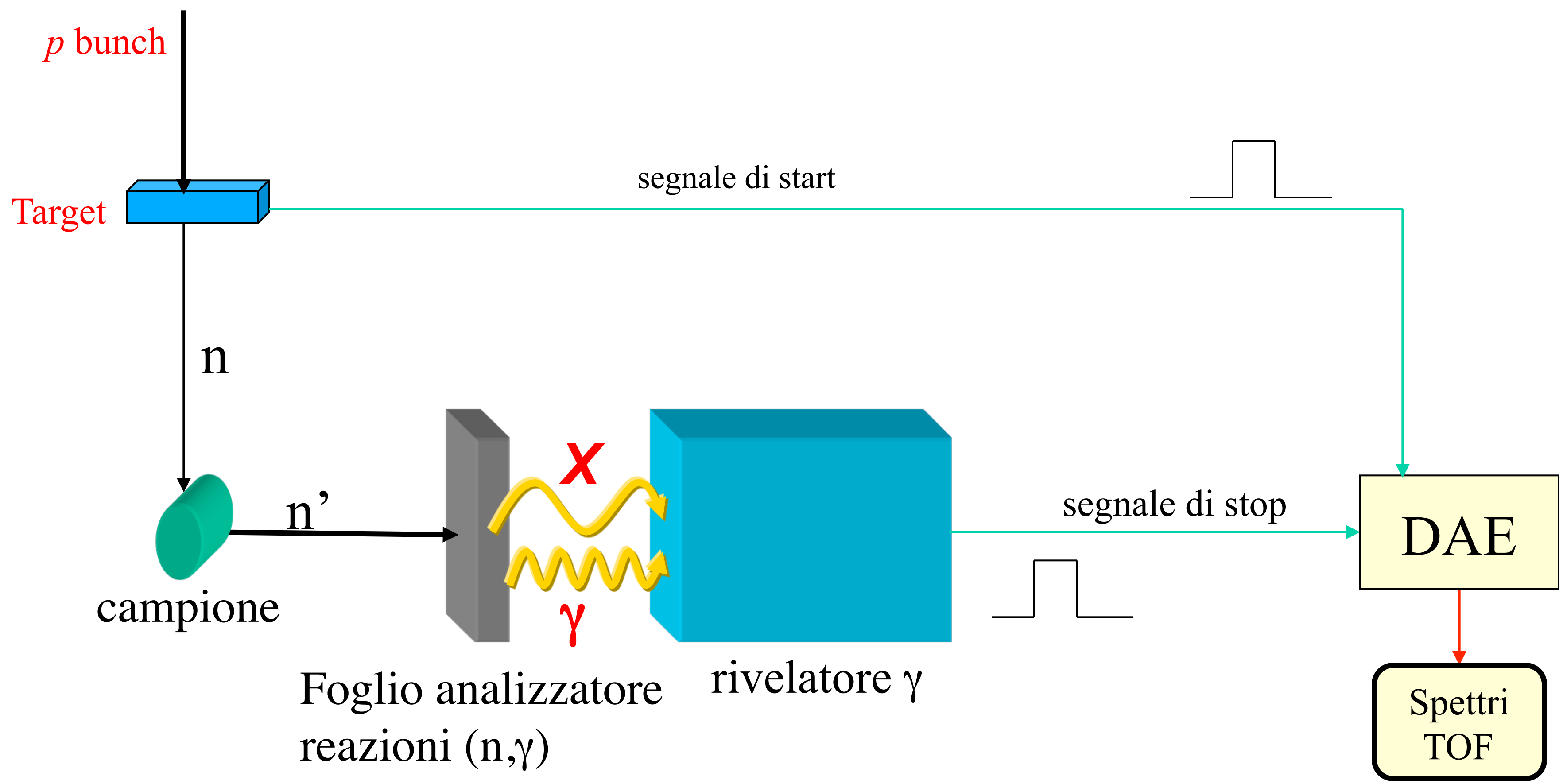

Suitable isotopes for eV neutron energy selection

	% isot.	Z	A	densita'	N	Eris	$\sigma 0$	σ eff a 295K	λ n	d*5*5*λ n	σ eff a 75K
				g/cm^3	atom/cm^3	eV	barn	barn	μm	g	barn
In	4,3	49	113	7,3	3,9E+22	14,6	9965	3837	66,9	1,223	5791
La	99,9	57	139	6,1	2,7E+22	72,2	5969	1762	213,2	3,275	2769
Sm	7,4	62	150	7,4	3,0E+22	20,7	56207	29108	11,6	0,214	39486
Gd	20,6	64	156	7,9	3,0E+22	33,2	11078	4854	67,5	1,334	6811
Dy	2,3	66	160	8,5	3,2E+22	10,5	19229	12179	25,5	0,545	15214
	2,3	66	160	8,5	3,2E+22	20,5	16165	9188	33,9	0,723	11923
Er	27,1	68	168	8,5	3,1E+22	79,7	11203	4096	79,8	1,703	5993
	14,9	68	170	8,5	3,0E+22	95,0	26393	23711	13,9	0,298	25396
Hf	0,2	72	174	13,3	4,6E+22	70,0					
	5,2	72	176	13,3	4,5E+22	48,0	36842	21132	10,4	0,346	26852
	5,2	72	176	13,3	4,5E+22	68,0					
	27,1	72	178	13,3	4,5E+22	7,8	153848	107369	2,1	0,069	127948
	35,2	72	180	13,3	4,4E+22	72,6	16838	6136	36,7	1,218	8657
W	26,3	74	182	19,3	6,4E+22	4,2	18828	10209	15,3	0,740	12354
	26,3	74	182	19,3	6,4E+22	21,1	46877	24395	6,4	0,310	29749
	26,3	74	182	19,3	6,4E+22	115,0					
Os	1,6	76	187	22,6	7,3E+22	12,7	16672	9563	14,4	0,812	11063
	26,4	76	190	22,6	7,2E+22	91,6	6777	2121	65,9	3,719	2625
U	100,0	92	238	18,9	4,8E+22	6,7	23564	7570	27,6	1,305	11250
U	100,0	92	238	18,9	4,8E+22	20,9	37966	9864	21,2	1,002	15119
U	100,0	92	238	18,9	4,8E+22	36,7	42228	13363	15,6	0,739	19913
U	100,0	92	238	18,9	4,8E+22	66,0	20134	4357	48,0	2,268	6813

Energy and relative intensities of γ-rays

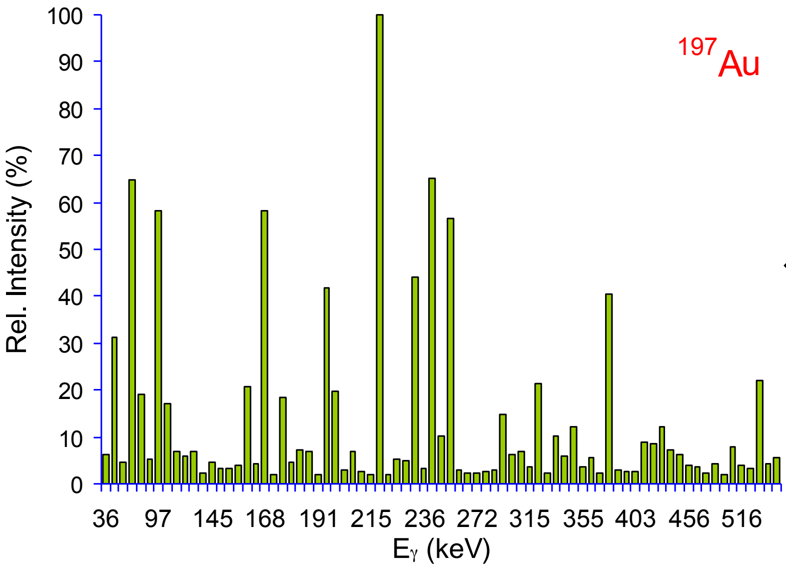

Intensità relative (I_r>2%) per l'emissione γ a seguito di cattura radiativa di neutroni termici in ^{197}Au.

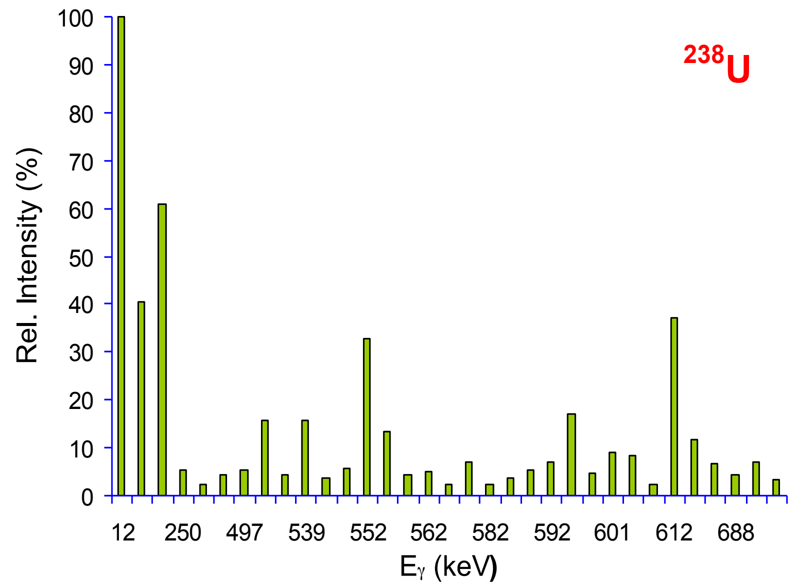

Intensità relative (I_r>2%) per l'emissione γ a seguito di cattura radiativa di neutroni termici in ^{238}U.

The VESUVIO spectrometer at ISIS

Molecular Physics

Foil cycling Technique

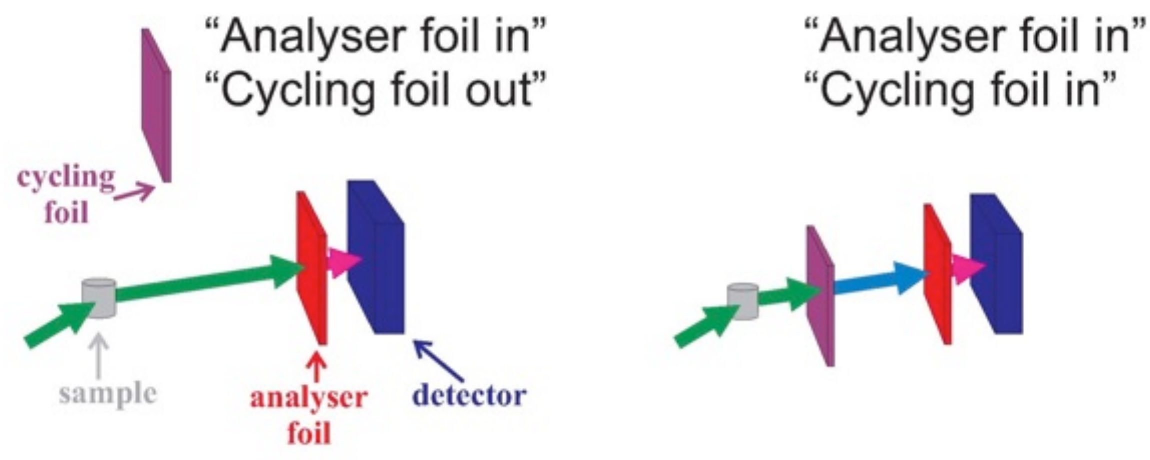

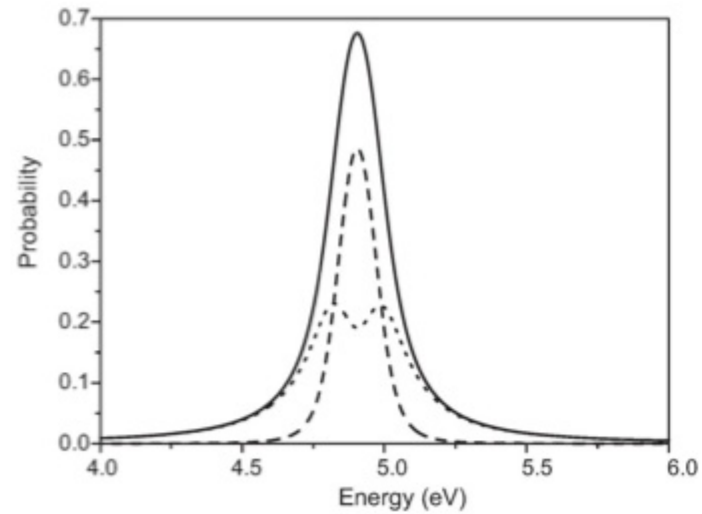

Deep Inelastic Neutron Scattering

or

Neutron Compton Scattering

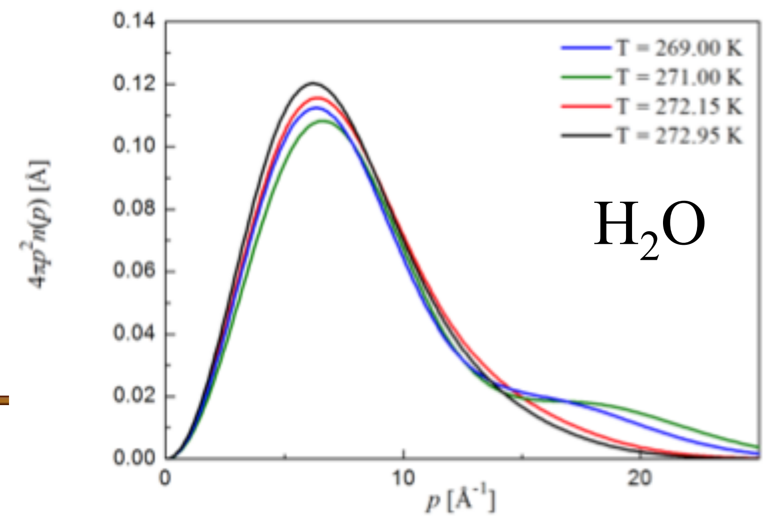

Attosecond time scale
Sub Angstrom lenght scale

Neutron Resonance Capture Analysis

Material analysis

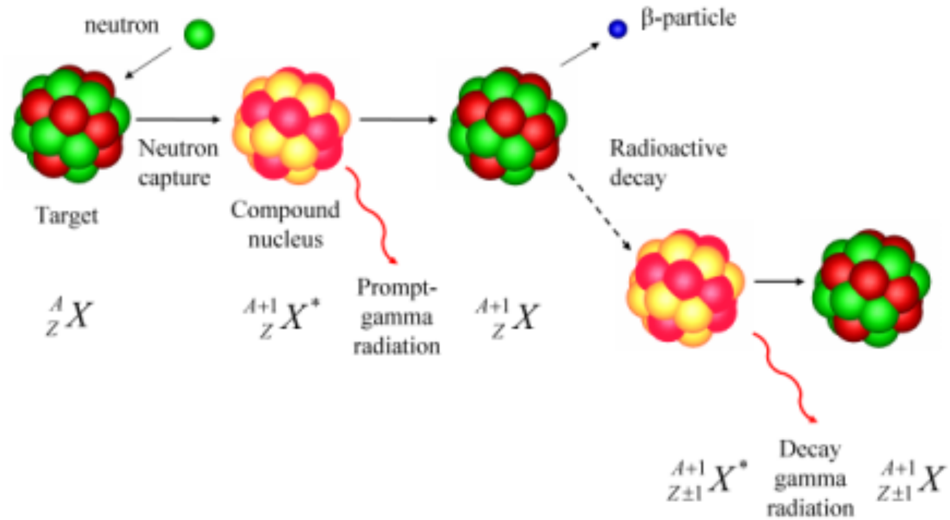

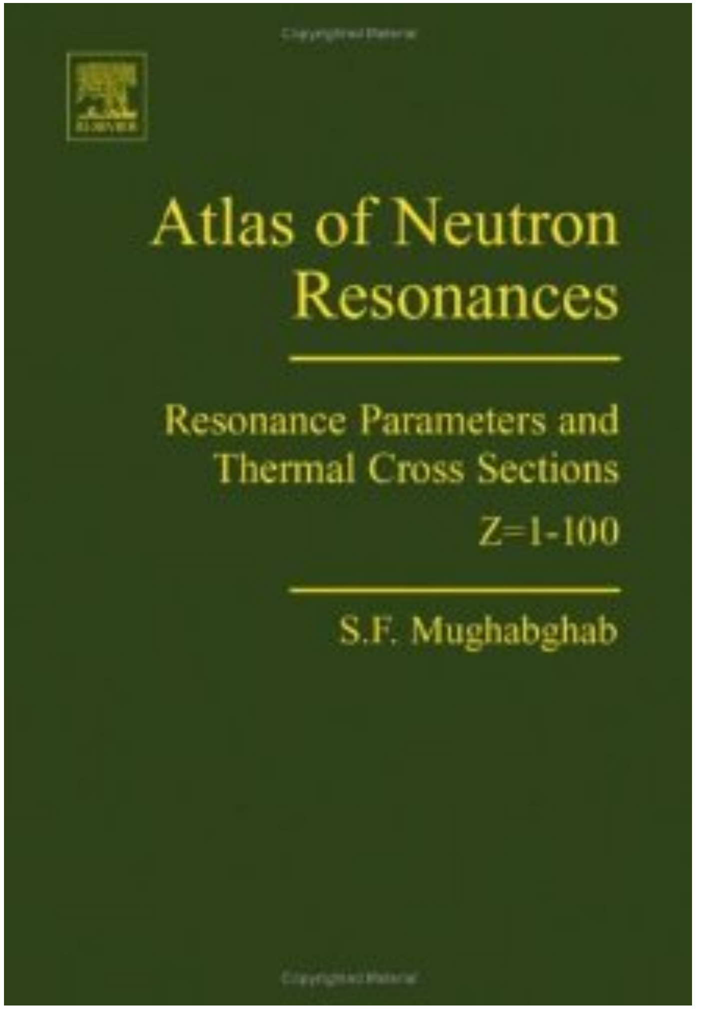

An experiment layout

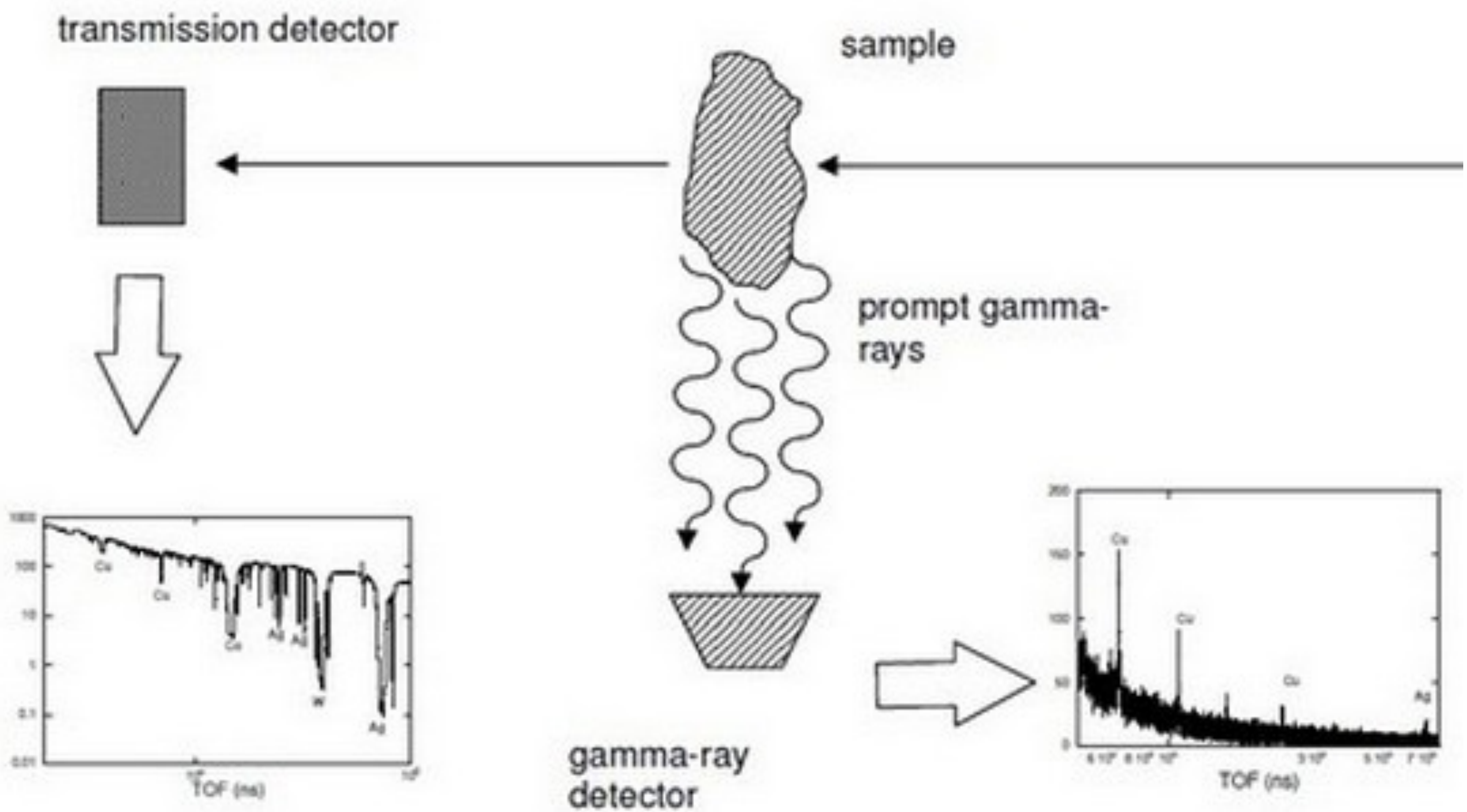

Suitable elements for NRCA

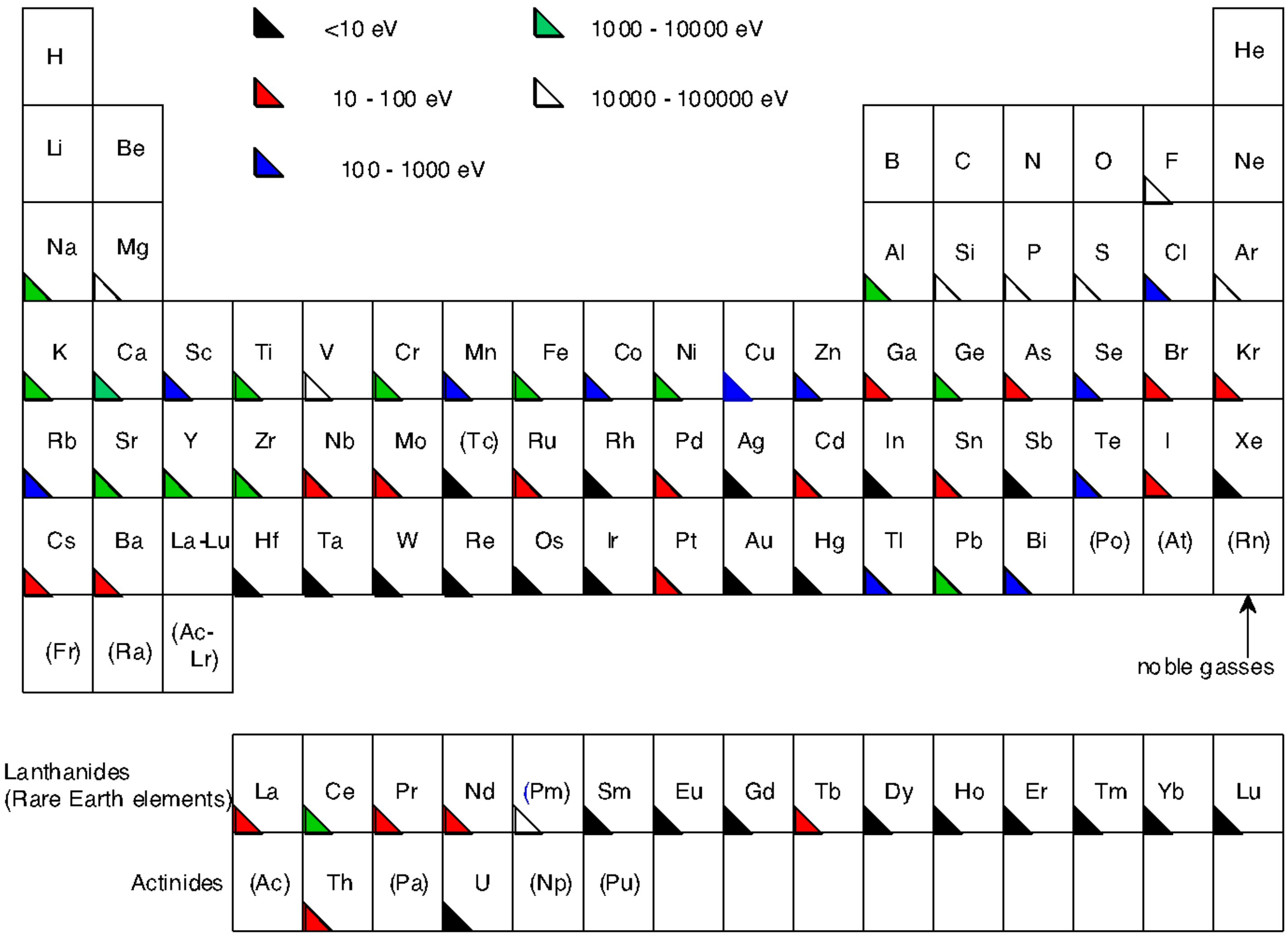

Delft University of Technology

Experimental NRCA tests at ISIS

t_{exp} [μs]	t_{calc} [μs]	E_r [eV]	^{A}X
742.6±0.3	743.1	4.91	^{197}Au
662.5 ± 0.3	663.9	6.16	^{121}Sb
419.7± 0.3	420.1	15.37	^{121}Sb
355.1± 0.3	354.8	21.59	^{123}Sb
108.4± 0.3	108.9	228.65	^{65}Cu
68.4± 0.3	68.2	583.30	^{63}Cu
64.3± 0.3	65.1	640.66	^{63}Cu

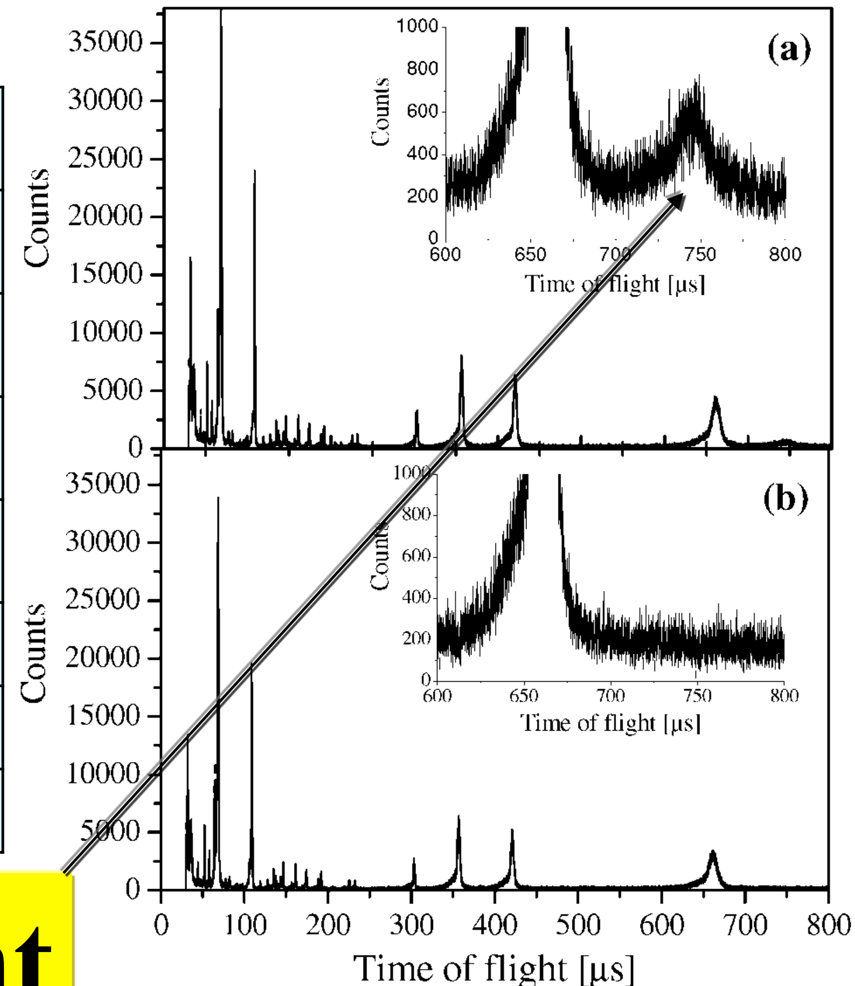

Au 40 ppm in weight

Layout

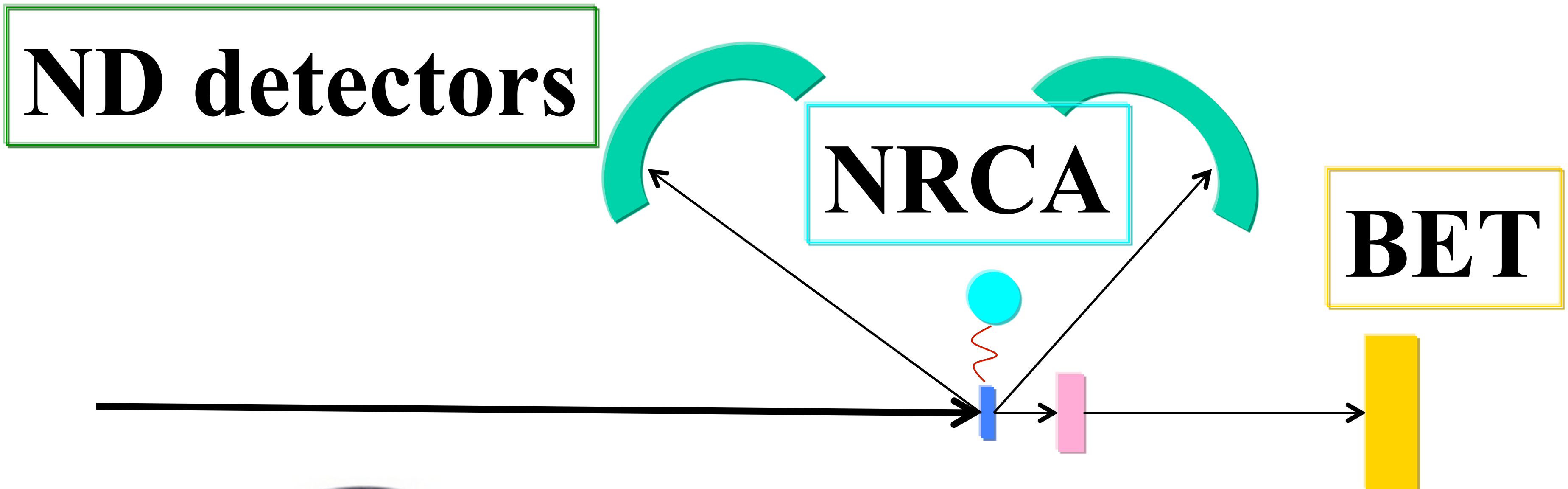

Tests on INES @ ISIS

Some results on INES

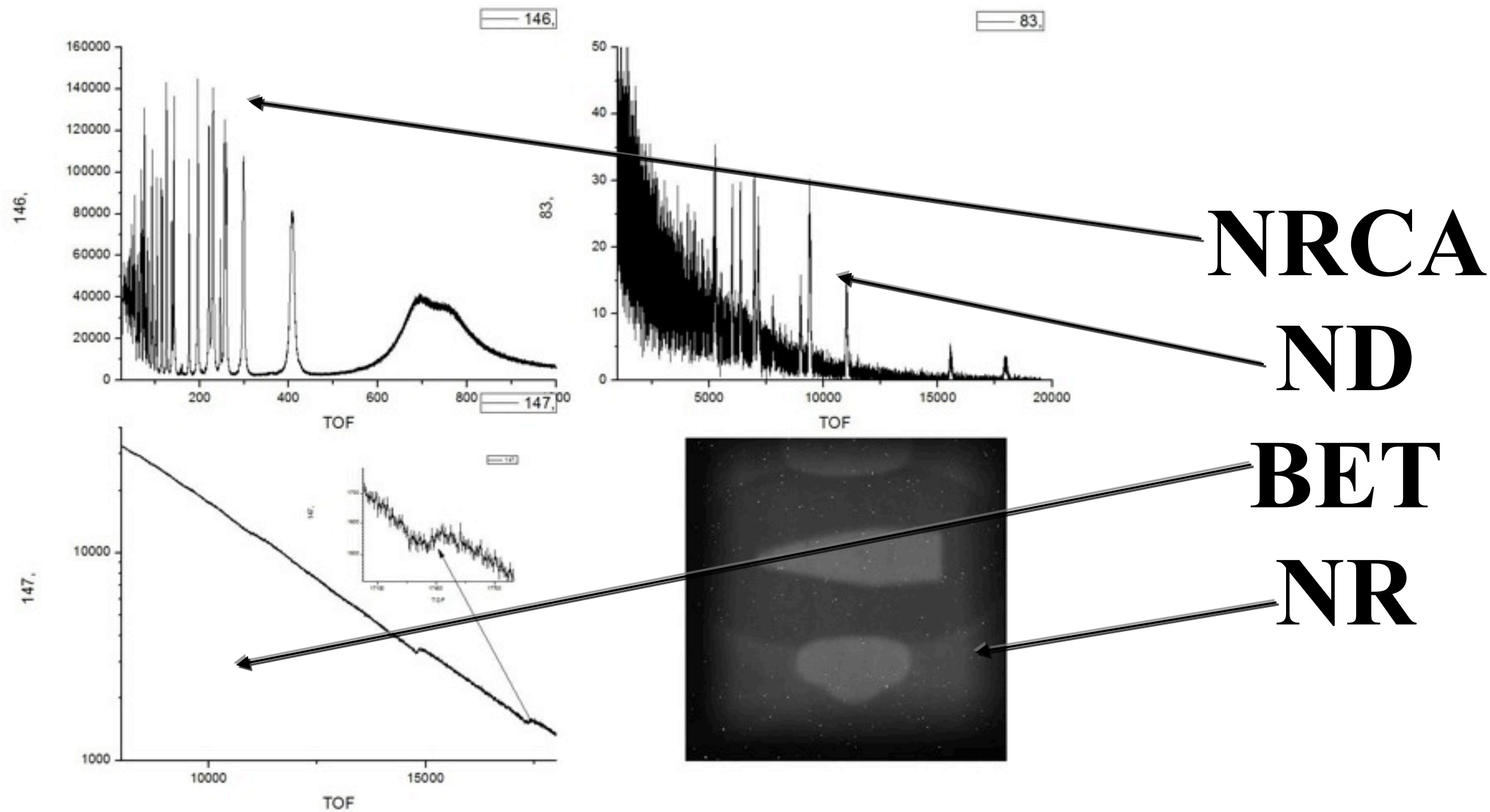

Fast neutrons

Aviation

motive

IT
Infrastructure

Medical

What has to be measured ?

- SEE cross sections

$$\sigma = \frac{\#SEE}{\varphi}$$

#SEE*:* number of errors of different type observed under different conditions:

Single Bit Upsets
Multiple Bit Upsets,
Single Event Latchup,
Single Event Transient

φ: neutron fluence (above 1 MeV)

<u>beam line requirements</u>:

- "atmospheric" neutron spectrum
- High acceleration factor: 10^6-10^8
- Beam uniformity (intensity and spectrum)
- Possibility to measure locally the fluence close to the irradiated chip

Neutron production in the atmosphere

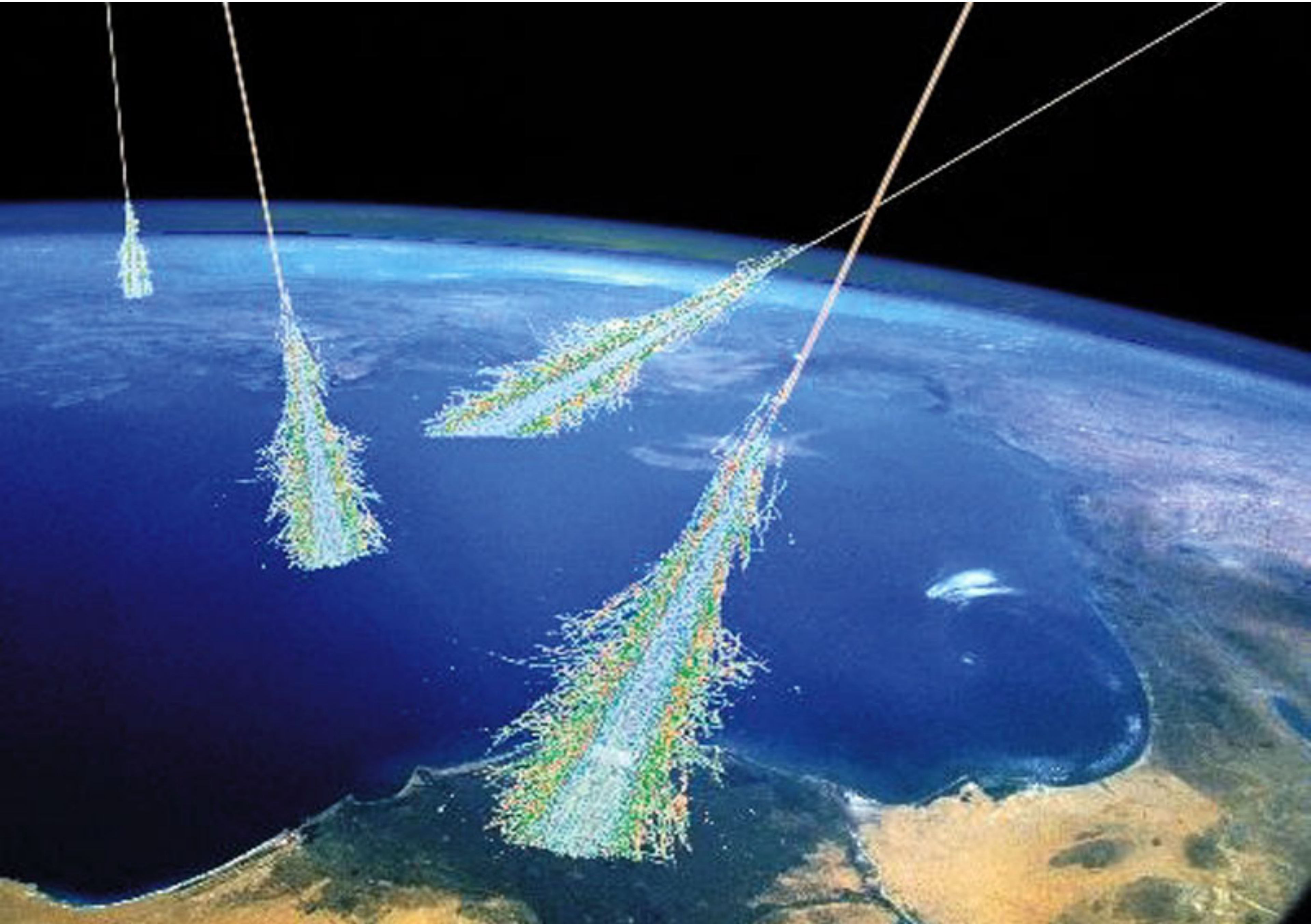

Neutron Radiation from primary cosmic rays

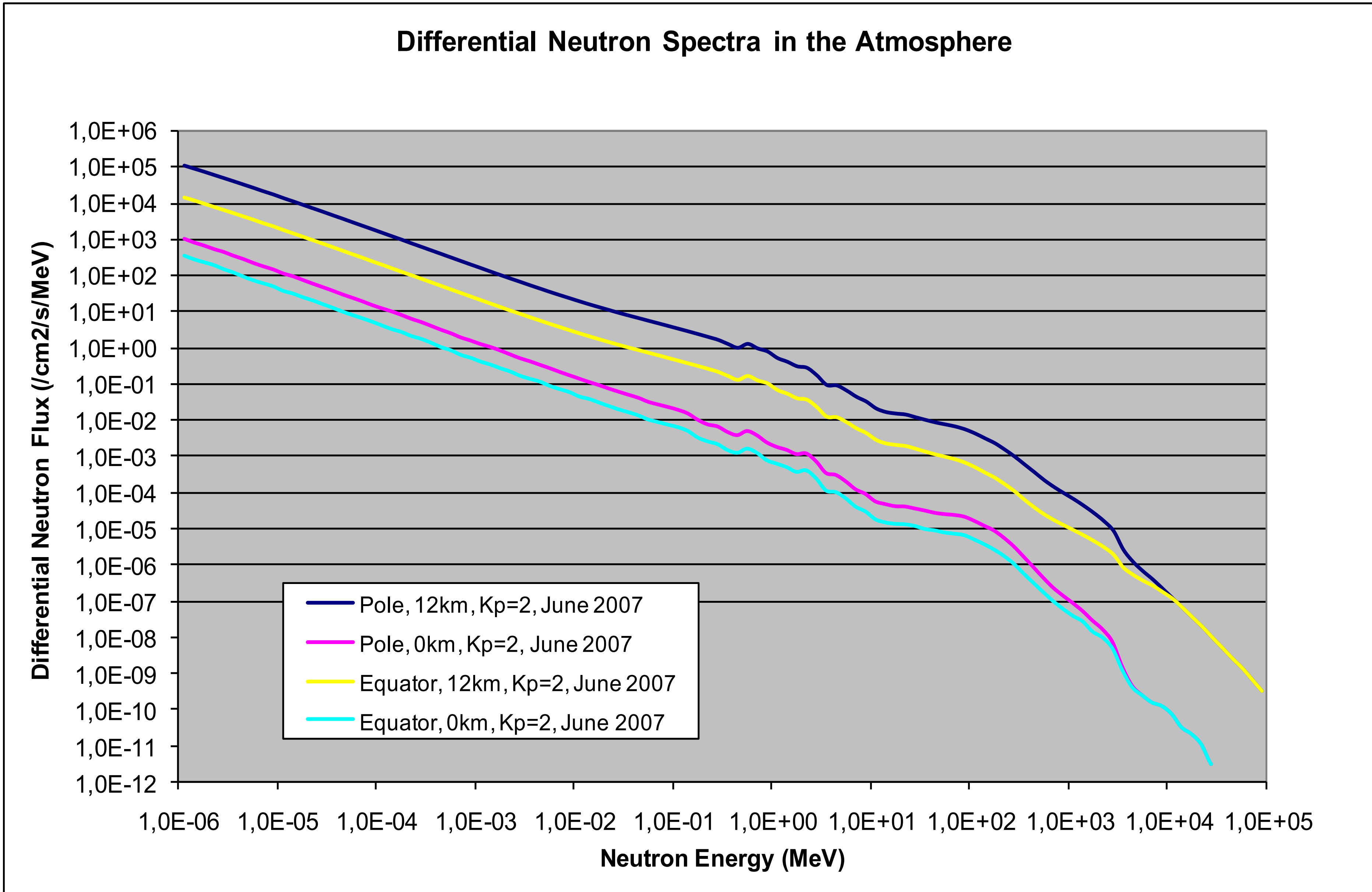

Worldwide irradiation facilities

- **The Bonner Spheres**

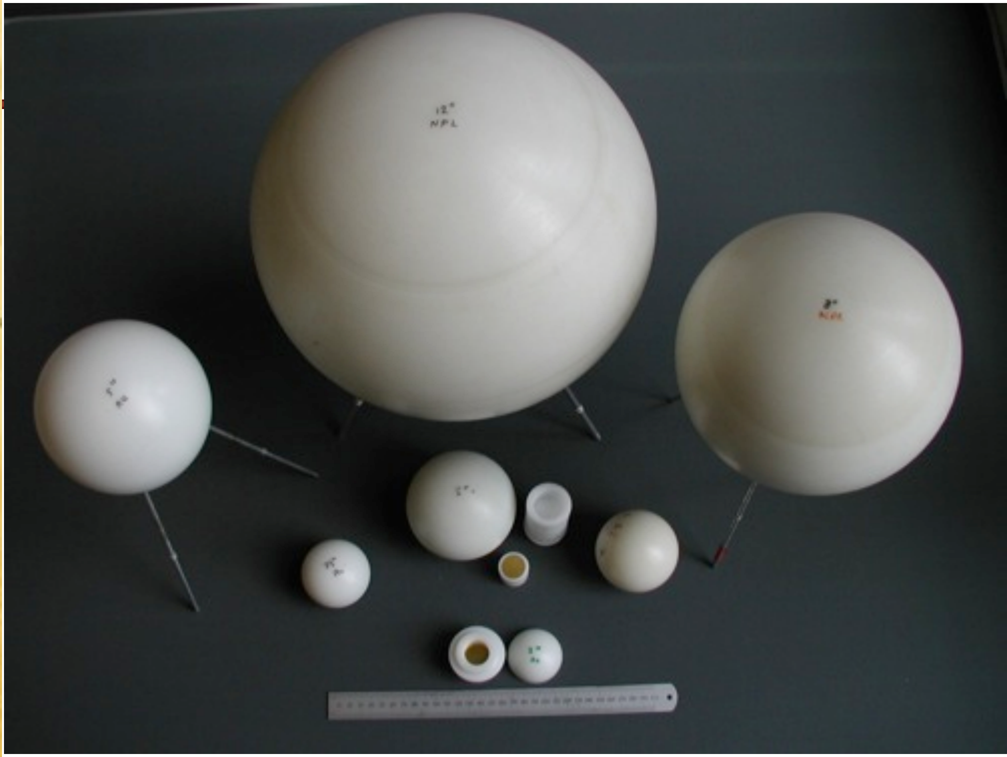

Geometry - Energy

Principle of operation

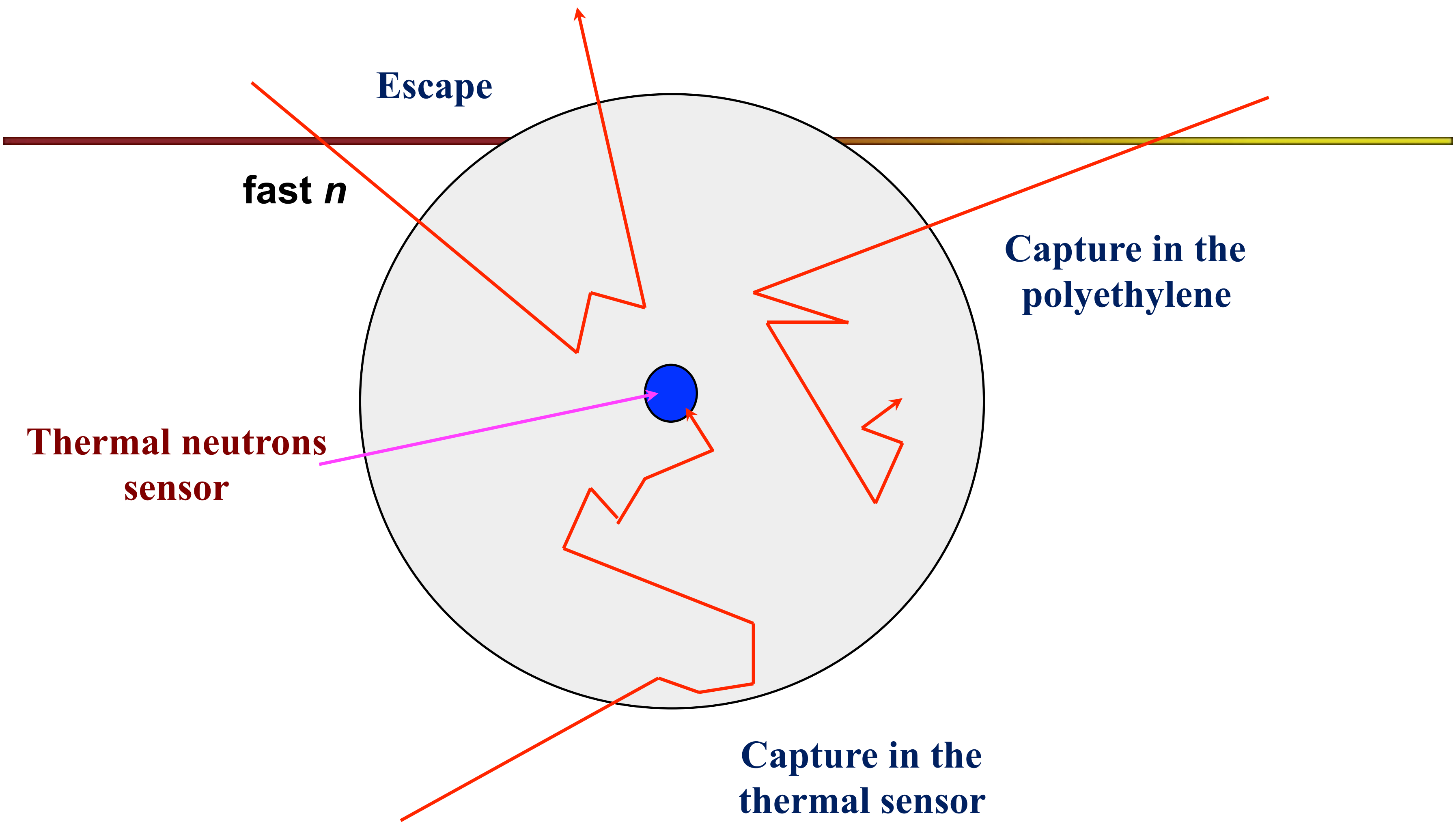

From the measured activity on the sensor after a period of irradiation the neutron flux at the selected energy range is found

Modified Bonner Spheres by including metal inserts to allow for *n(x,n)* reactions to occur

Response Functions of Bonner Spheres

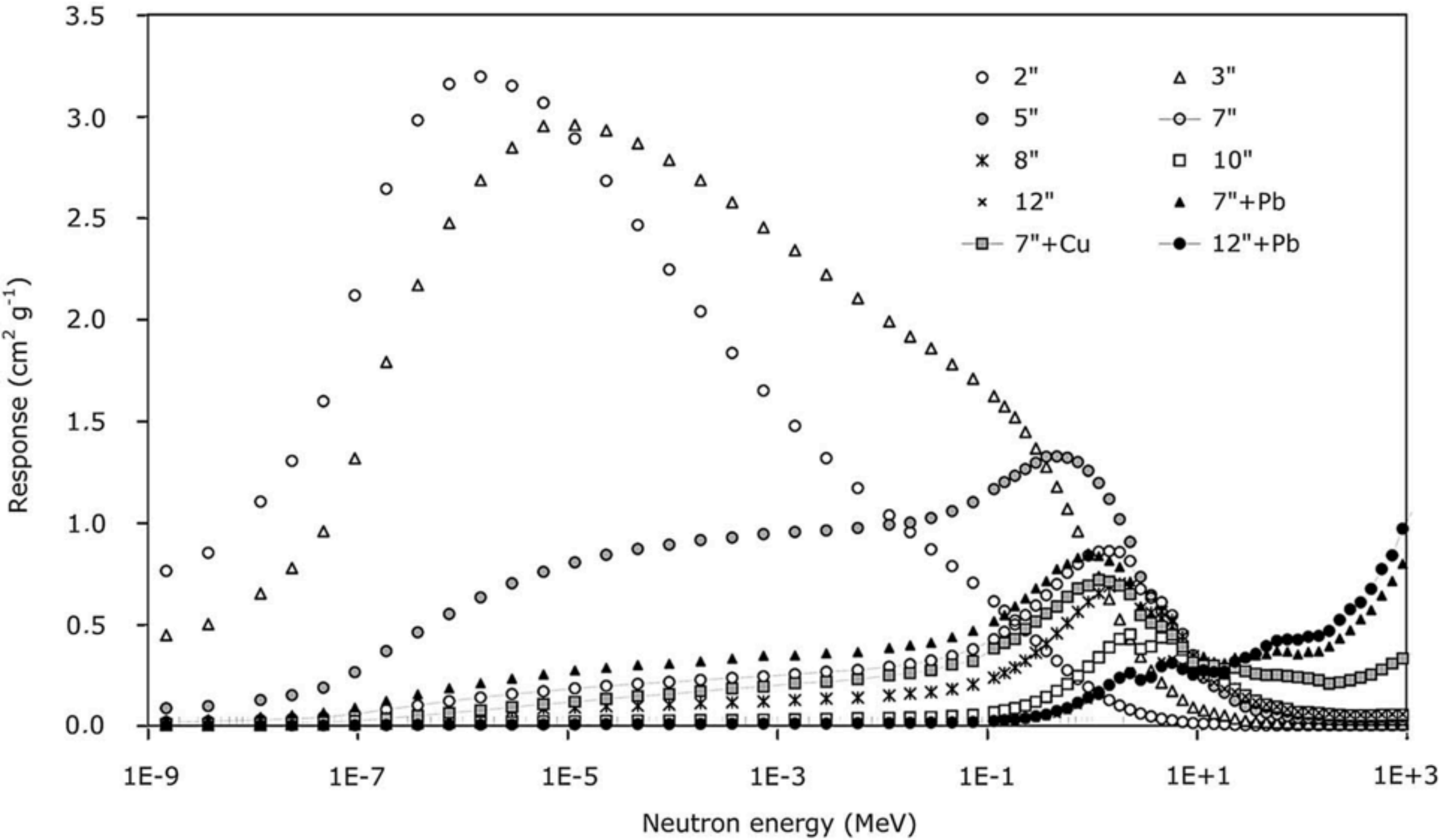

Measurements on VESUVIO beam ine @ ISIS-TS1

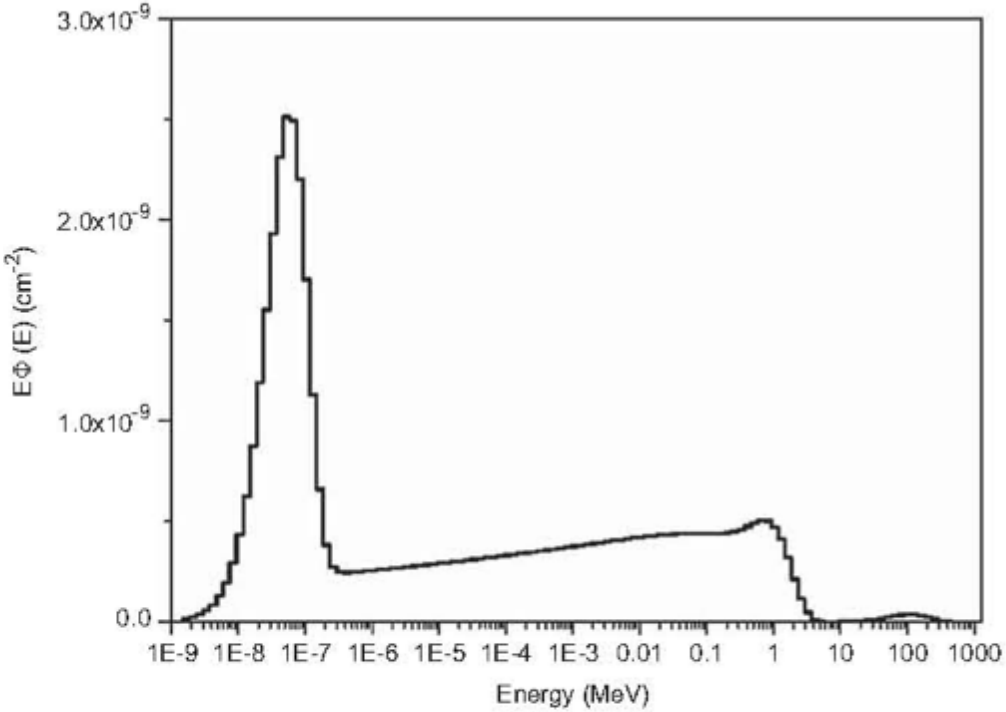

The spectrum, in equi-lethargy representation, normalized to one incident proton

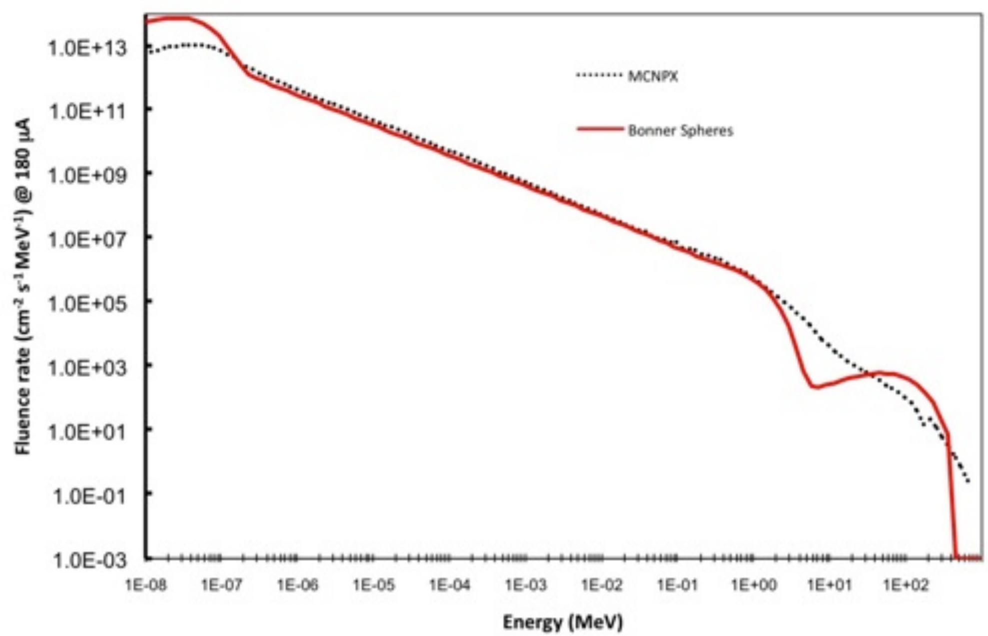

Energy distribution of the neutron fluence rate normalized @ 180 mA proton current

MCNPX simulations by S. Ansell

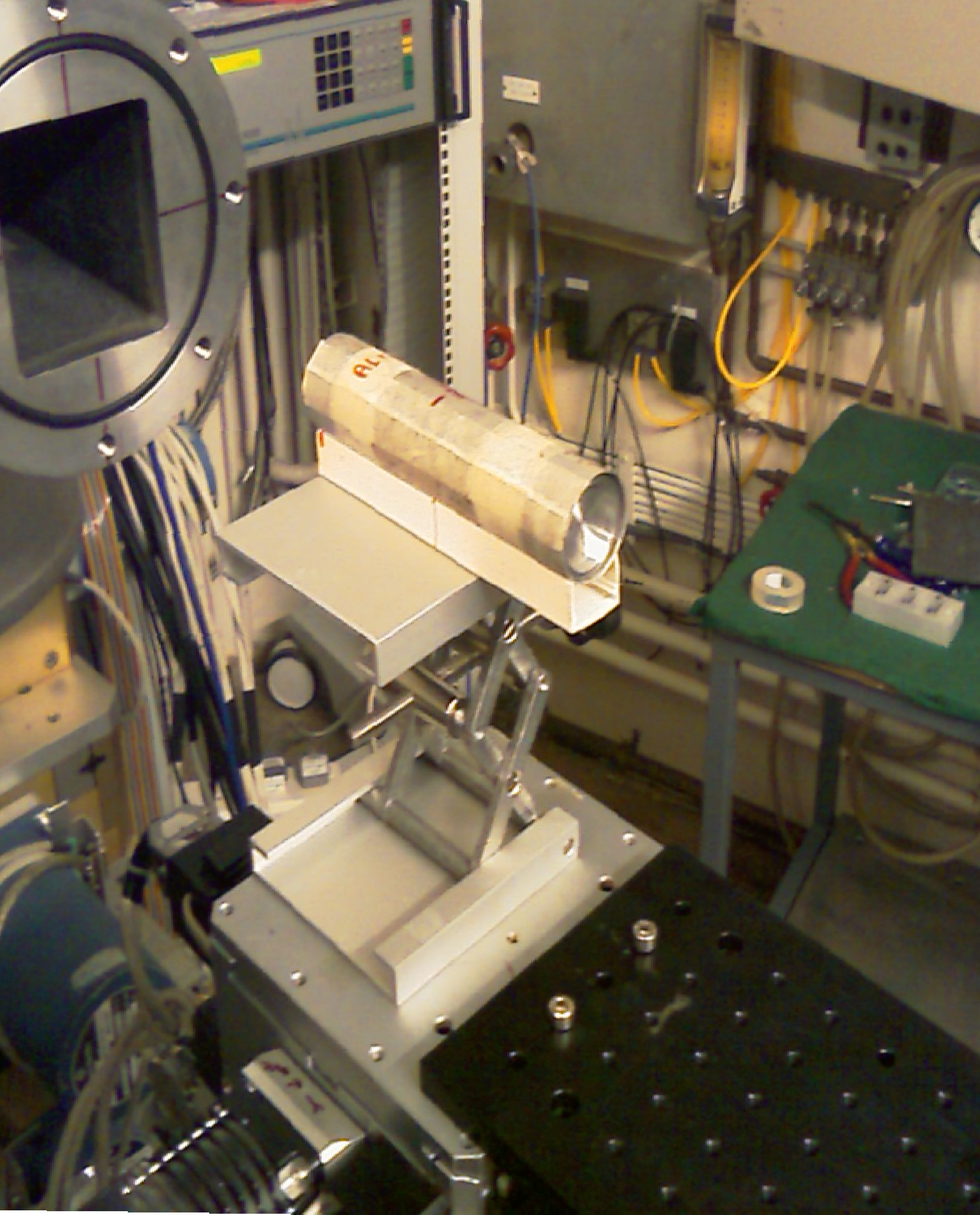

A different geometry

"**Bonner Cylinders**"

More suitable for collimated beams

Measurements on Rotax in December 2009

Simulation of the response functions and data analysis ongoing

- **Thin Film Breakdown Counters TFBC**

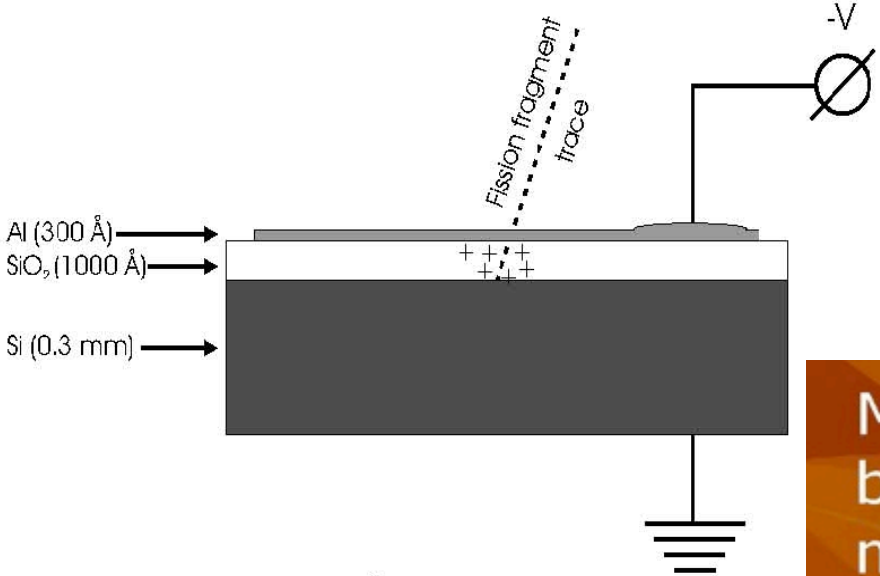

A. Smirnov and A. Prokofiev

Schematic of a TFBC and the principle of its operation: an incident fission fragment produces an electrical breakdown in the SiO_2 layer.

Real time counter suitable for Time of Flight measurements

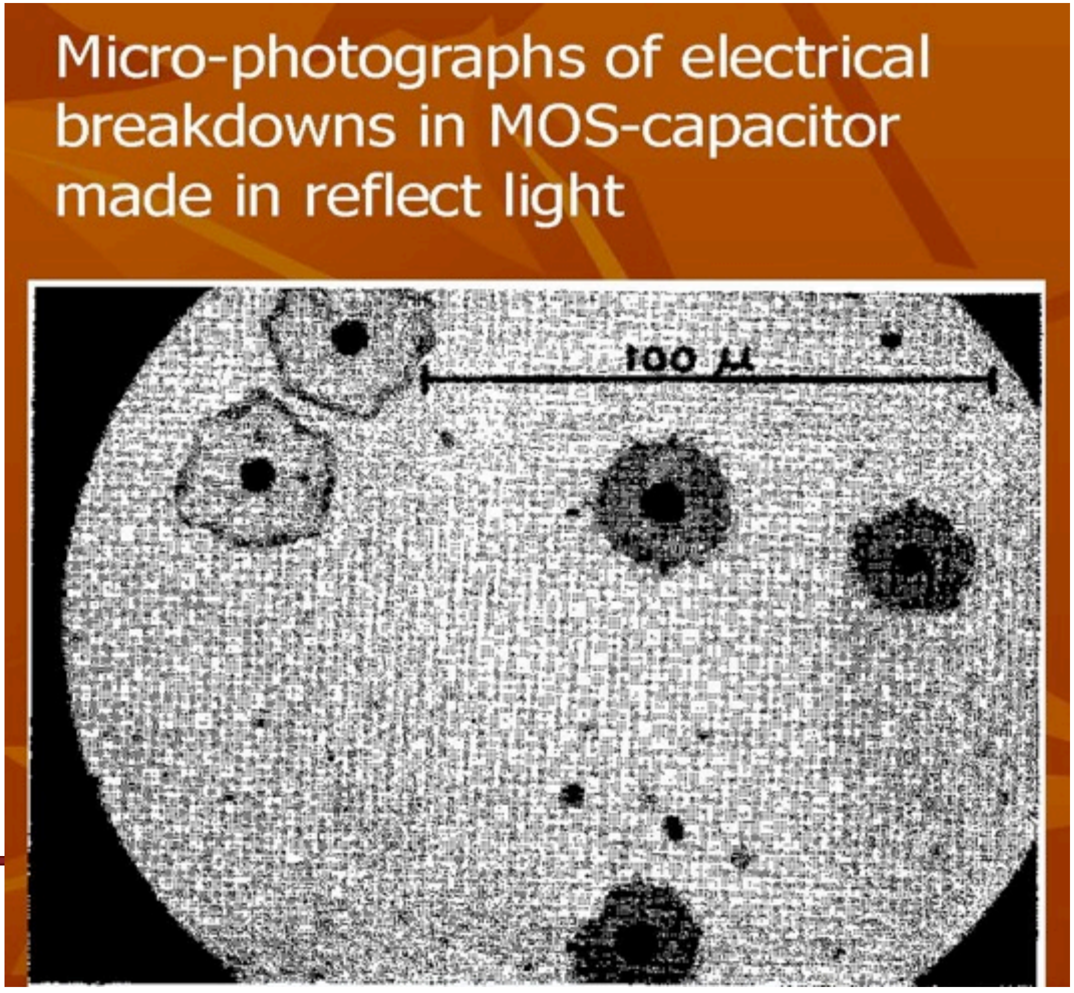

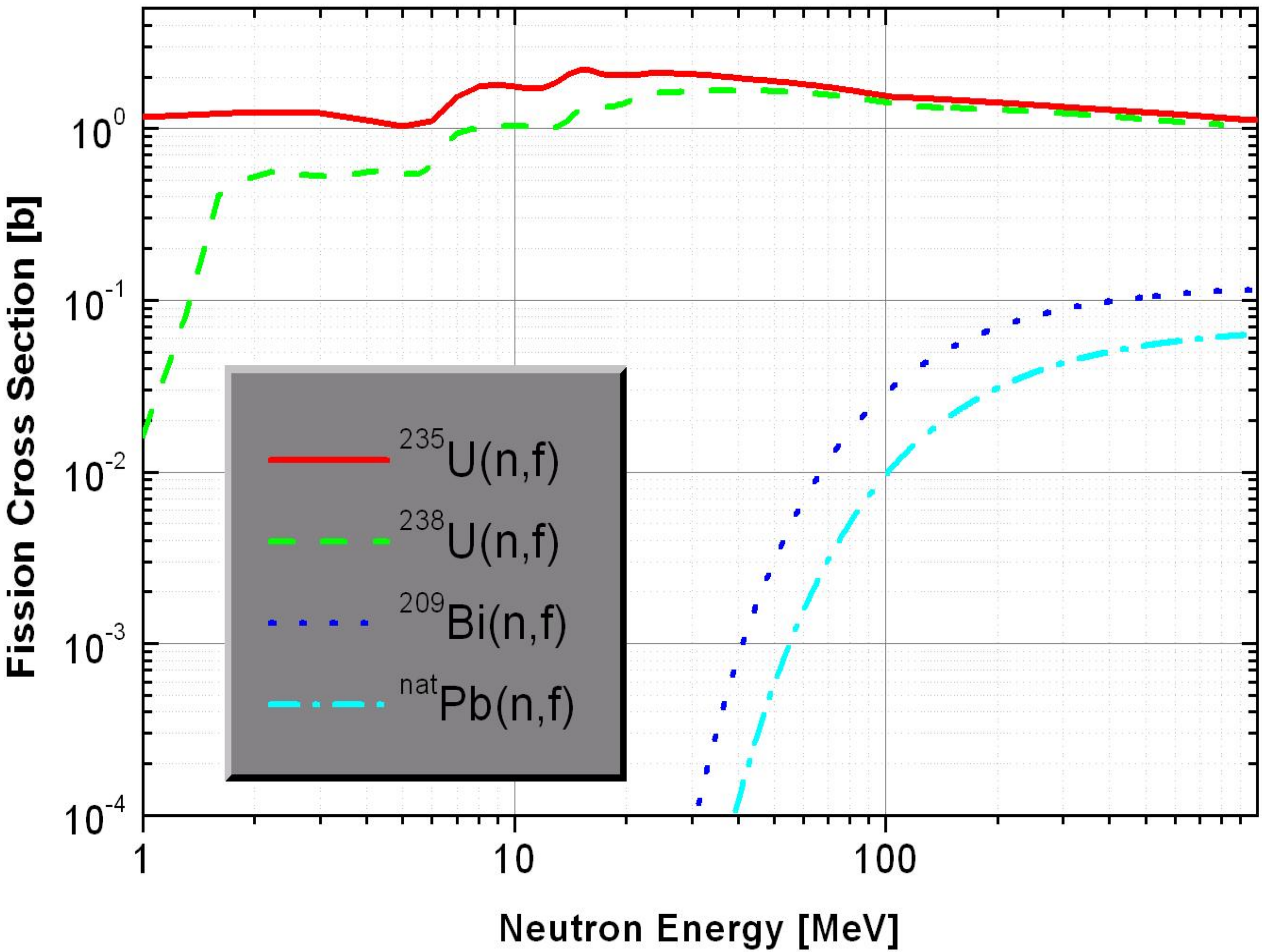

Fission Cross Section [b]
10^{0}
10^{-1}
10^{-2}
10^{-3}
10^{-4}
1
10
100
Neutron Energy [MeV]
$^{235}U(n,f)$
$^{238}U(n,f)$
$^{209}Bi(n,f)$
$^{nat}Pb(n,f)$

Picture of a TFBC array used for tests on VESUVIO beam line at ISIS-TS1

A. Smirnov and A. Prokofiev

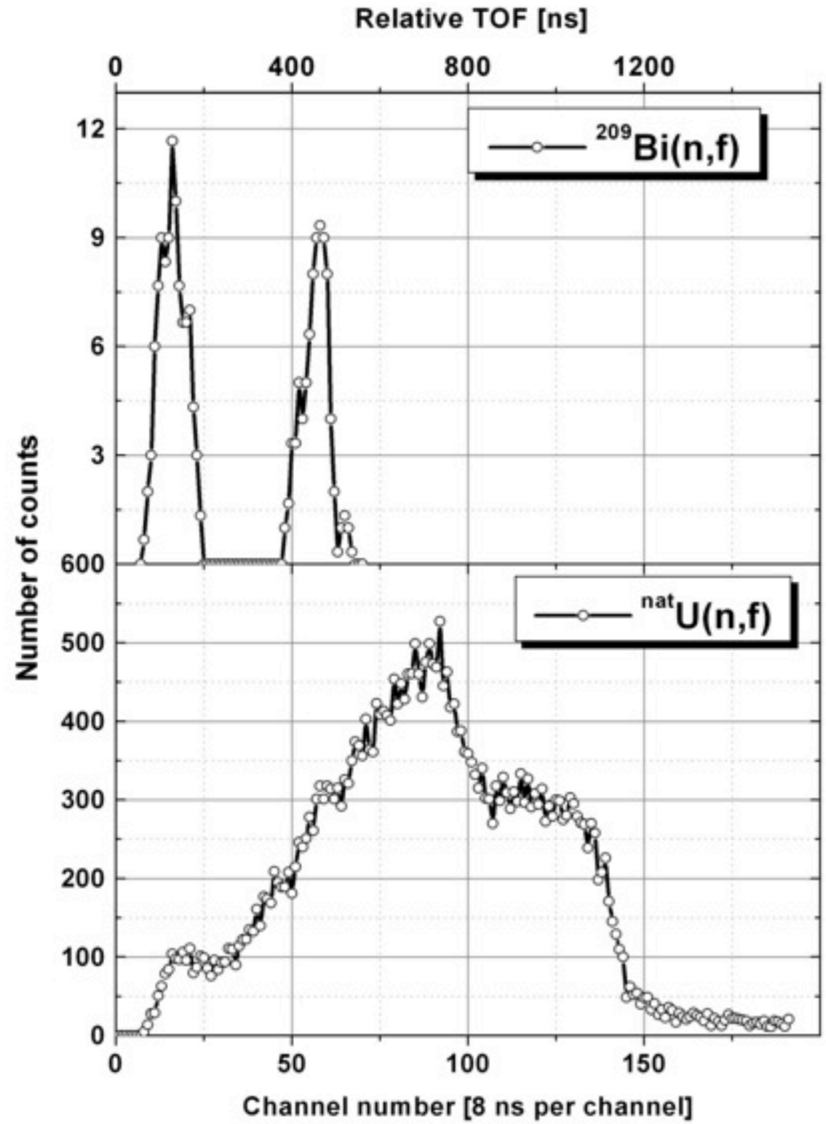

Neutron ToF spectra

Results are going to be presented at the RADECS conference

- **Localized flux monitoring:**

Single Crystal Diamonds

SCD by Chemical Vapor Deposition

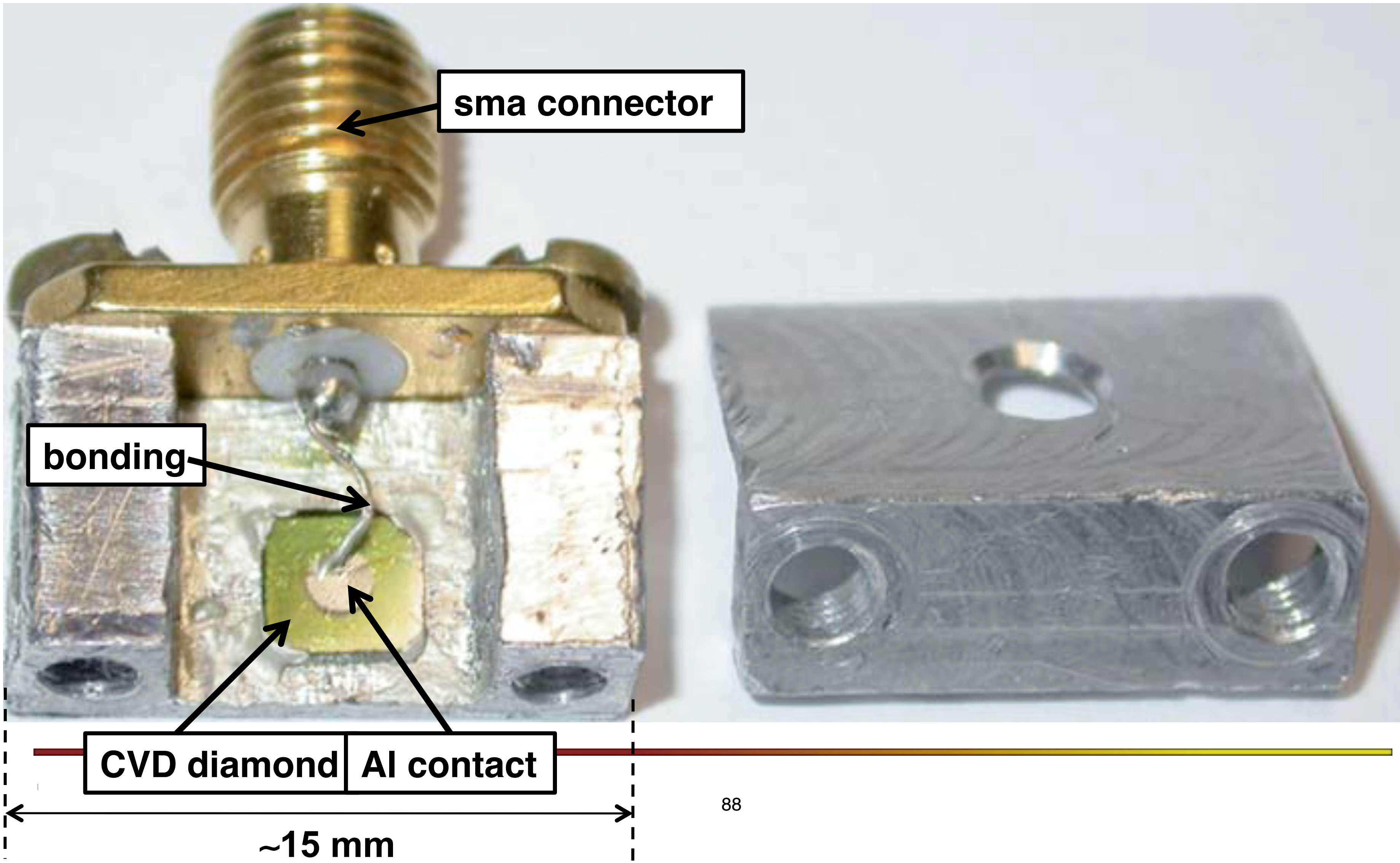

n-^{12}C neutron cross sections

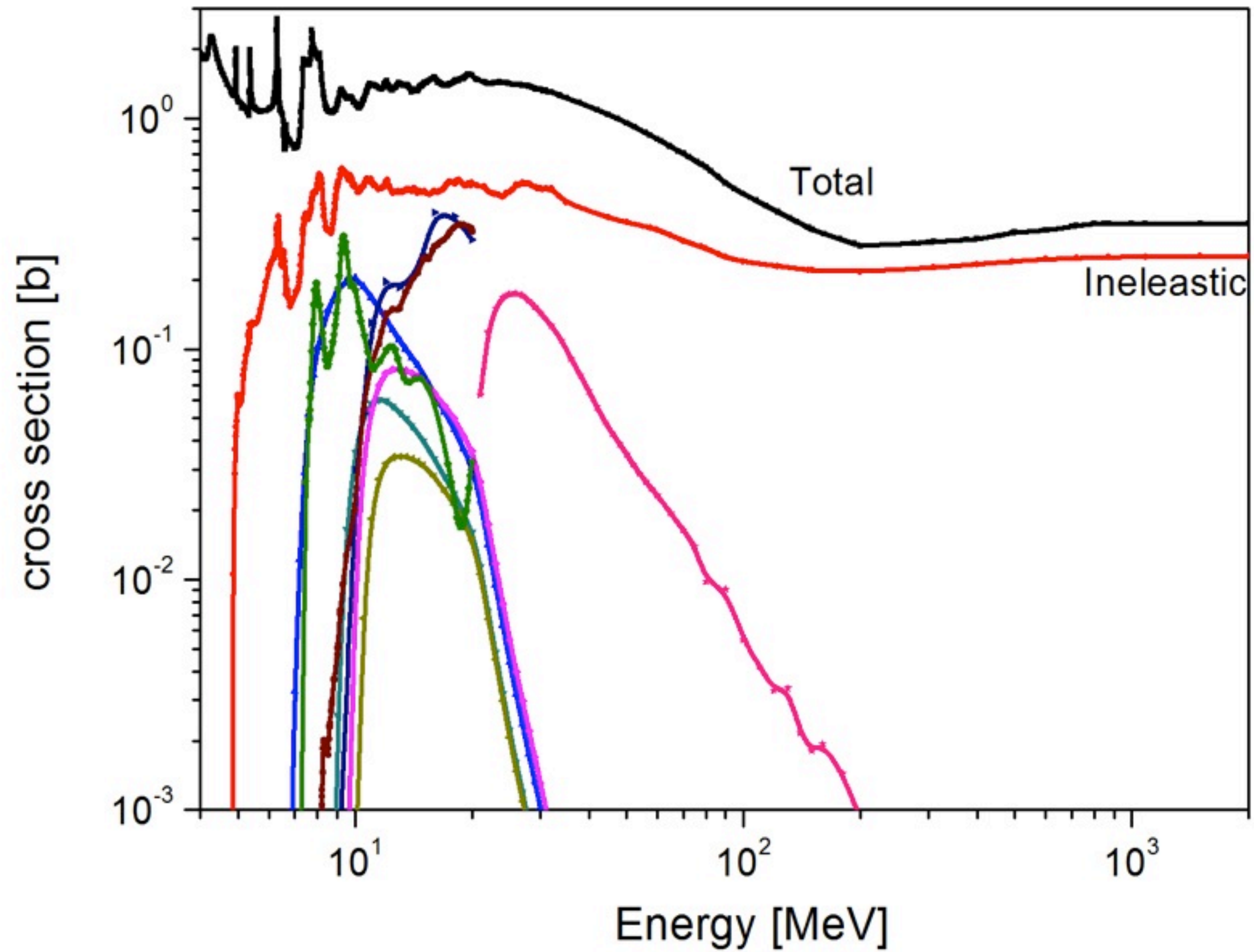

- **Test results: TOF spectra on ROTAX beam line at ISIS-TS1**

SET UP

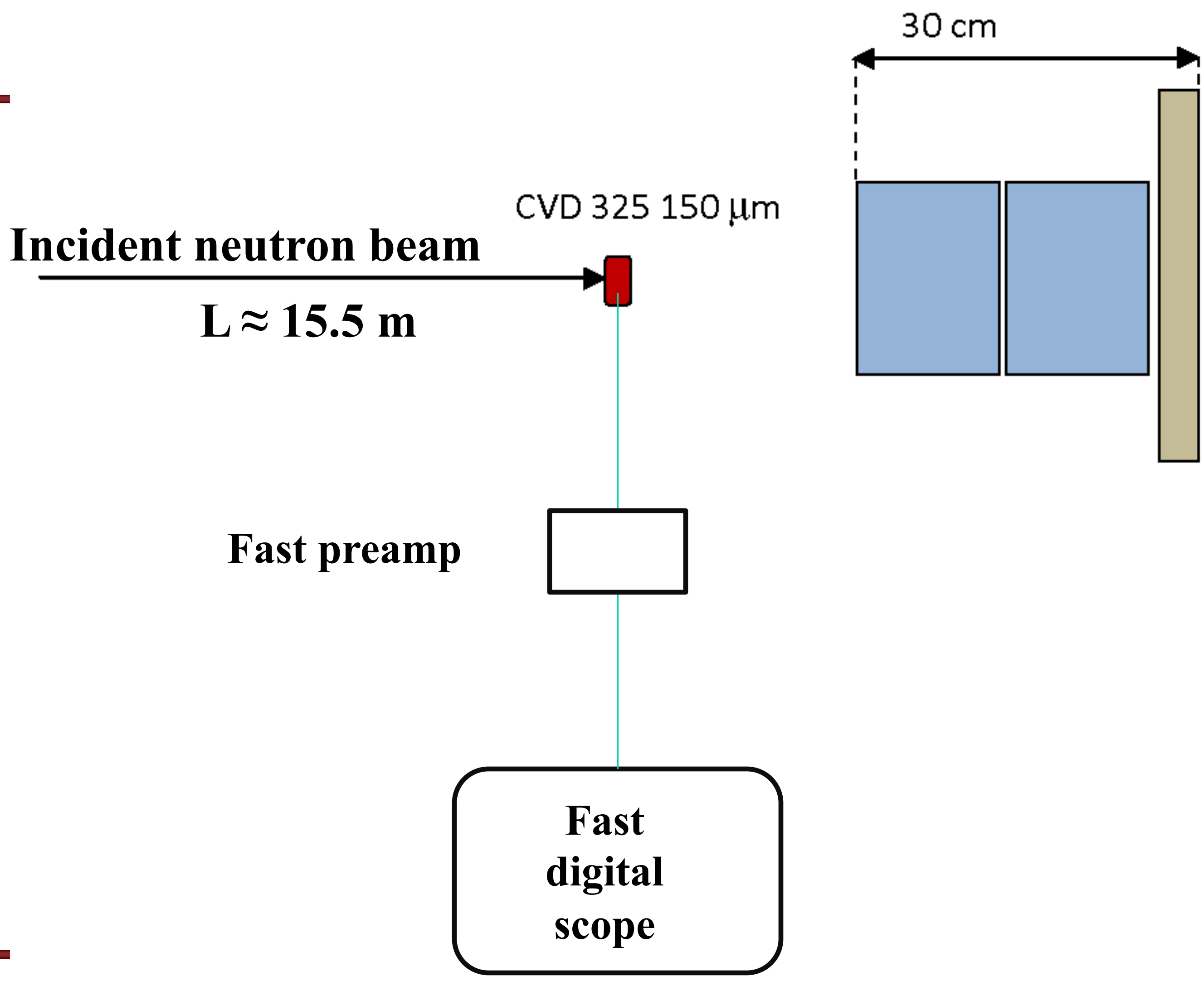

30 cm
CVD 325 150 µm
Incident neutron beam
L ≈ 15.5 m
Fast preamp
Fast
digital
scope

SET UP

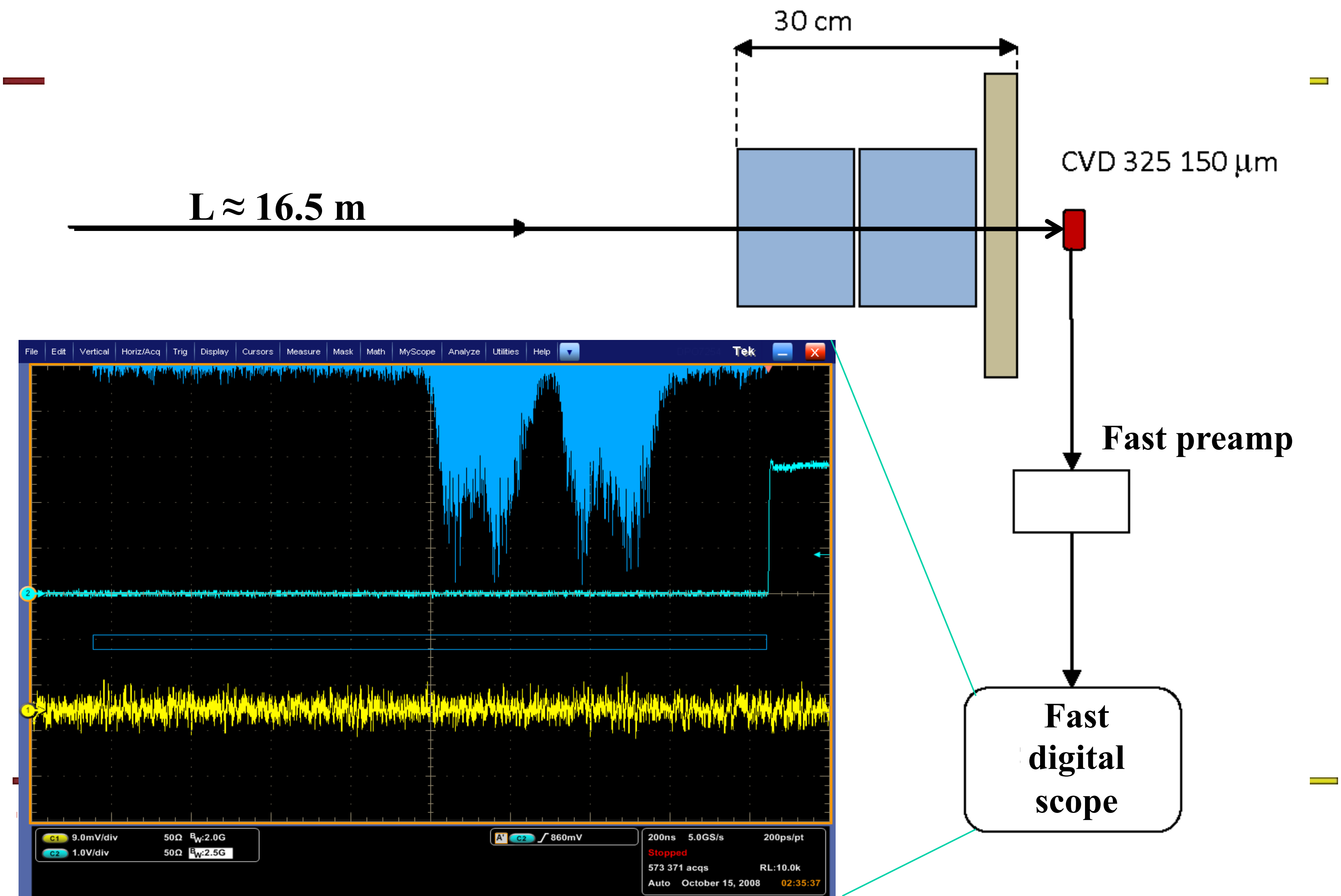
30 cm
L ≈ 16.5 m
CVD 325 150 µm
Fast preamp
Fast digital scope
200ns 5.0GS/s 200ps/pt
Stopped
573 371 acqs RL:10.0k
Auto October 15, 2008 02:35:37

TOF SPECTRUM FROM DIAMOND
1- ROTAX beam

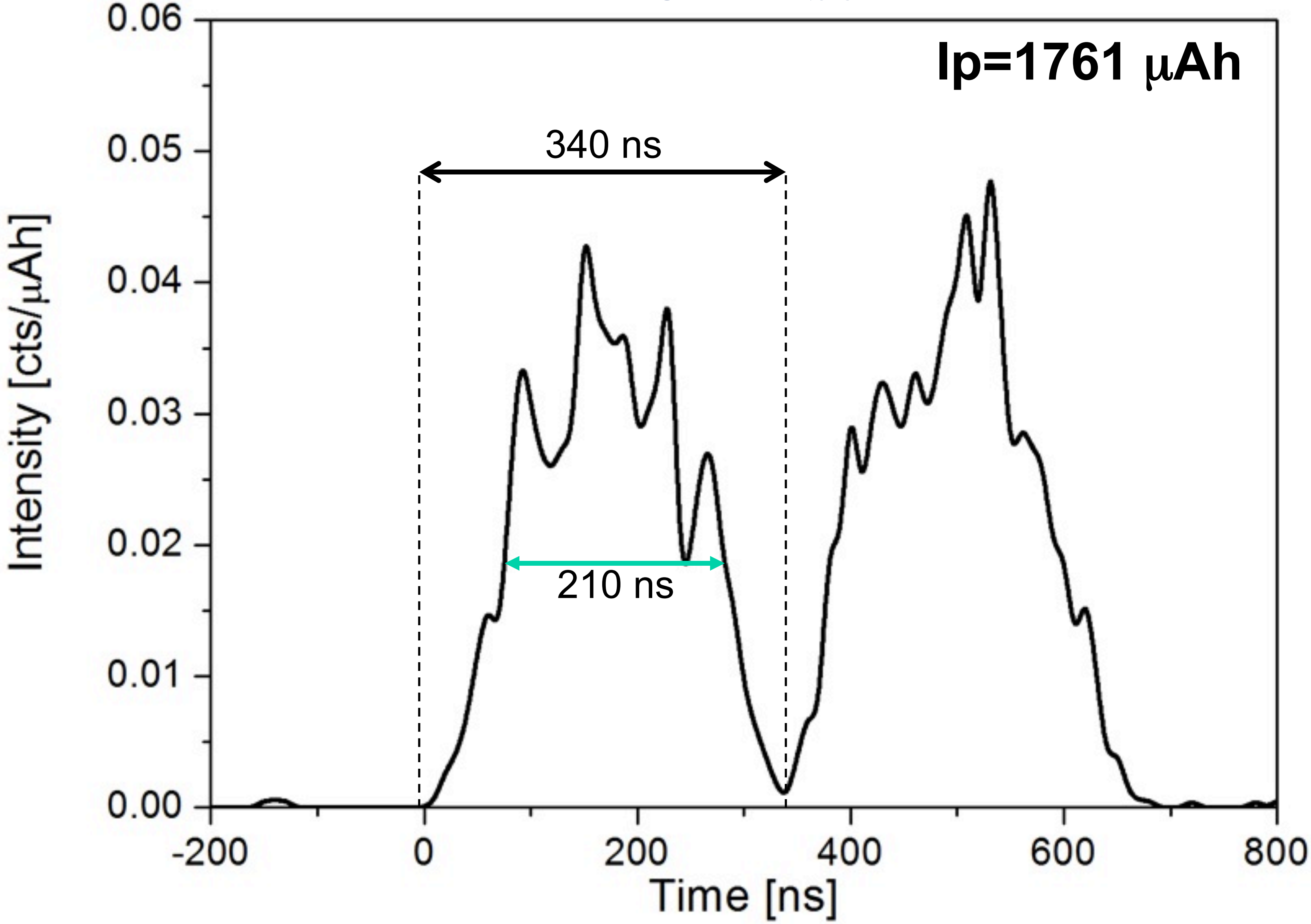

TOF SPECTRUM FROM DIAMOND
2- Moderated beam

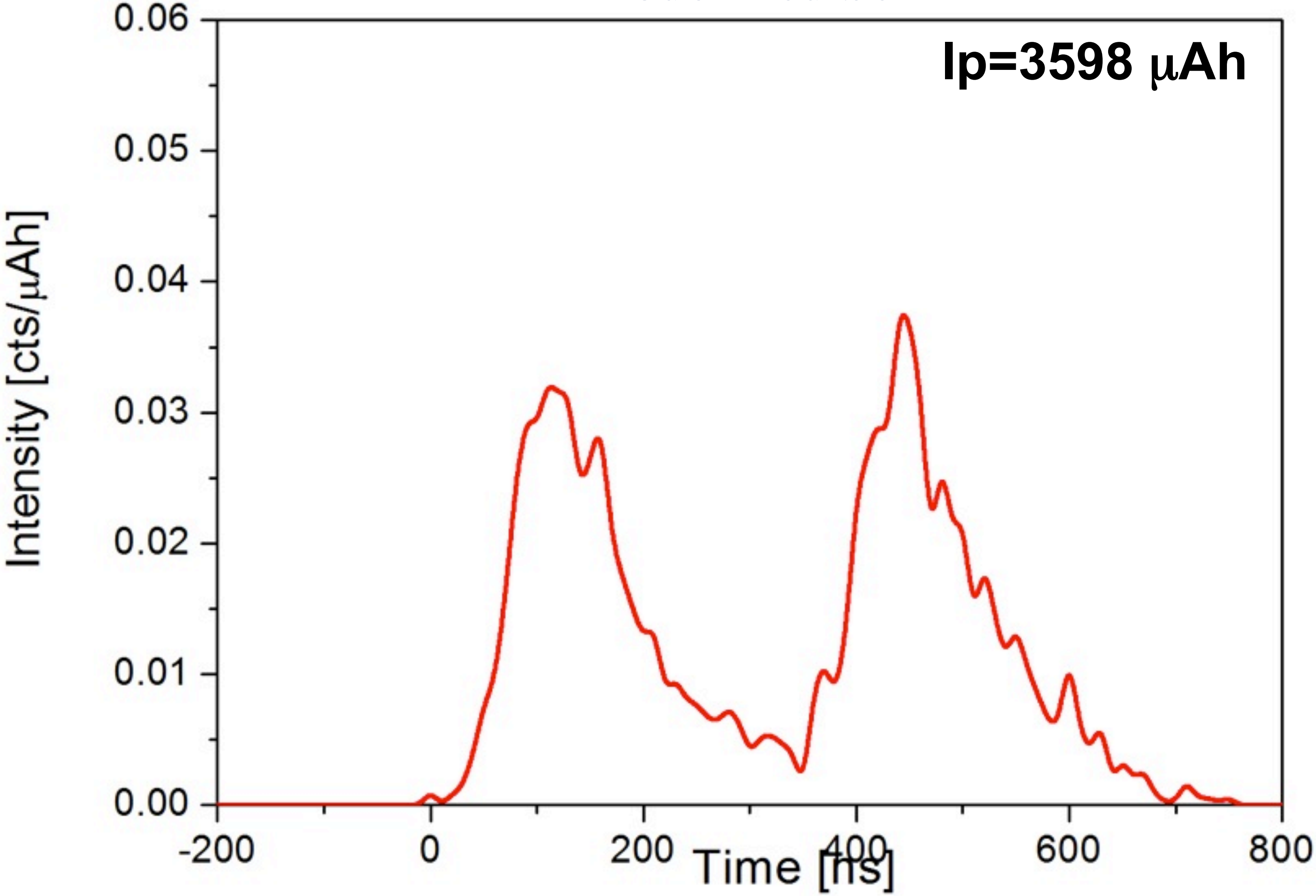

TOF SPECTRA FROM DIAMOND

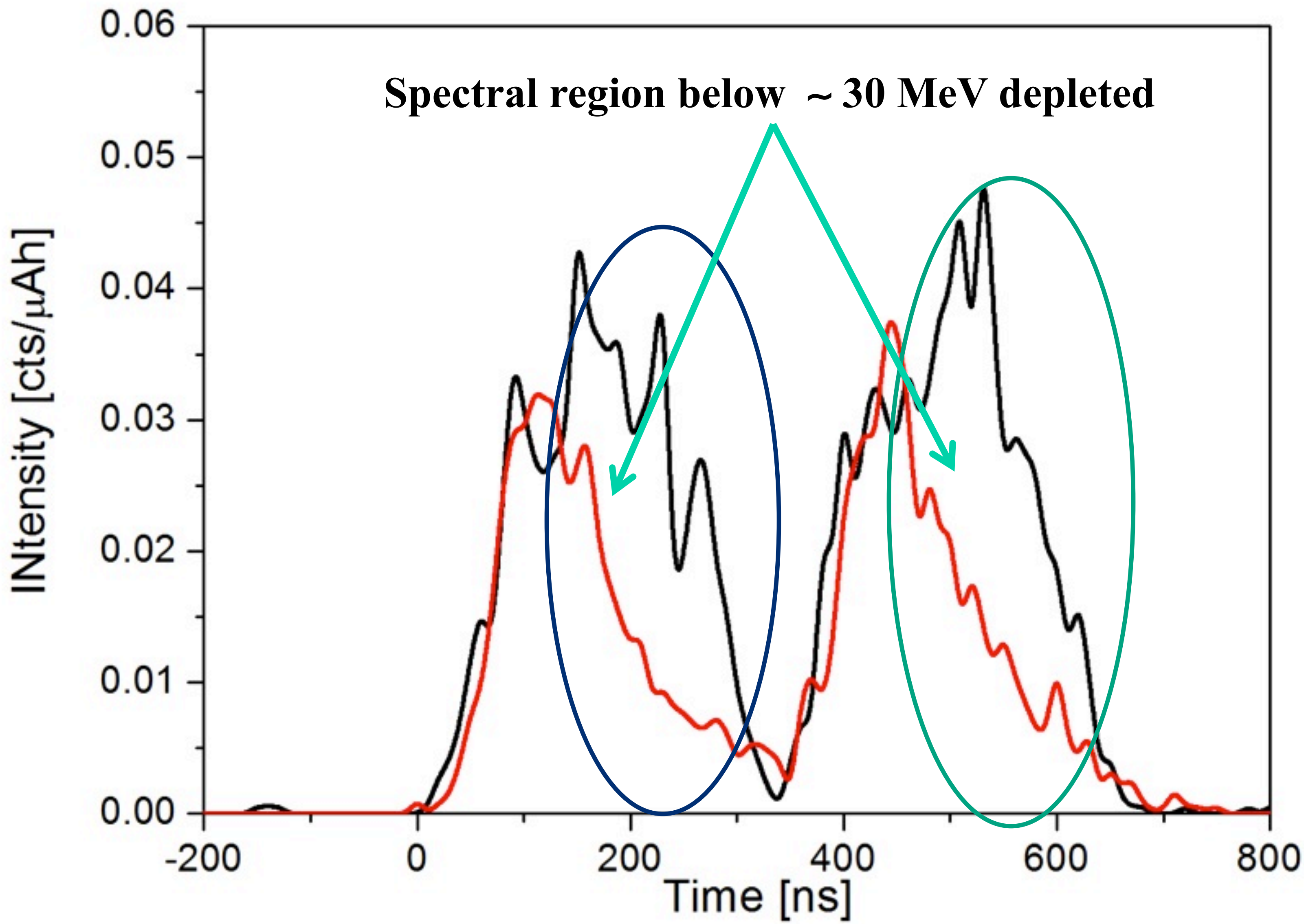

Modifying the diamond response:

1- with a fissile material

Only diamond (25 μm)

Diamond + ^{nat}U sheet 30 μm

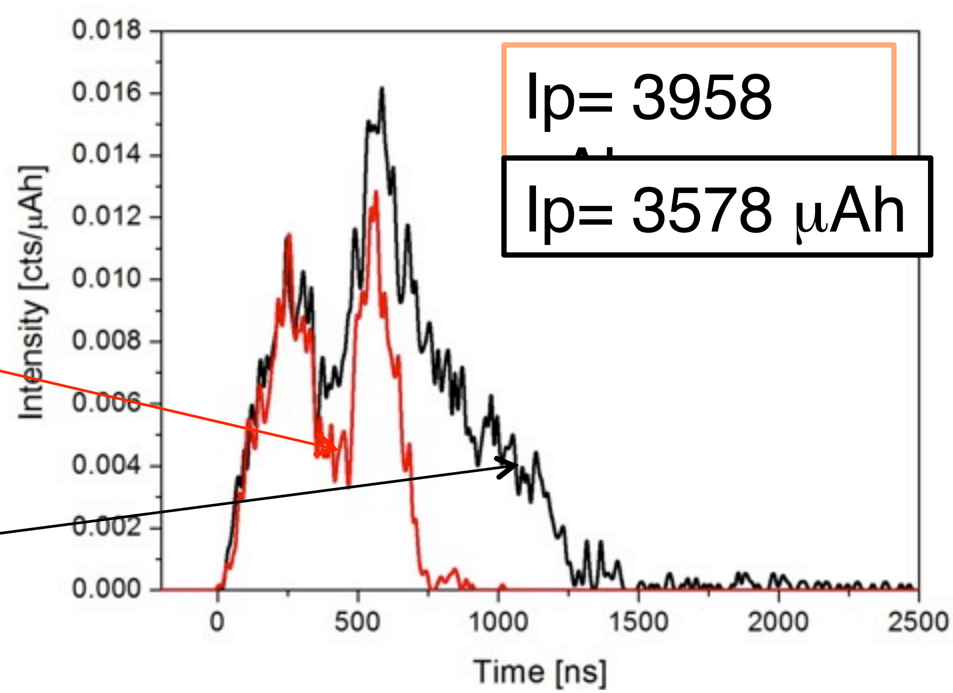

Diamond detectors at JET

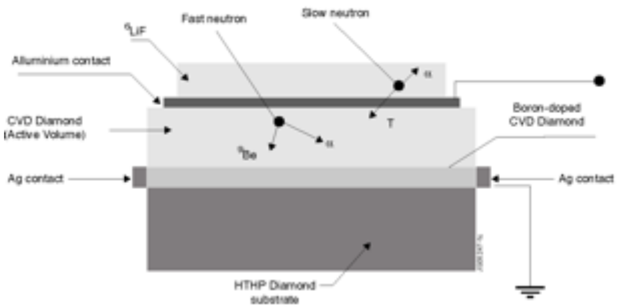

Detector configuration

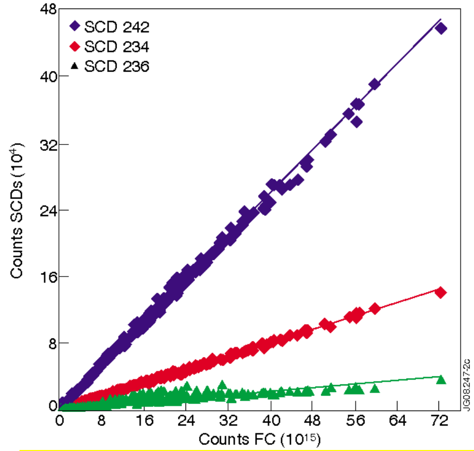

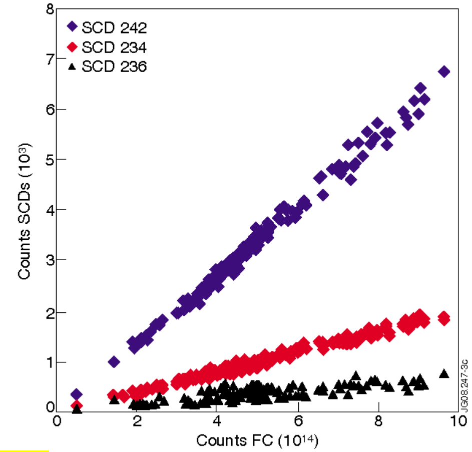

Correlation between the three diamond detectors and the FC for 900 JET shots examined.

Correlation between the three diamond detectors and the FC for the shots with low total neutron yields (< 1. E15).

A typical JET Pulse No: (72331) showing the matching between the FC and the three SCD detectors (normalized counts). Pulse duration 6.2s; neutron yield = 1.109 E16.

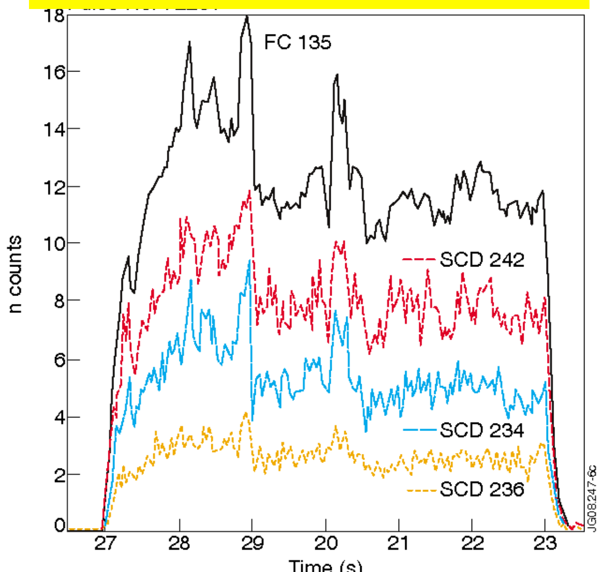

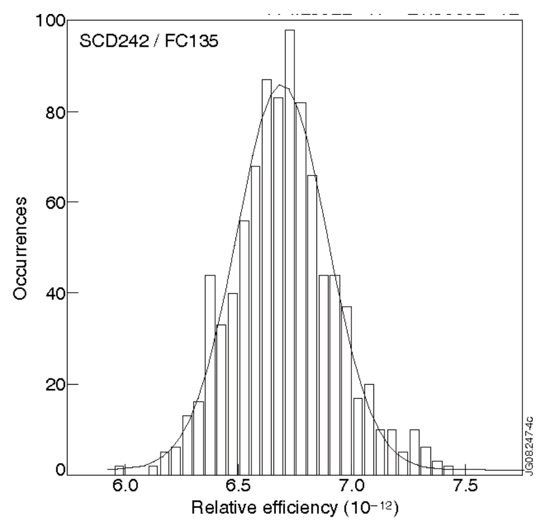

Statistical distribution of the relative efficiency (SCD242/ FC135) for all the 900 JET shots.

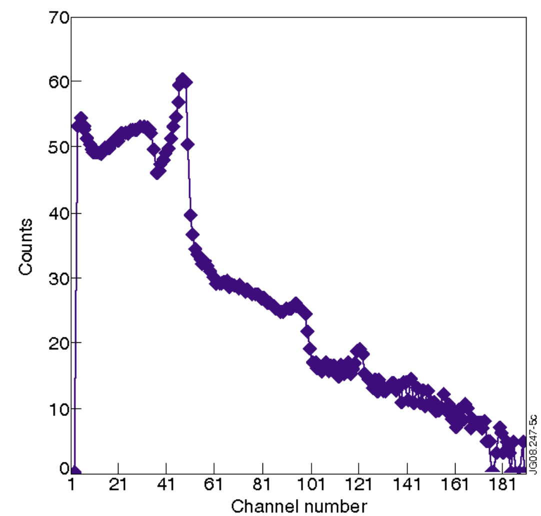

Sum of more than 800 JET spectra (total neutrons) as measured by SCD 234.

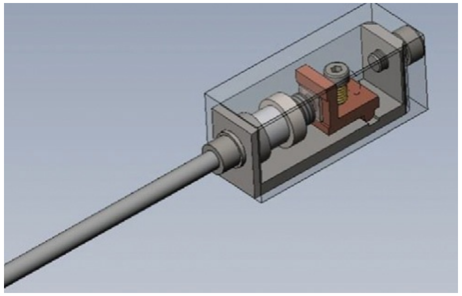

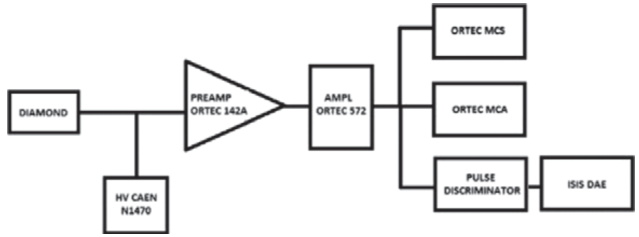

Test ad alta T

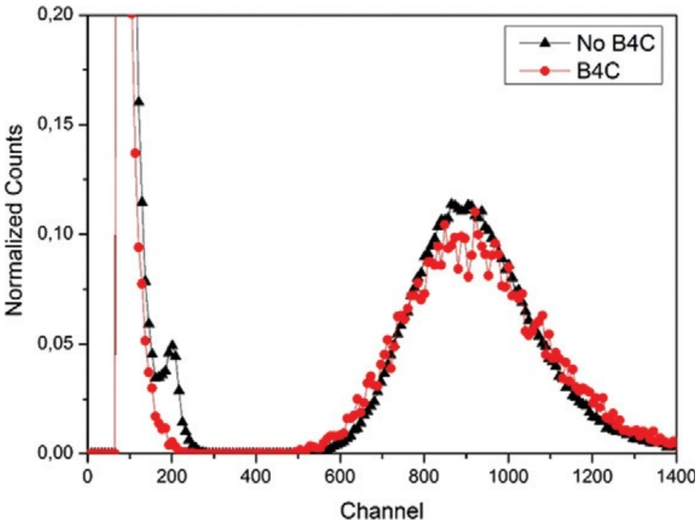

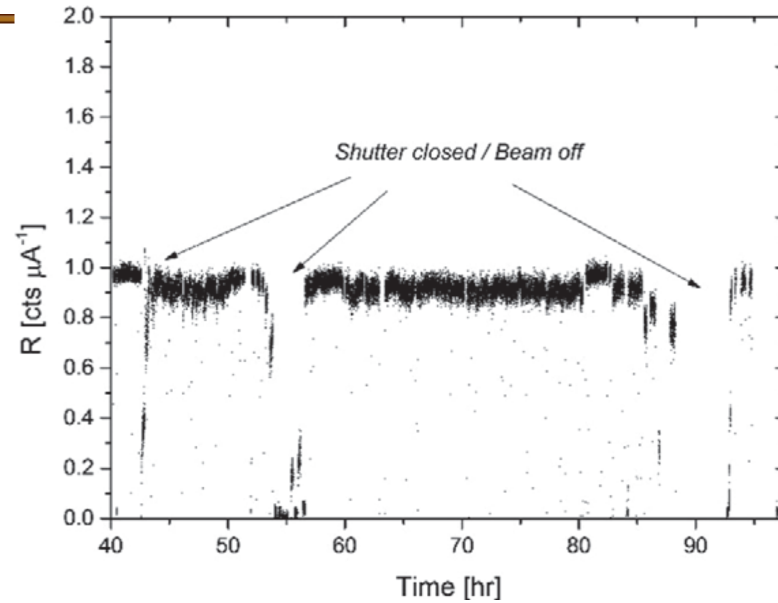

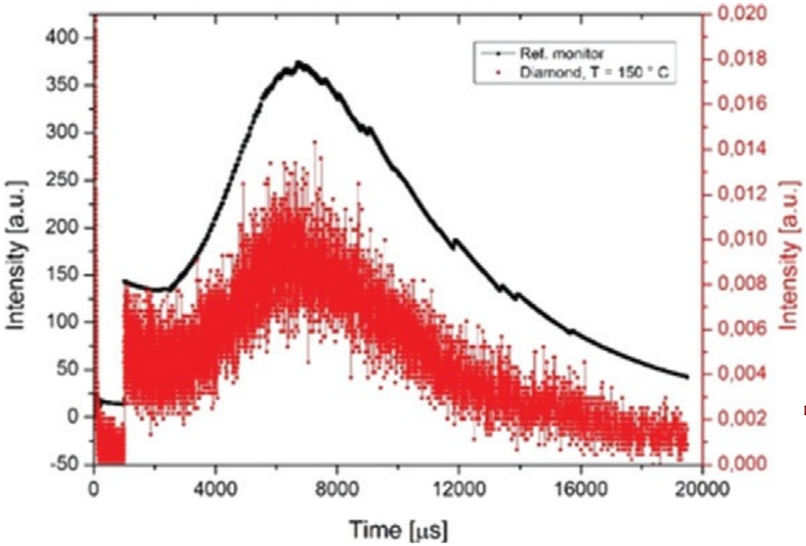

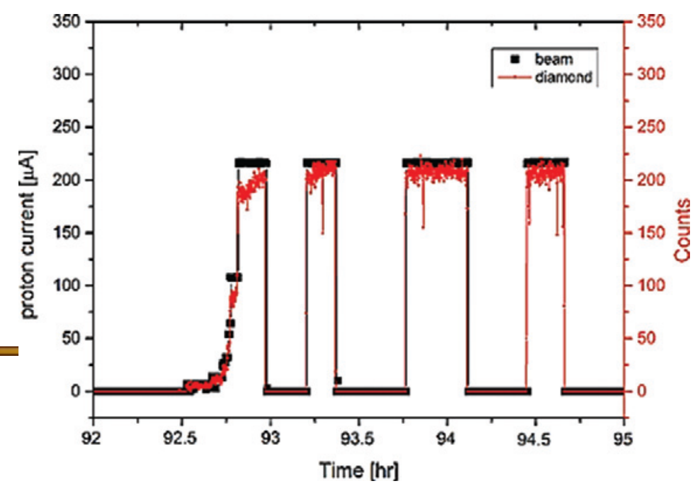

14 MeV neutrons for medical application: a scientific case $^{99}Mo/^{99m}Tc$

30 milion SPECTs every year

85% of whole nuclear medicine diagnostics

$^{99}Tc^{m}$ tracer radiopharamceutical

Tc-99m Thyroid Imaging

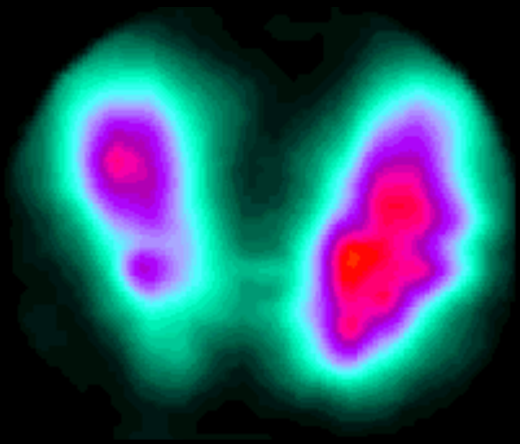

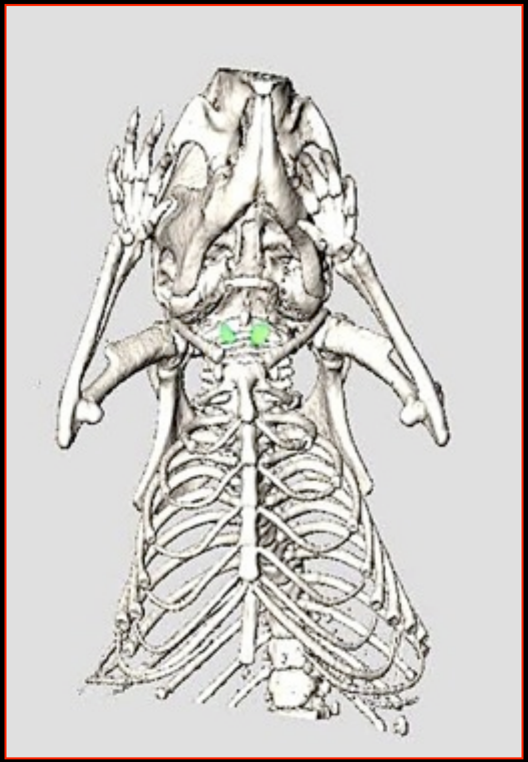

CARDIAC TOMOGRAPHY

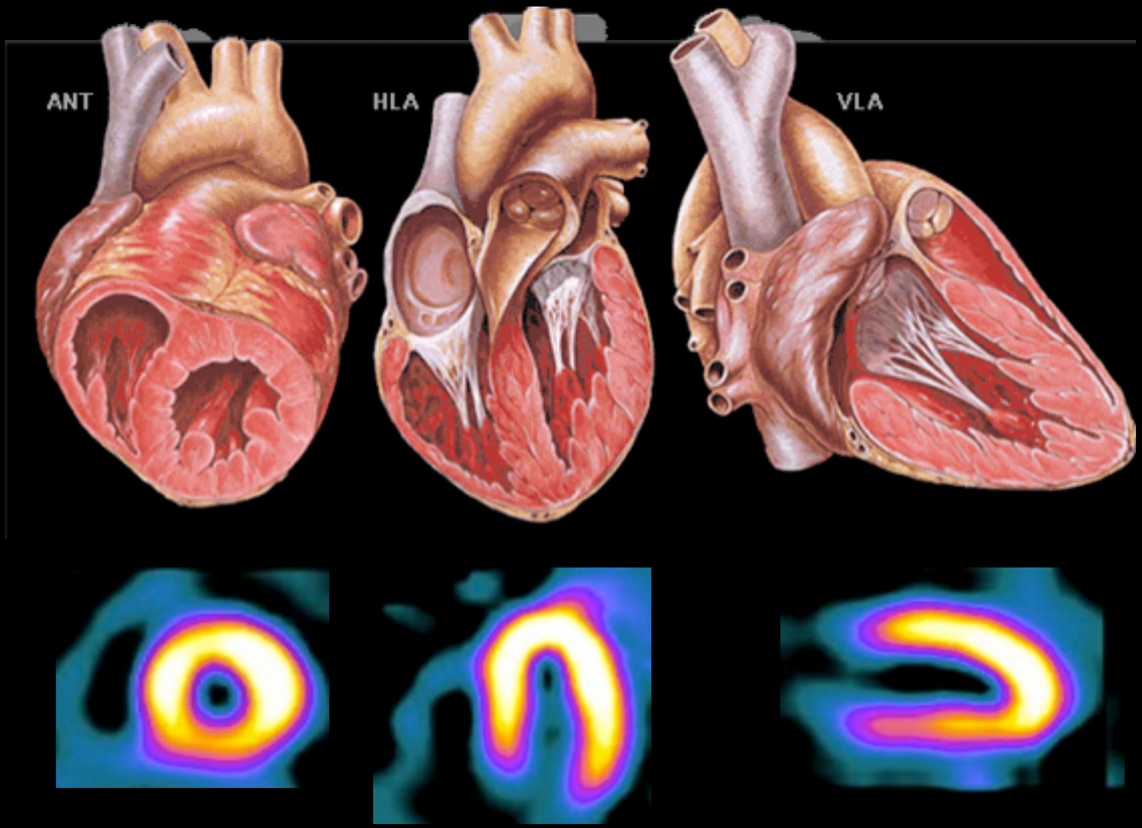

3D-TOMOGRAPHY

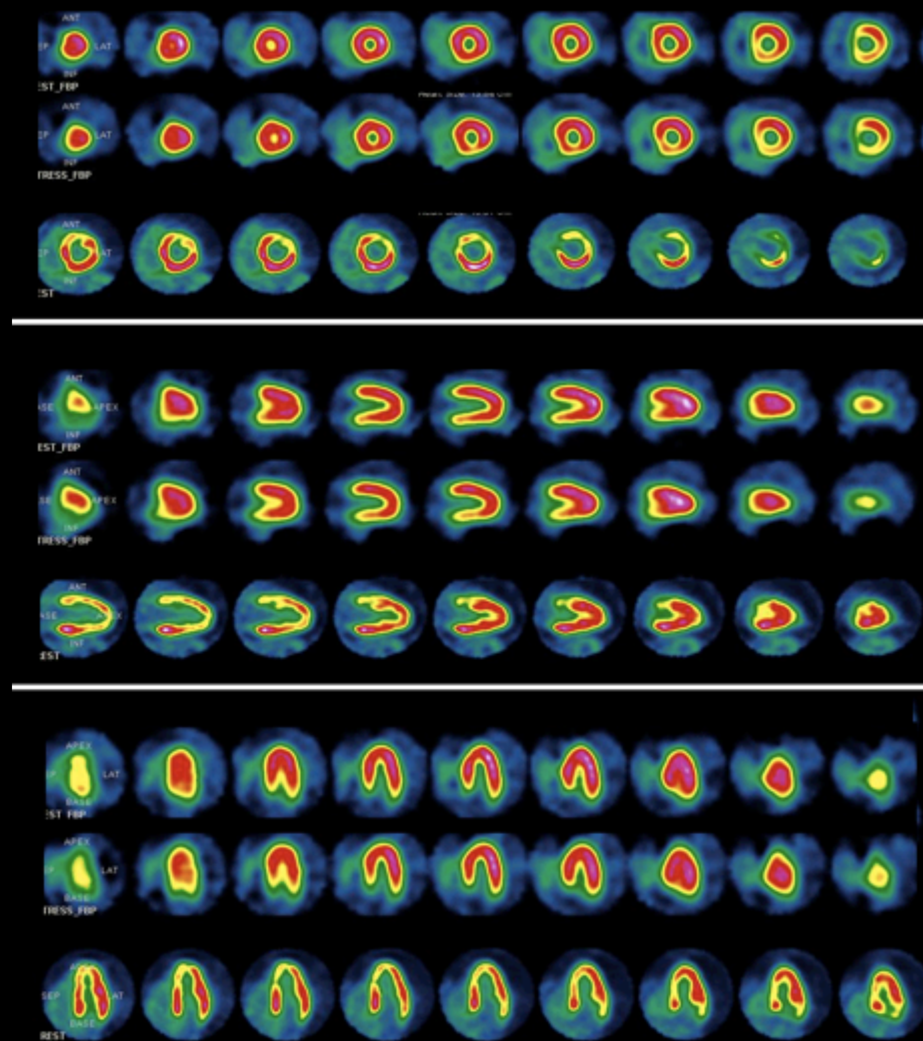

4D Cardiac Images

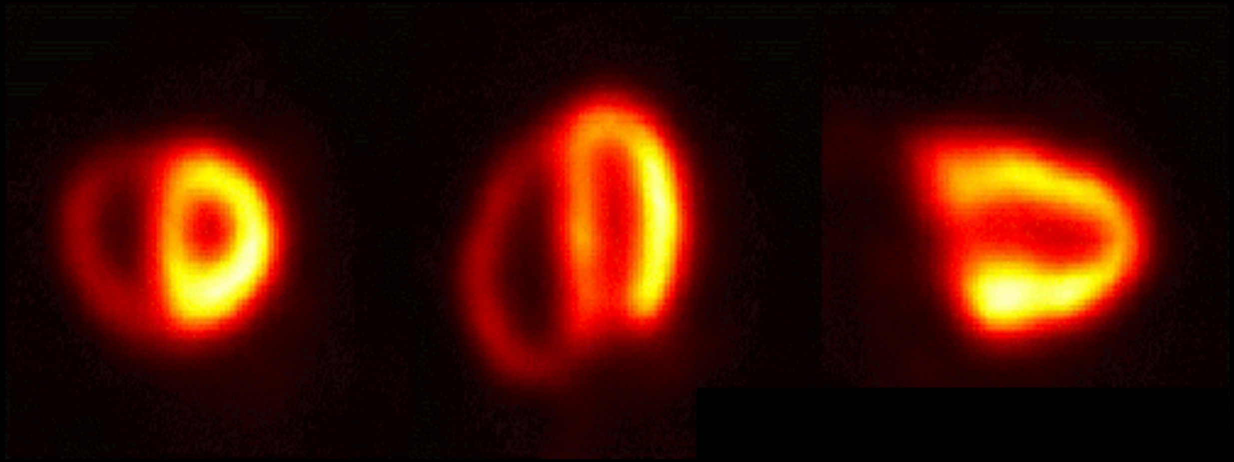

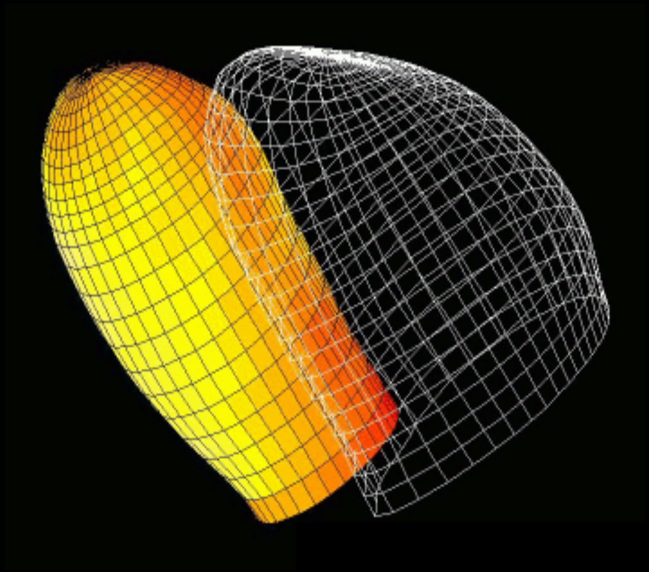

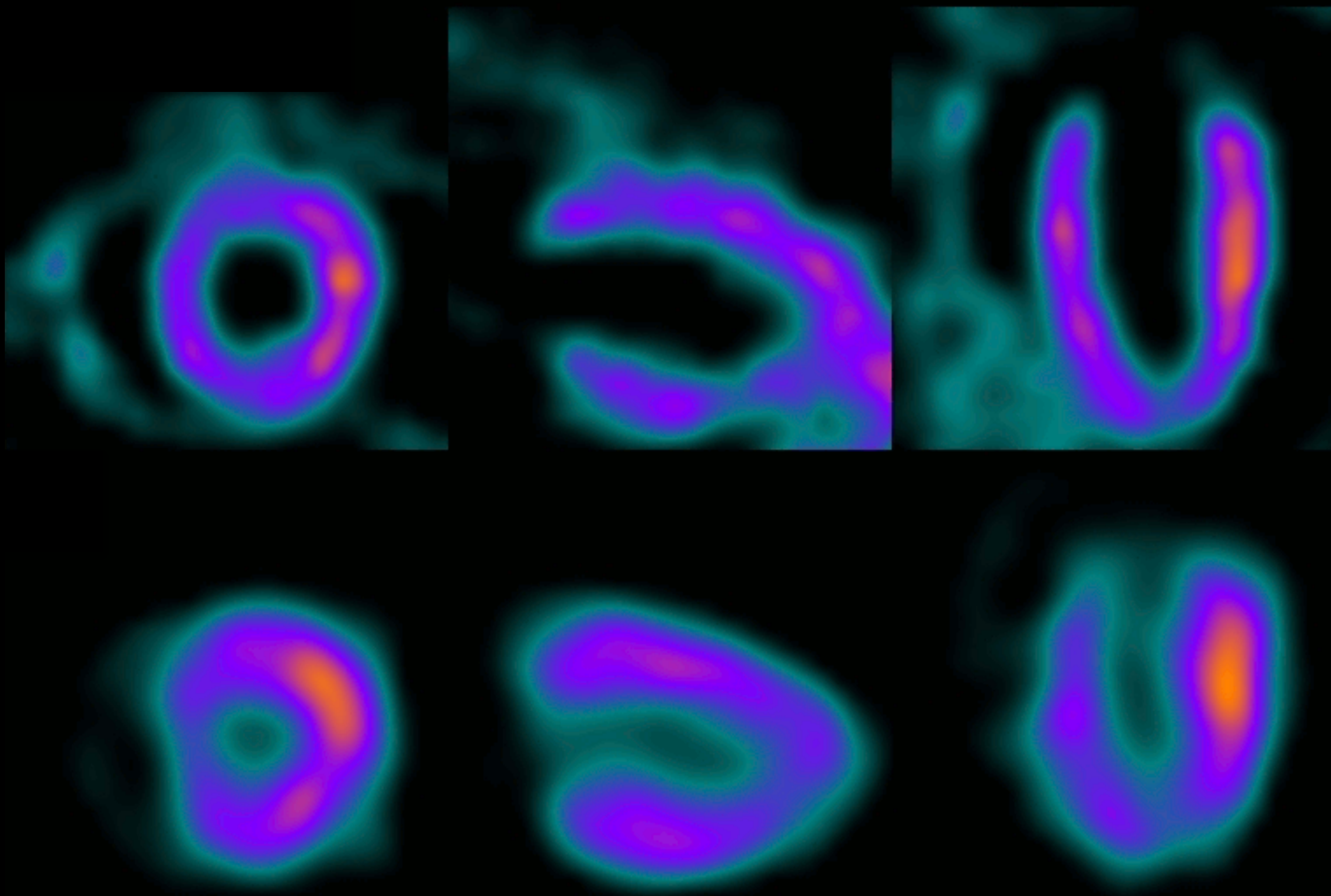

14 MeV neutrons for medical application: a scientific case $^{99}Mo/^{99m}Tc$

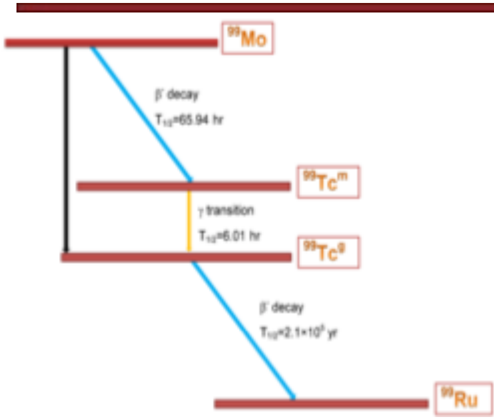

2009 Global crisis

Finding alternative solutions to reactors

$^{100}Mo(n,2n)^{99}Mo$ using 14 MeV neutrons

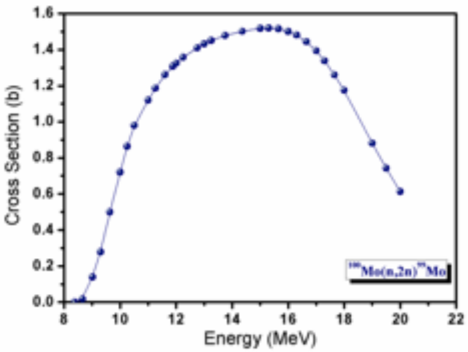

FNG

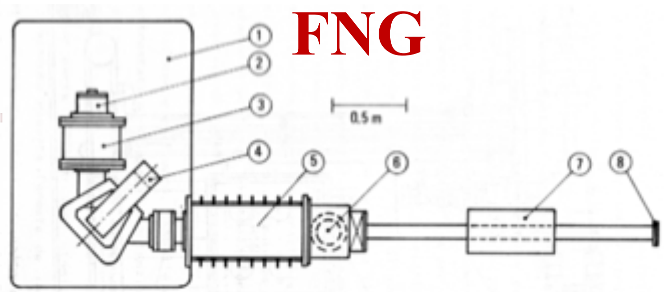

Z	Radionuclide	SA_M [Bq g-1]	SA_{Exp} [Bq g-1]
40	^{89}Zr	46.35±1.6%	48±4.9%
	^{95}Zr	0.96±5.5%	0.97±6.4%
	^{97}Zr	16.1±9.1%	16.6±5.8%
41	$^{93}Nb^{m}$	39.1±1.8%	40±4.5%
	$^{95}Nb^{m}$	42.3±2.9%	0.64±327%
	^{95}Nb	189.7±2.5%	187±1.8%
	^{97}Nb	1424.6±9.4%	17.3±6%

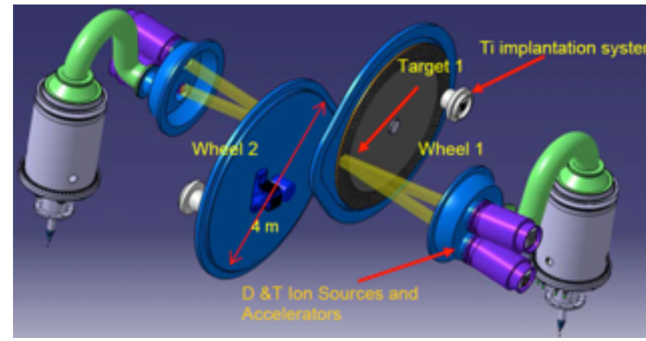

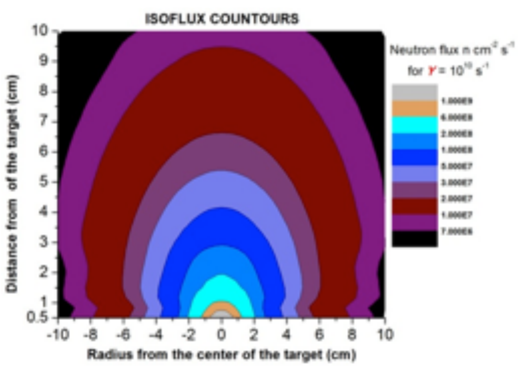

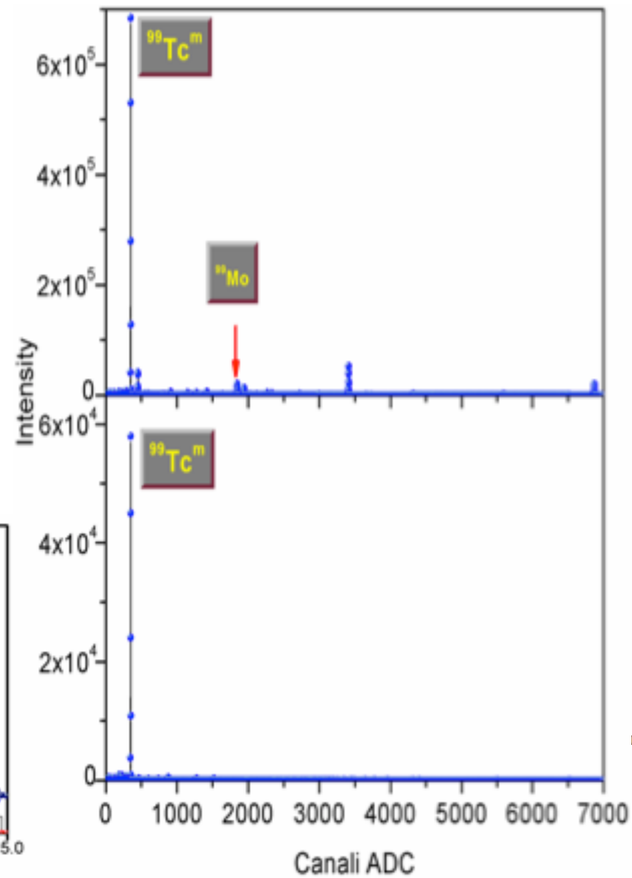

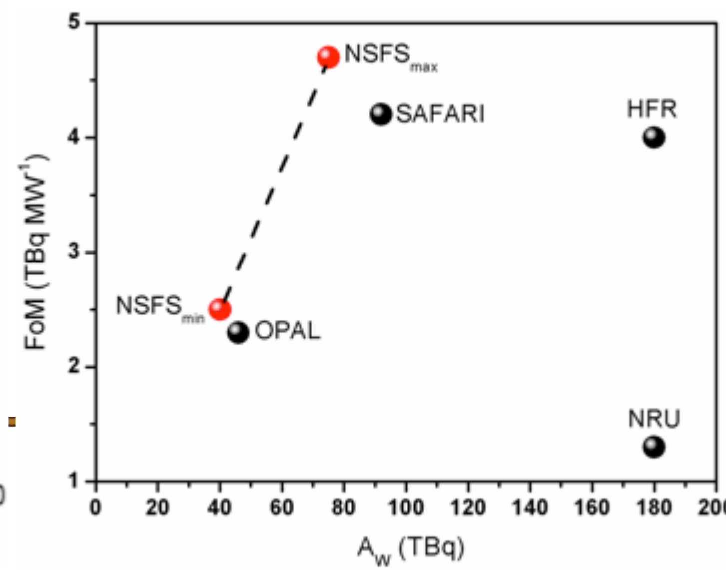

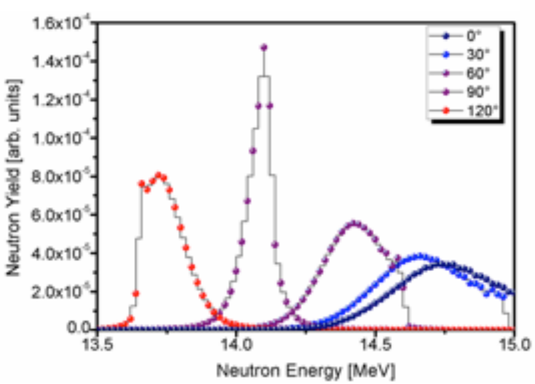

Detector development

Hybrid Superconducting Neutron Detectors

In beam cold neutron imaging

The basic idea

Hot-spot

Superconducting thin films detect energetic charged particles

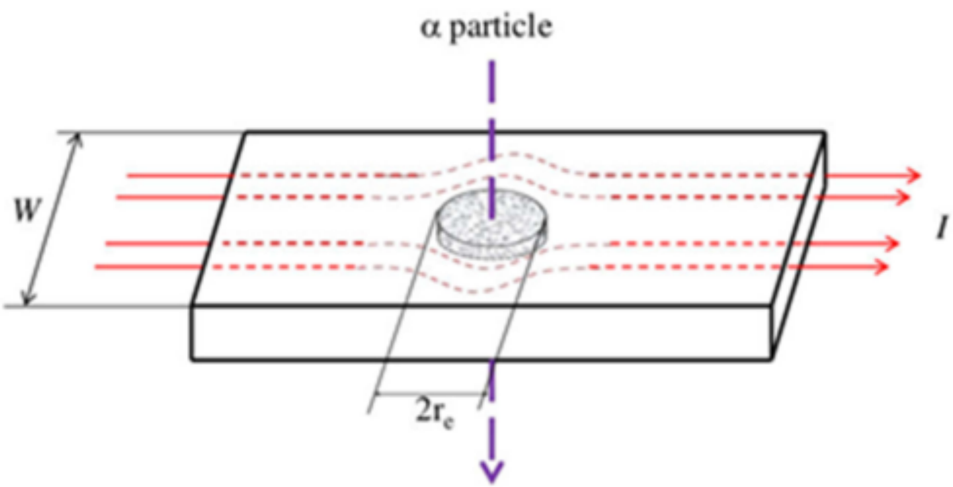

Bolometric model

$$V = 2\, r_c \rho\, J_B$$

r_c : hot spot radius
ρ : electrical resistivity
J_B: biased transport current density

D. H. Andrews et al. Phys. Rev. 76, 154 (1949)	CbN-α
D. E. Spiel et al. App. Phys. Lett. 7, 292 (1965)	Sn-α
E. C. Crittenden and D. E. Spiel. J. App. Phys. 42, 3182 (1971)	In-α
A. Gabutti et al. Nucl. Instrum. Methods Phys. Res. Sect. A 289, 274 (1990)	Al-x/γ
R. Wedenig et al. Nucl. Instrum. Methods Phys. Res. Sect. A 433, 646 (1999)	NbN-α

HSND working principle

$$^{10}\mathrm{B} + \mathrm{n} \rightarrow \alpha + {}^{7}\mathrm{Li} \qquad (\mathrm{BR}\ 6\%)$$

$$^{10}\mathrm{B} + \mathrm{n} \rightarrow \alpha + {}^{7}\mathrm{Li} + \gamma(478\,\mathrm{keV}) \qquad (\mathrm{BR}\ 94\%)$$

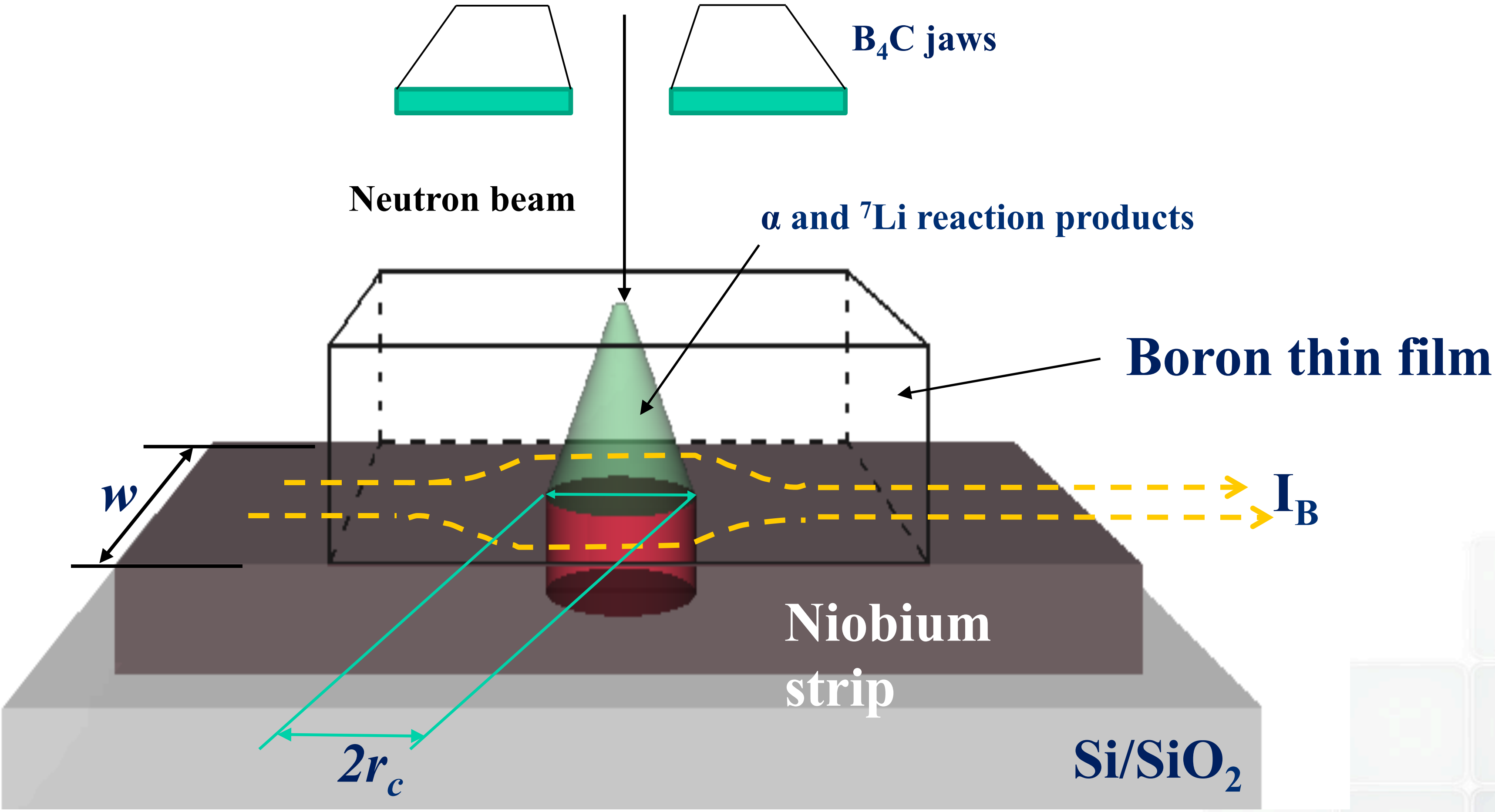

The detector

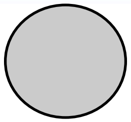

Silver contacts or
Si/Al wire bonding

samples made by means of optical lithography

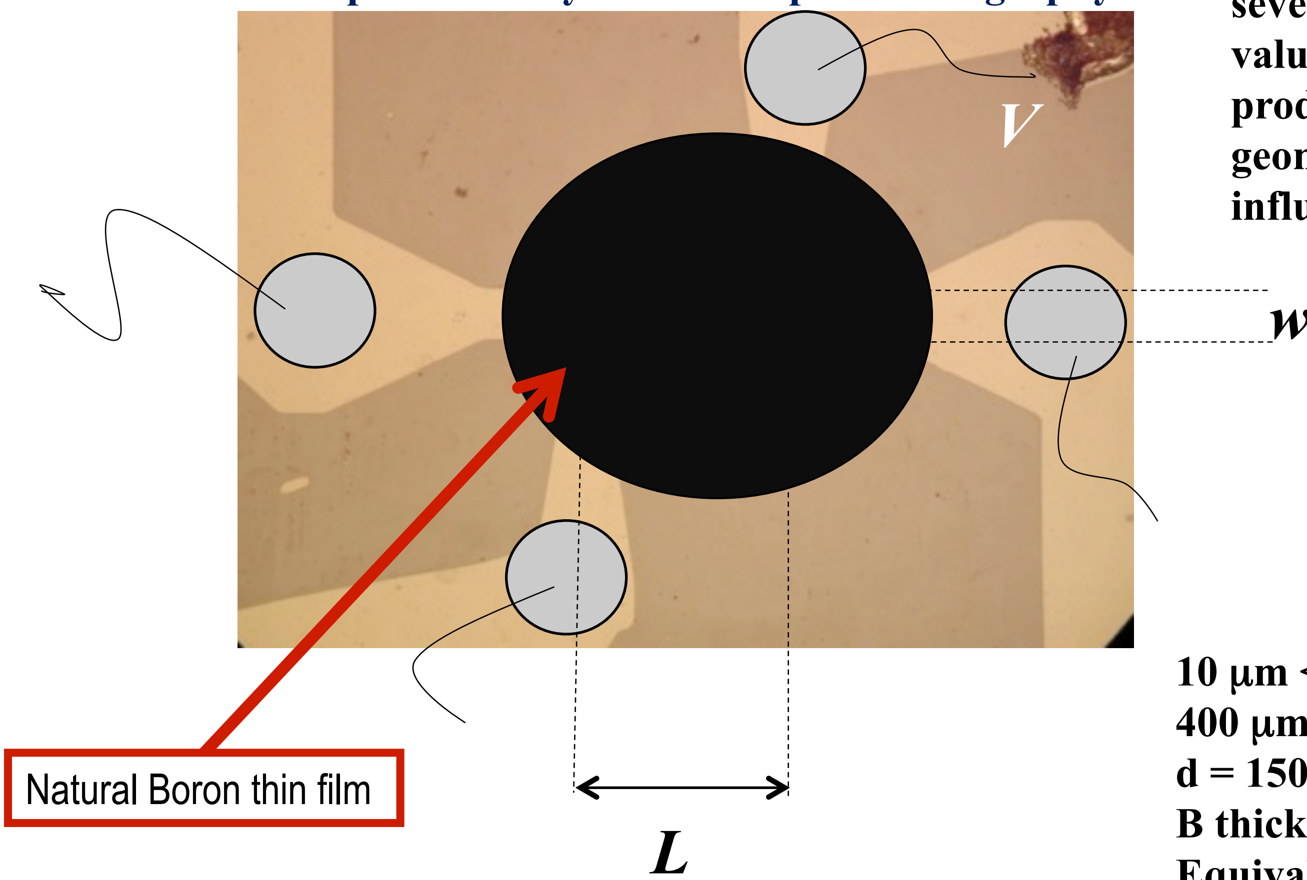

several samples with different values of w and L have been produced for optimizing the geometry, these parameters influence the performance

10 μm < w < 50 μm
400 μm < L < 800 μm
d = 150 nm (Nb thickness)
B thickness = 450 nm (natural B)
Equivalent to 90 nm of ^{10}B

Experimental set-up

Flow cryostat used 1.8-10 K with nominal uncertainty in temperature 0.01 K

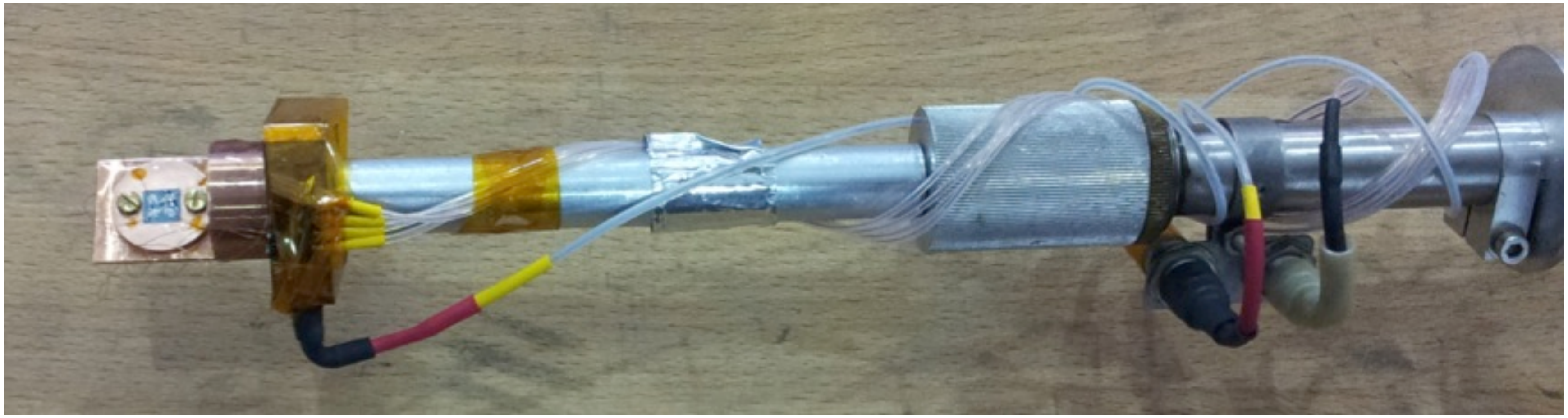

Silver contact strip

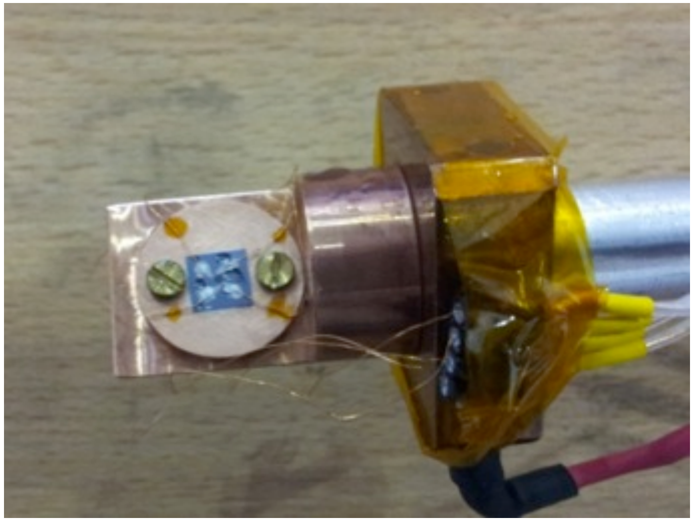

Bonded contact strip

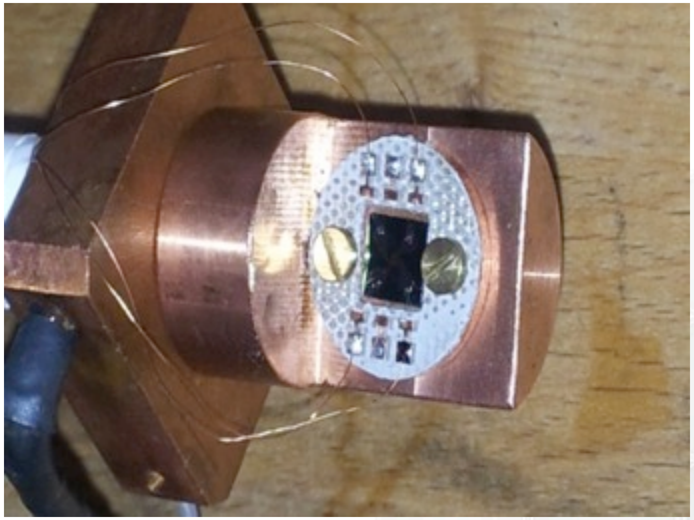

Experimental set-up

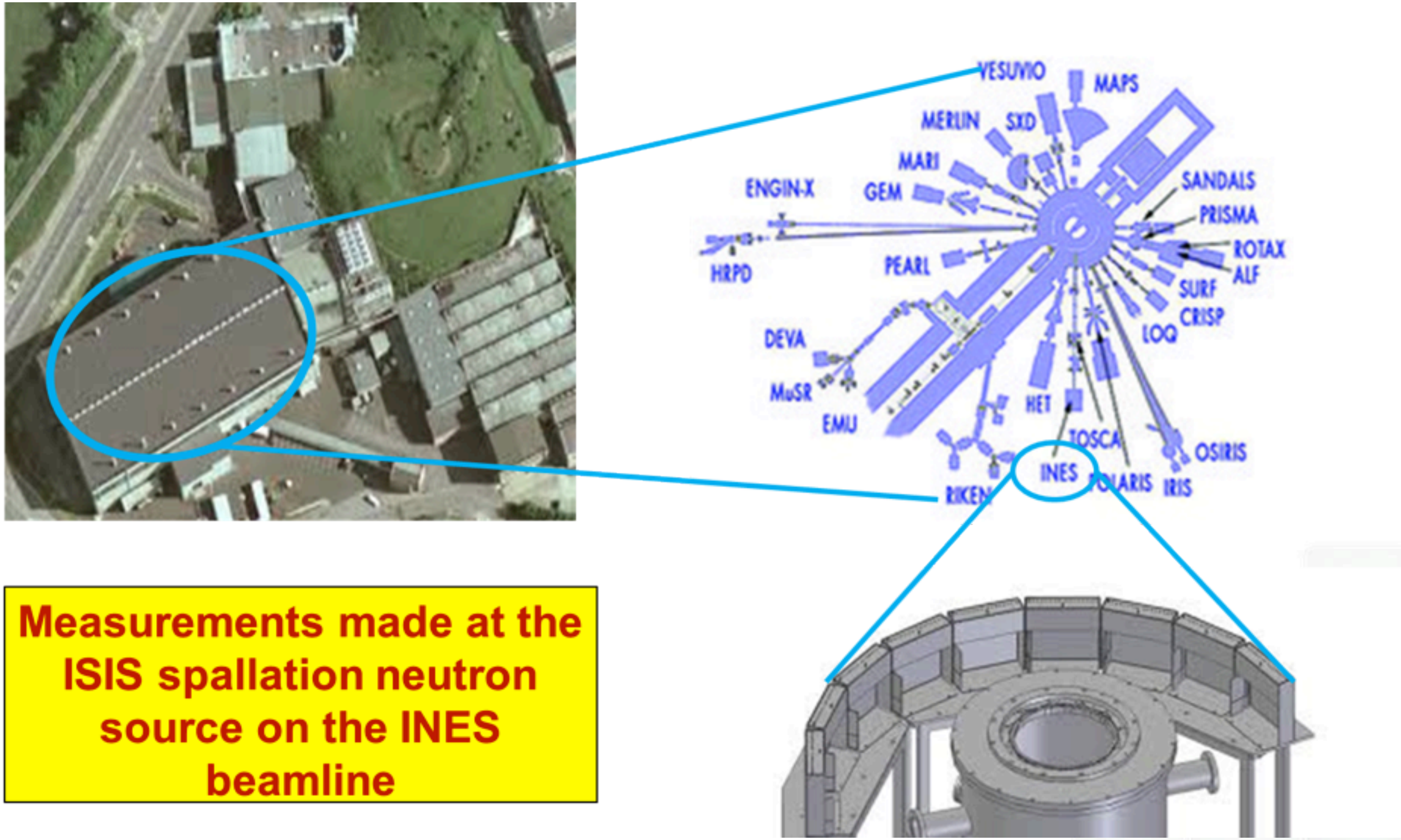

Measurements made at the ISIS spallation neutron source on the INES beamline

Experimental data

Nb-B 600 μm x10 μm bonded

T_{op}=8.12 K; T_c=8.6 K; T_{op}/T_c= 0.94 I_c=13 mA

Nb-B I_B=4.5 mA I/I_C=0.35

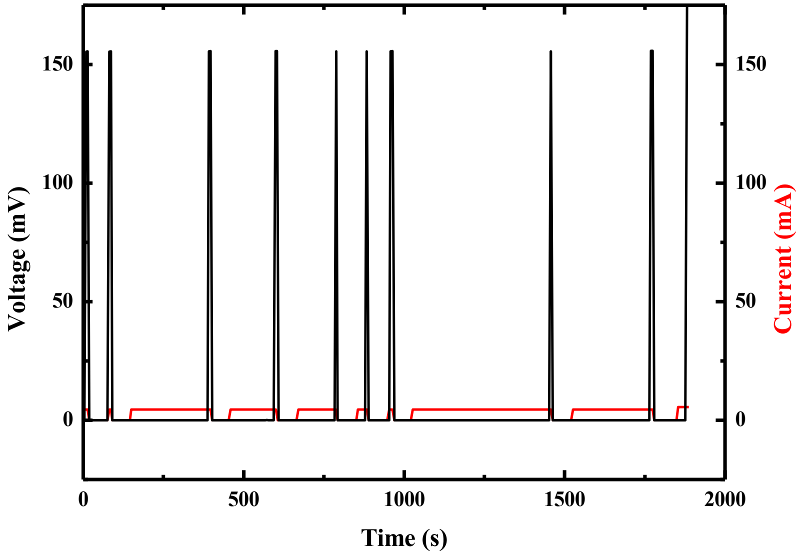

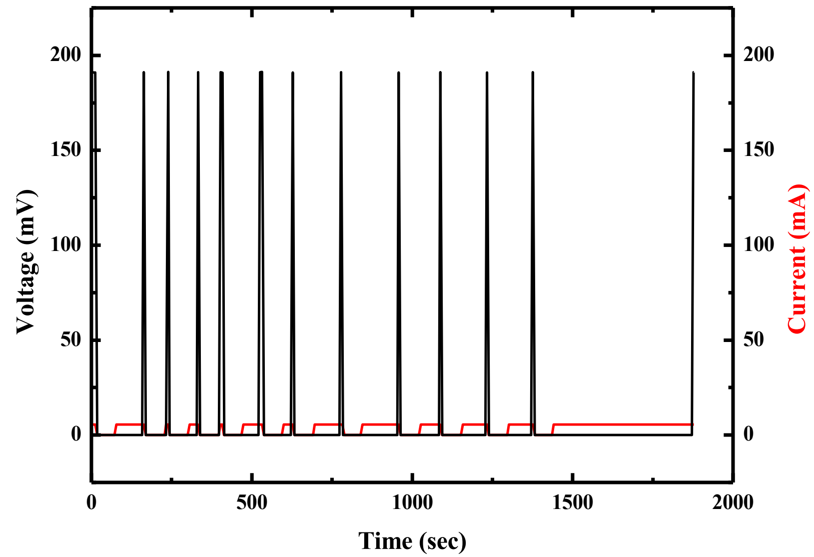

Nb-B I_B=6.5 mA I/I_C=0.5

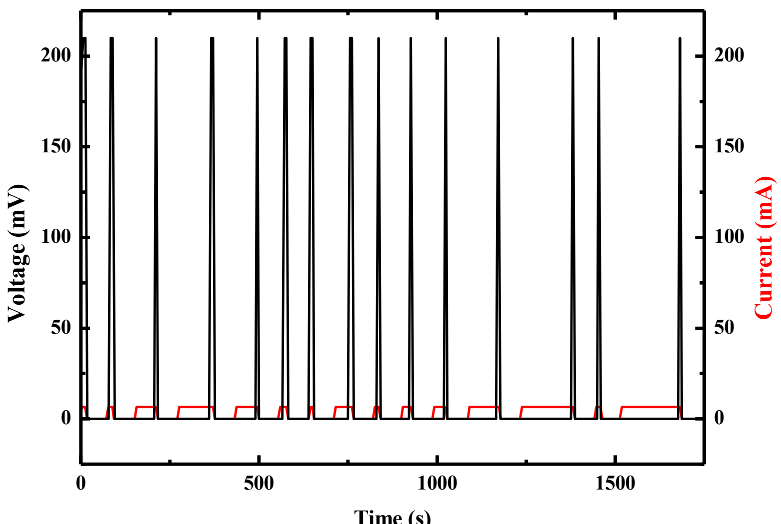

Nb-B I_B=10.5 mA I/I_C=0.78

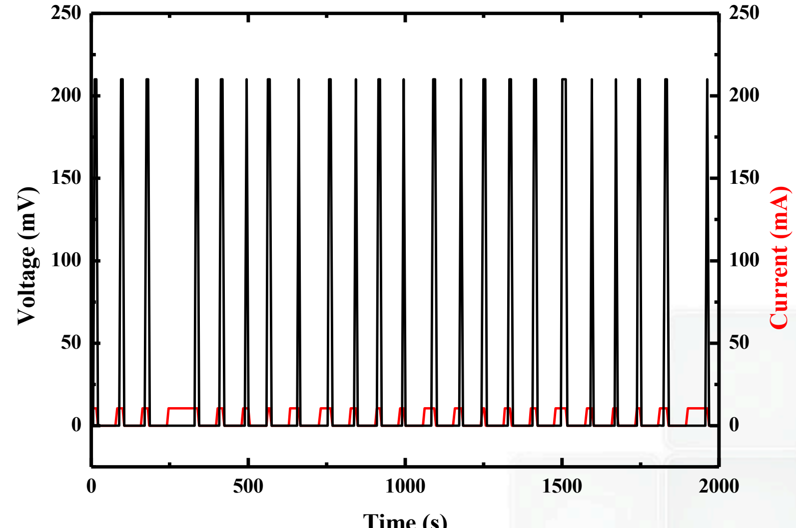

Experimental data

Fixed T_{op} measurement

Nb-Strip d=150 nm w=20 µm L=800 µm

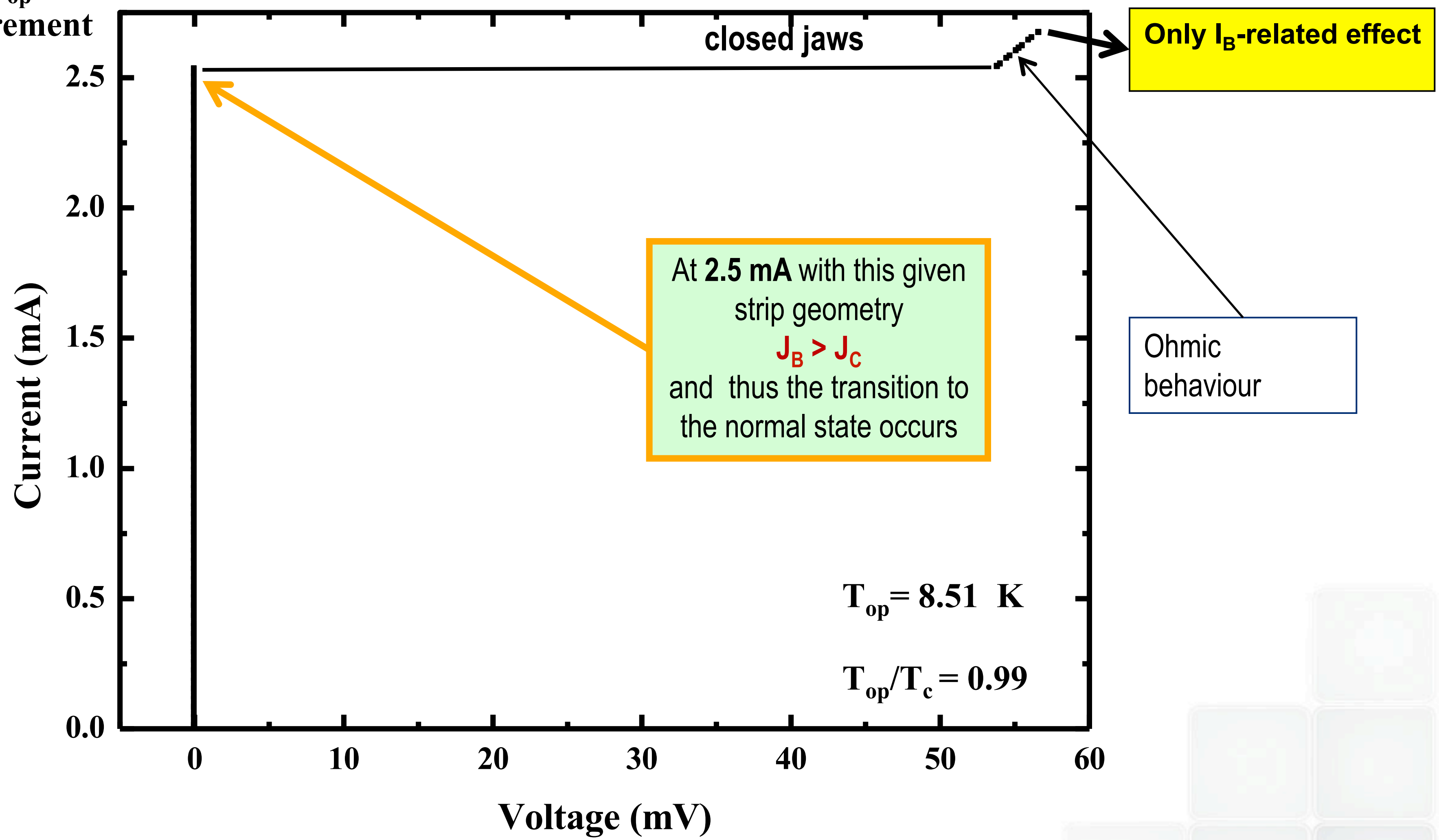

Experimental data

Fixed T_{op} measurement

Nb-Strip d=150 nm w=20 μm L=800 μm

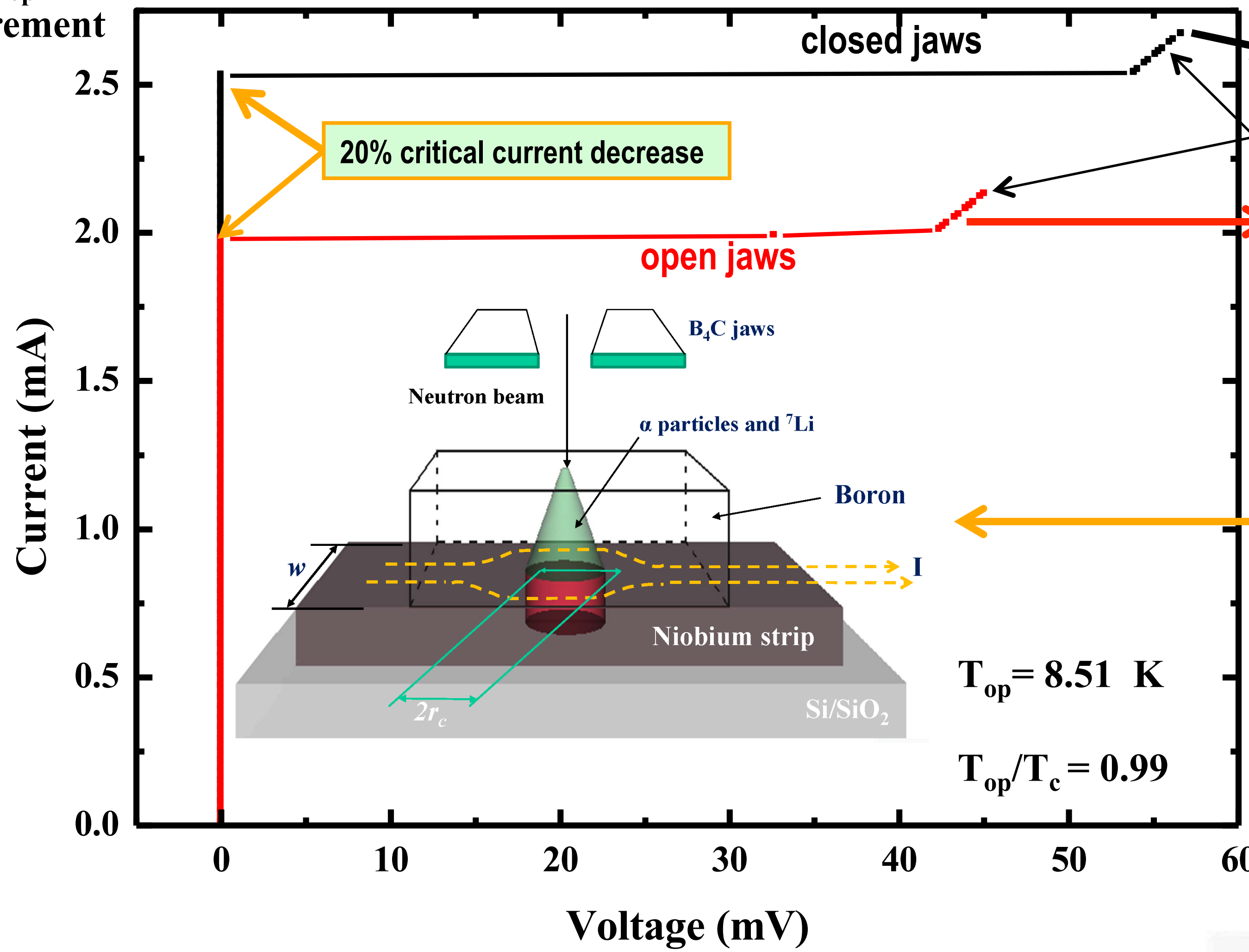

Only I_B-related effect

Ohmic behaviour

A+^{7}Li-related effect

Transition to Normal state occurs at lower I_B due to hot spot formation

$J_B > J_C$

Experimental data

Fixed I_B measurement

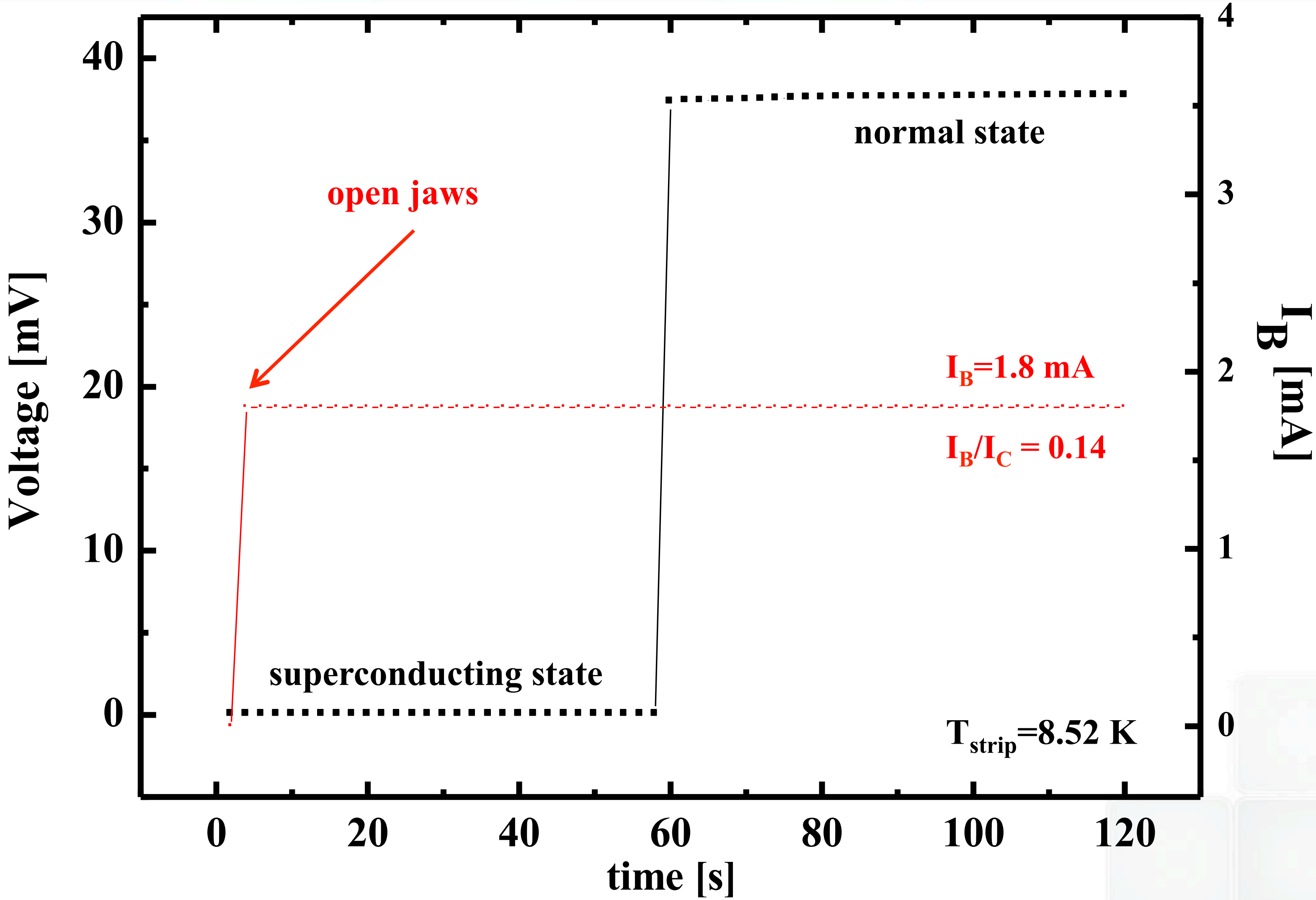

Experimental data

Nb-Strip d=150 nm w=20 µm L=800 µm

I_B synchronized to Jaws opening

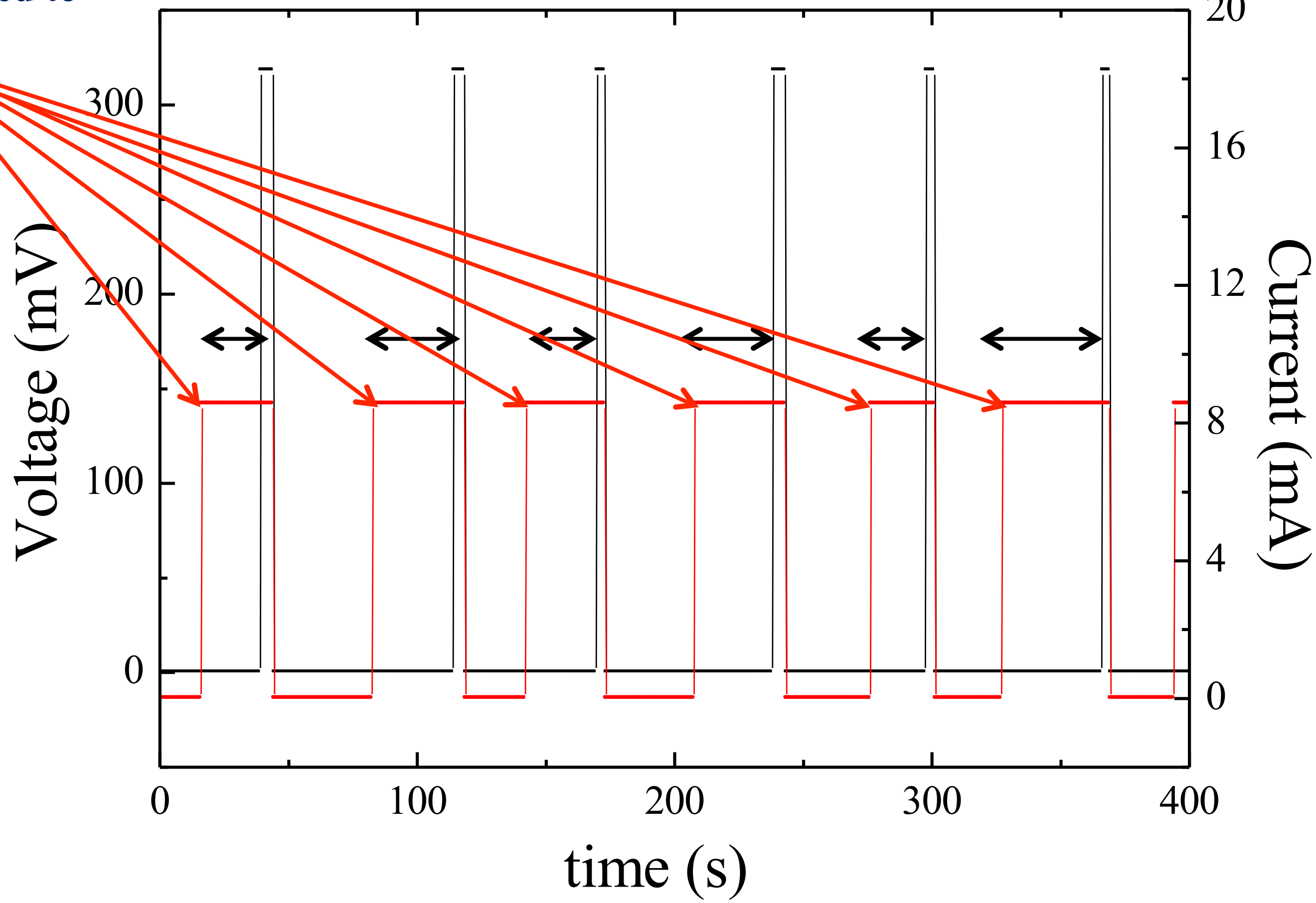

Detection of events takes place at different times after each I_B switch-on (jaws opening)
Confirmirmation of the statistical nature of the phenomenon

Analysis

slope of the weighted least-squares line is 4.47 ± 0.39 counts/(s·A)

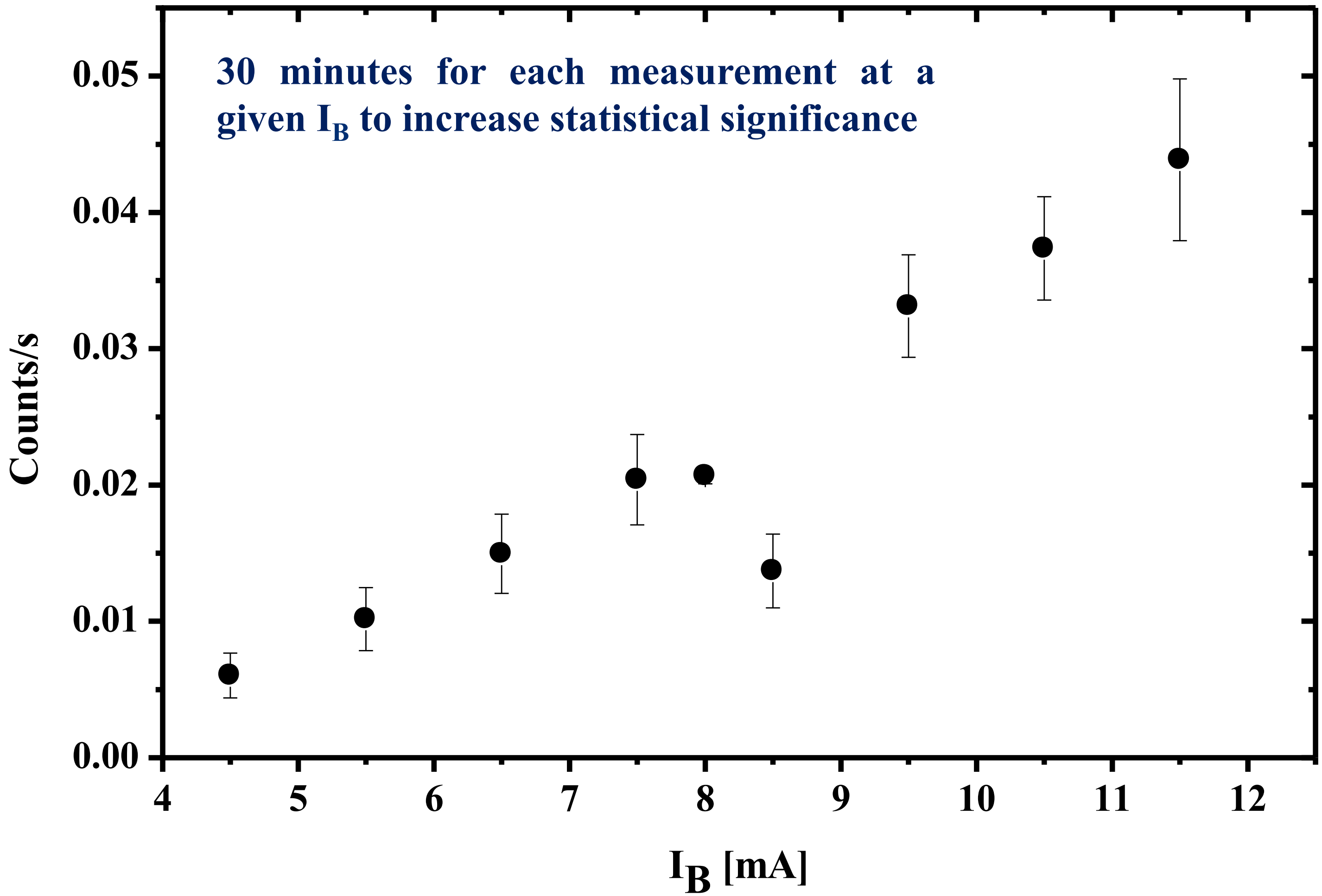

Maximum 3 counts/min

On going

Sviluppo di un calcolo analitico e calcolo agli elementi finiti per studiare le caratteristiche temporali del rivelatore

Sviluppo di rivelatori ad alta TC

YBCO

Detector development

GEM-based Gaseous detectors

^{3}He replacement

Gas Electron Multipliers Detectors

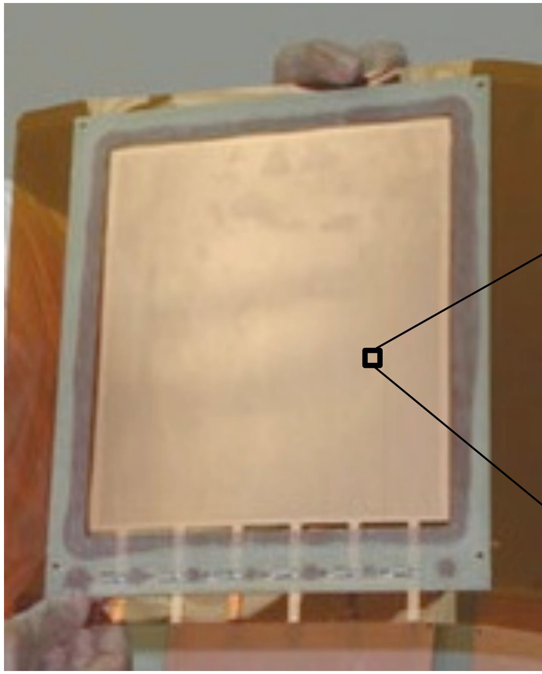

A Gas Electron Multiplier (F.Sauli, NIM A **386**, 531) is made by 50 µm thick kapton foil, copper clad (5 µm thick) on each side and perforated by an high surface-density of bi-conical channels;

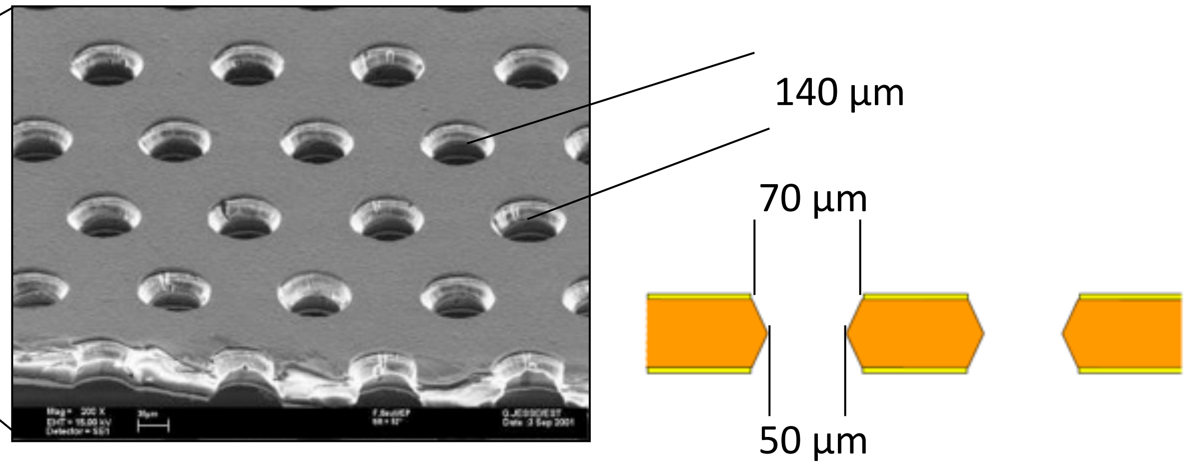

Applying a potential difference (typically between 300 and 500 volts) between the two copper cladding, an high intensity electric field is produced inside the holes (80-100 kV/cm).

GEM is used as a proportional amplifier of the ionization charge released in a gas detector.

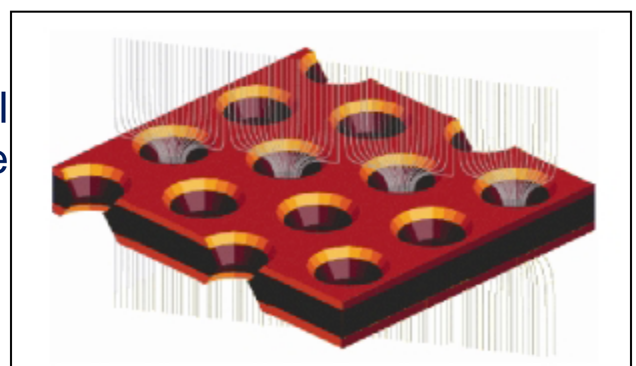

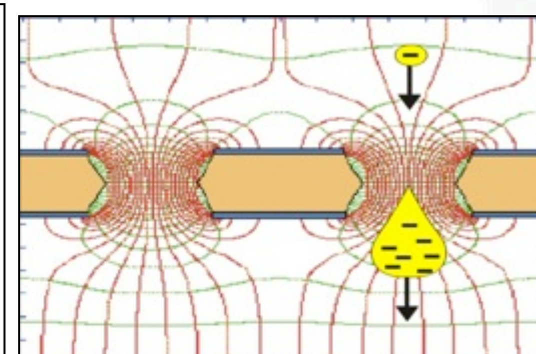

Triple-GEM detectors

Layout of a typical Triple GEM detector constructed with standard 10 x 10 cm²

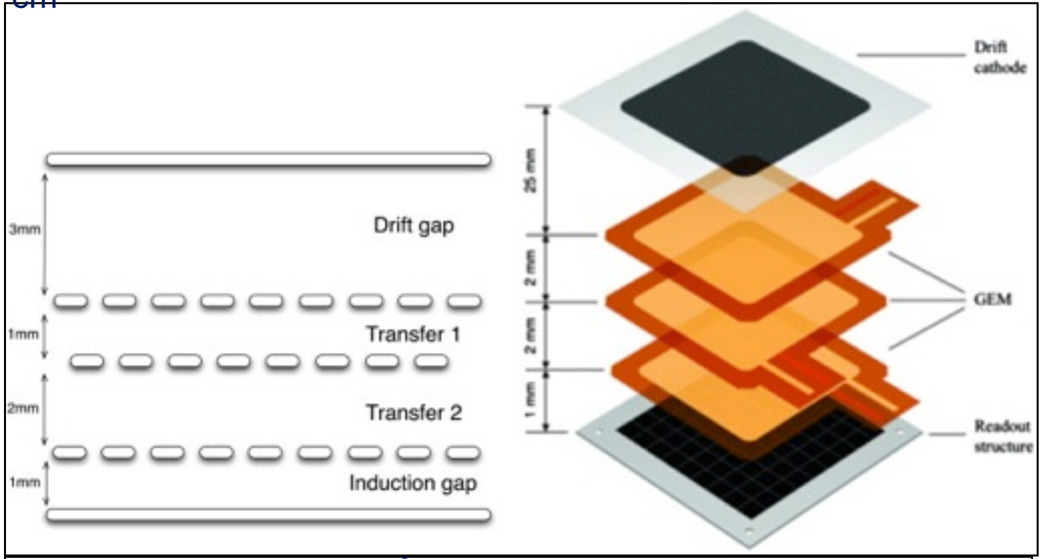

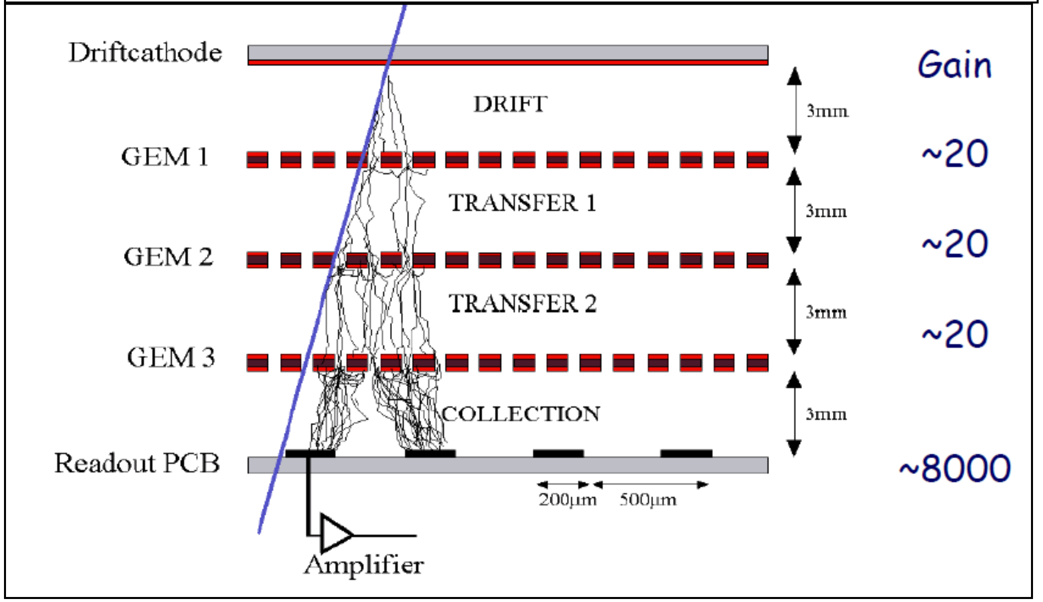

The anode has 128 pads. Each PAD can have a different geometry depending on detector applications.

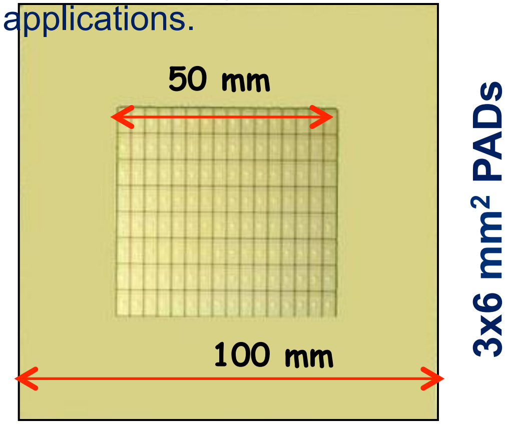

Gas Gain Curves

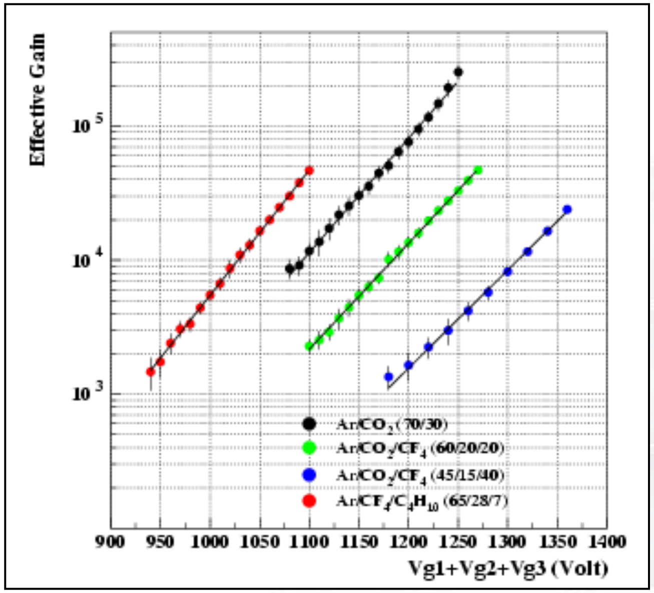

A GEM for thermal neutrons

The idea was to insert a sequence of borated strips attached to the aluminum cathode.
The drift region was extended and the detector was equipped with a side window.

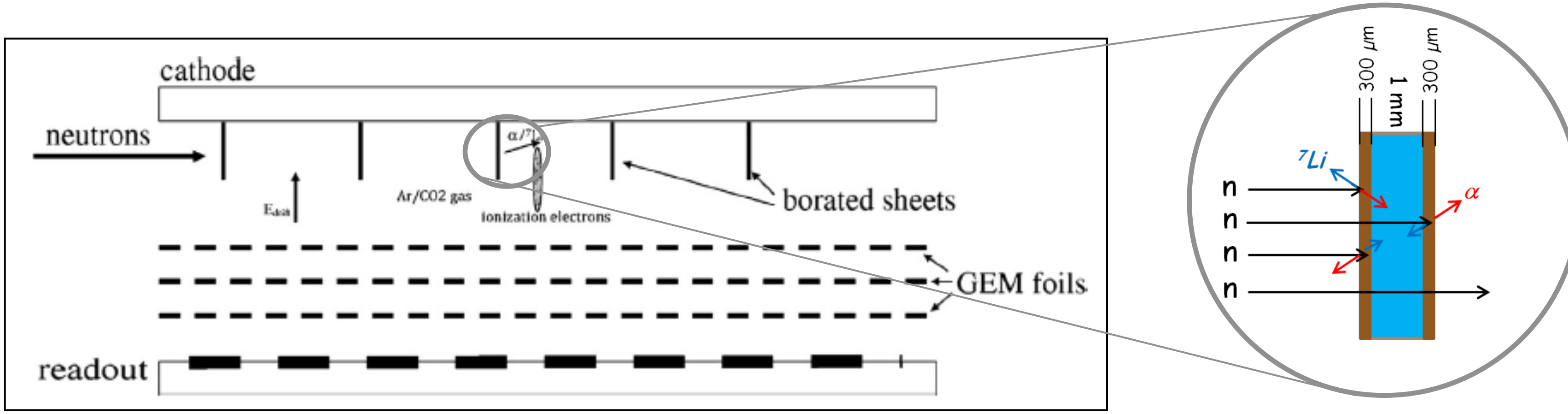

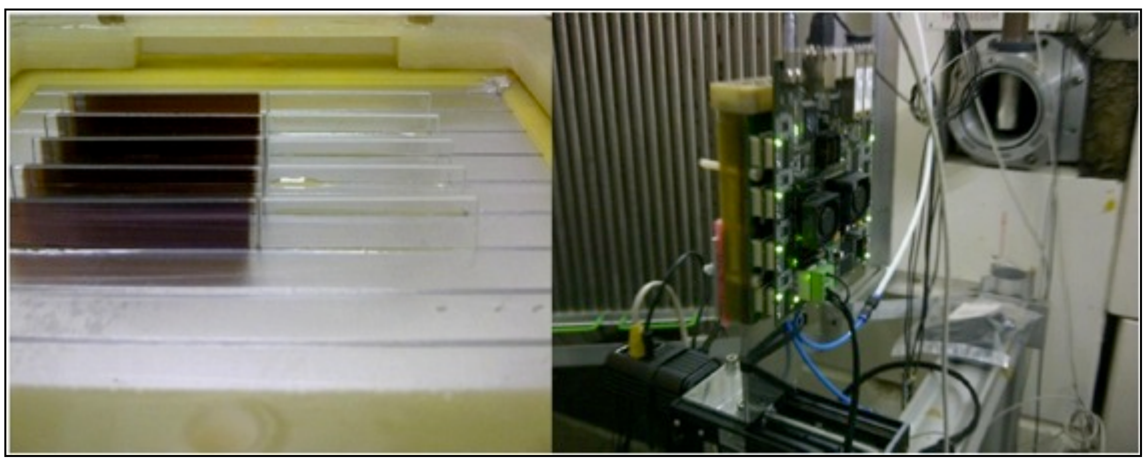

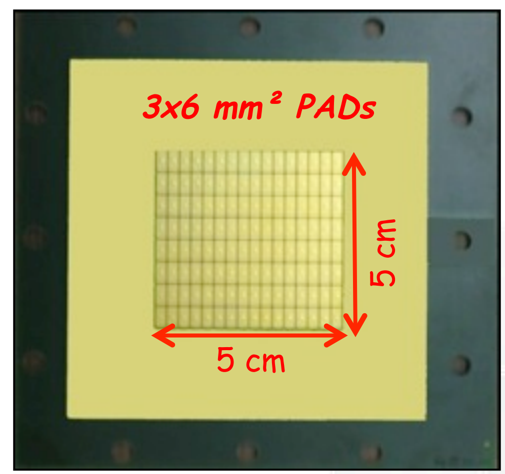

Boron Reaction: $^{10}B + n$ —> $\alpha + {}^{7}Li + 2.79$ MeV (6 %)

—> $\alpha + {}^{7}Li^{*} + 2.31$ MeV $+ \gamma$ (478 keV) (94%)

Neutron Facilities used

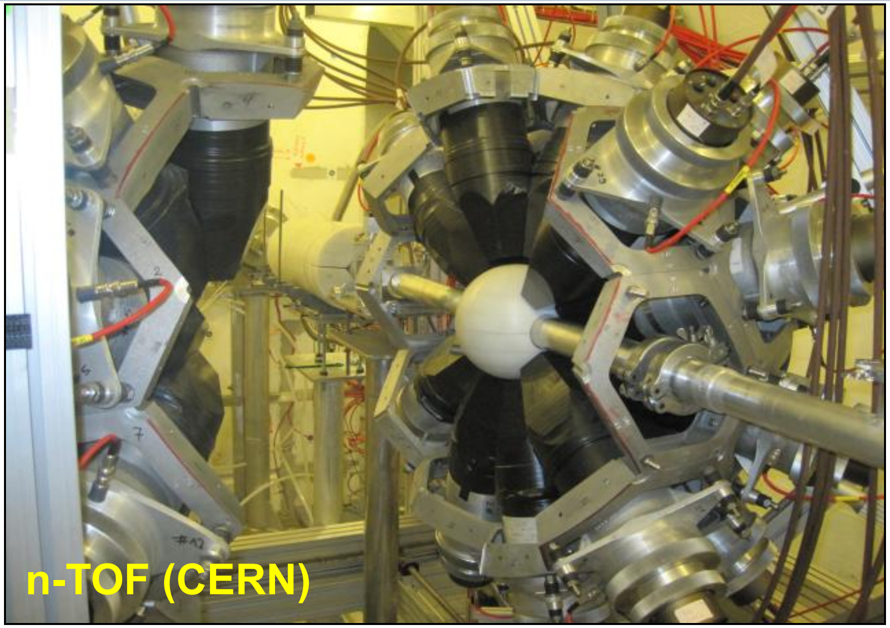

Tests @ TRIGA reactor (ENEA)

TRIGA Power: 1 MW (variable)
Beam line: radial channel
Flux @ 1 MW: $\phi = (2{,}3 \pm 0.2) \times 10^{6}\ ncm^{-2}s^{-1}$
Spectrum: Maxwell-Boltzmann at 25 meV
FWHM ~ 70 meV

The flux was changed varying the reactor power from 100 W to 1 MW.
Side-on GEM detector was able to follow these variations.

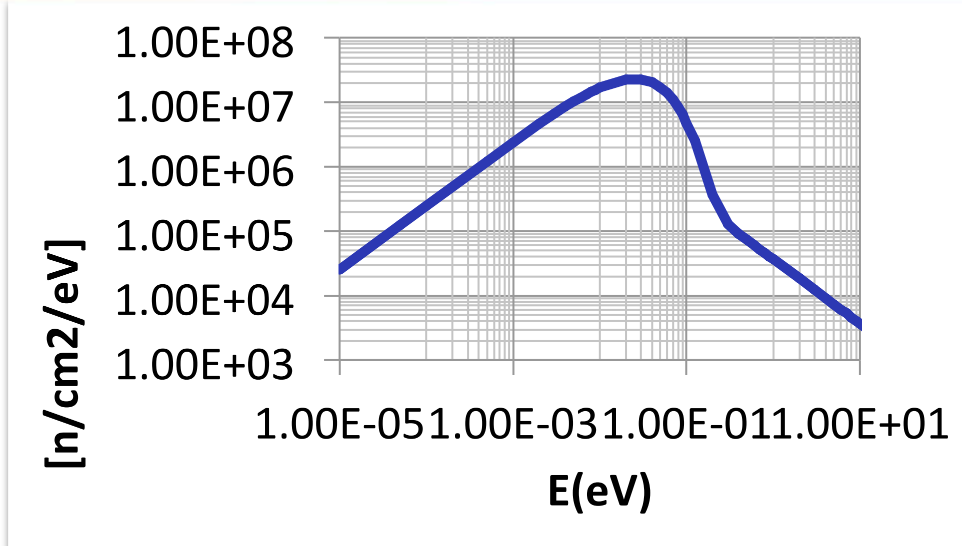

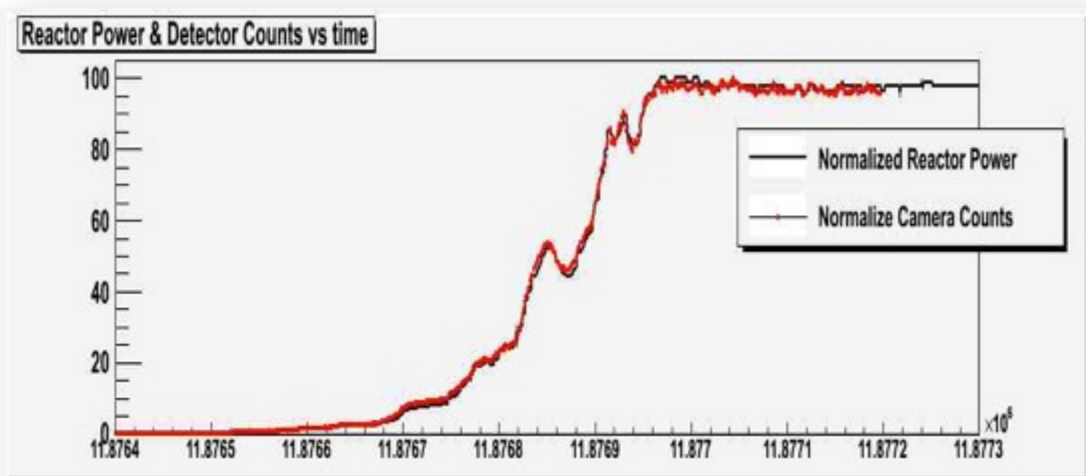

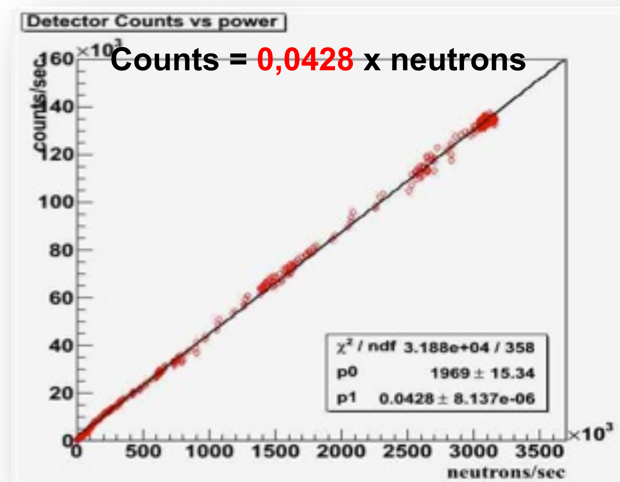

Knowing the incident flow and the detector active area of we estimated an **absolute efficiency** of **4.3 ± 0,5%**, over the whole range of reactor thermal energies.

Test @ ISIS: ToF measurements

ISIS facility is a pulsed neutron source. Energy spectrum ranges from thermal to fast neutrons. We used our detector to make Time of Flight (ToF) measurements of thermal neutrons.

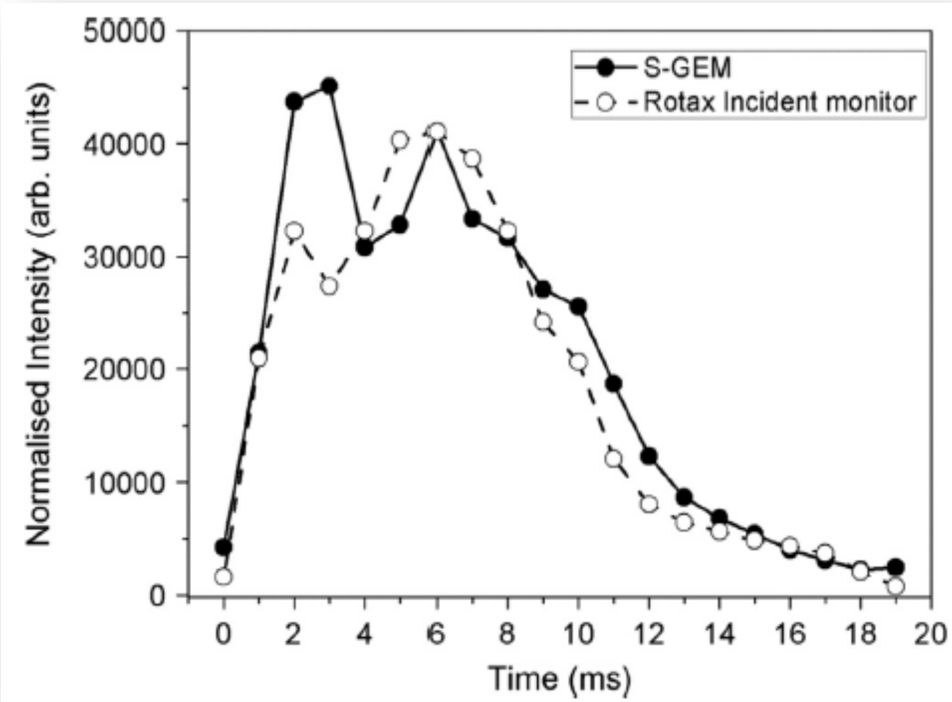

An external trigger starts the detector acquisition of the detector which records data in a time window of 1 ms.

The typical ISIS double-peak profile was obtained applying an increasing delay in step of 1 ms.

Results are in agreement with those obtained from the beam monitor of ROTAX.

Our FEE electronics is very fast and allows ToF measurements, widely used in neutron spectroscopy. It is possible to scan using time windows that can reach a temporal amplitude a few tens of μs.

The second prototype

We developed a new prototype increasing the number of borated strip up to 16, in order to obtain an higher efficiency.

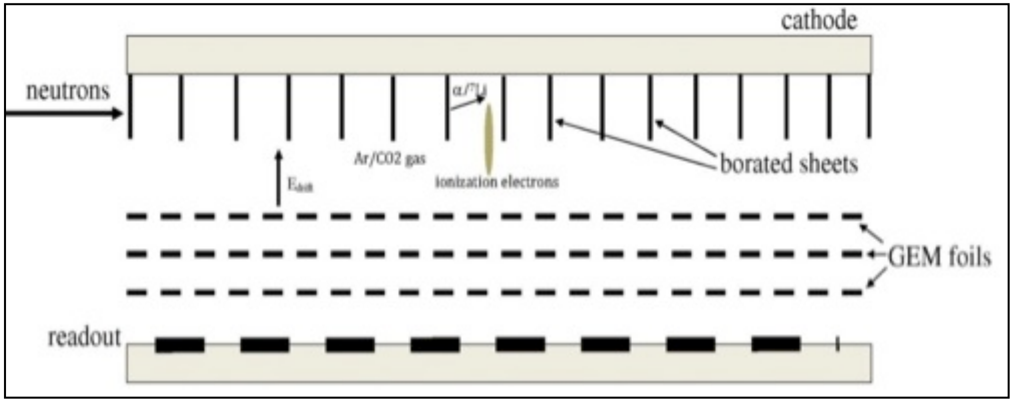

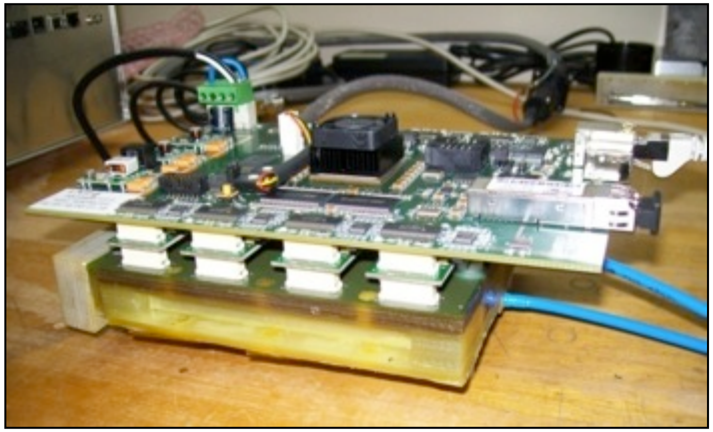

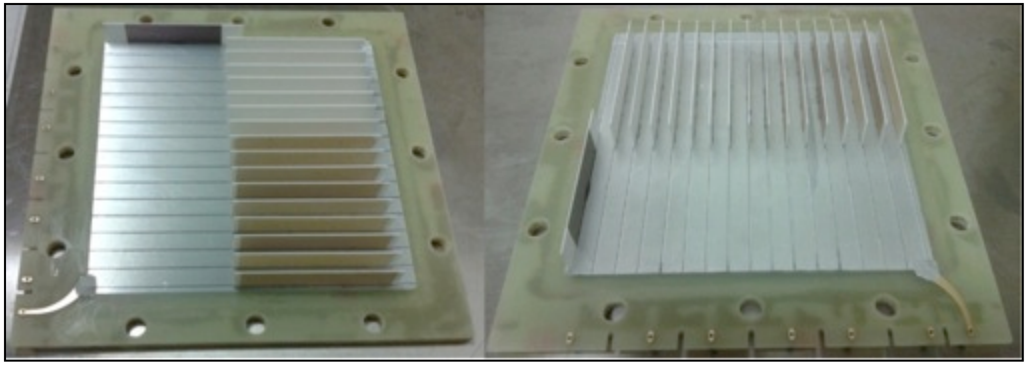

We used ceramic strips (Al_2O_3) 400 μm thick.

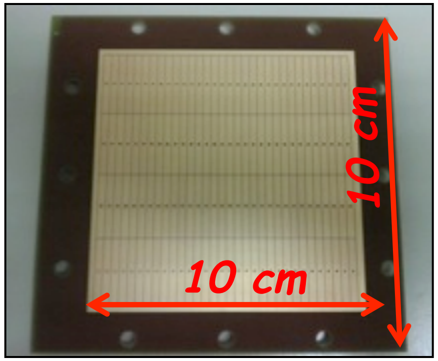

We used an anode with PADs having different geometry. There are 32x4 PADs and each PAD is 3x24 mm².

Detector window is placed on the side of the anode with 32 PADs. In this way detector is able to measure also position of small spot beams impinging on the side-on window.

Tests @ HFIR Oak Ridge National Laboratory (ORNL, US)

HFIR Power: 85MW
beam line:CG1A (detector test station)
estimated flux: 2×10^6 n cm^{-2}.
λ_P~ 4.23 Å (**E**~4.57 meV)
FWHM ~0.11 Å
irradiation area: 5×5 cm^2
angular divergence: < 1°
well suited for resolution, uniformity, distortion and performance measurements with a high neutron flux.

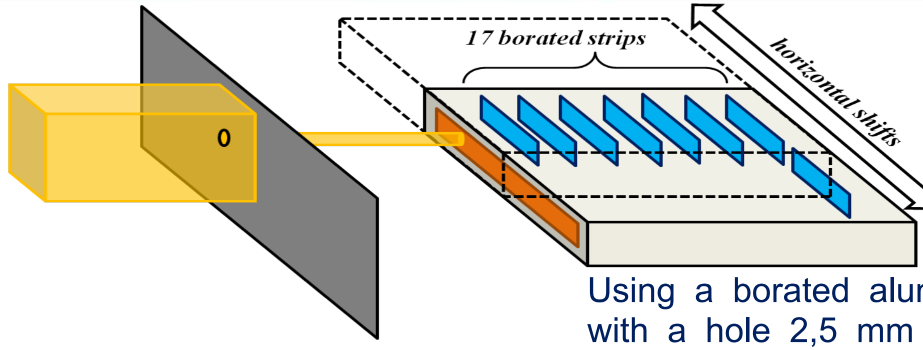

Using a borated aluminum mask with a hole 2,5 mm in diameter, we made a position scan moving the GEM detector.

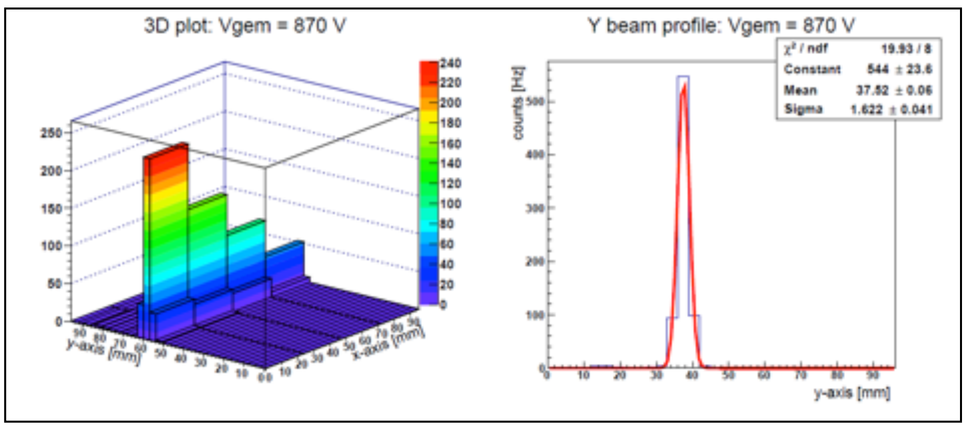

We obtain a beam position resolution of about 0.8 mm.

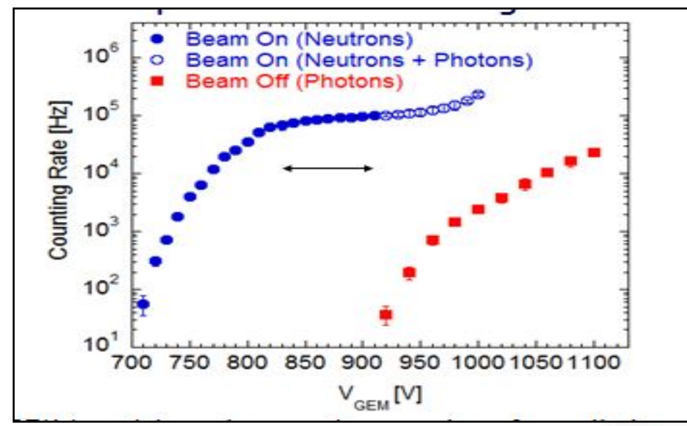

Low γ-rays sensitivity!

Comparison with He gas tube at pressure

	S-GEM	^{3}He Tube
Overall mean counts [s^{-1}]	1863	6011
Background mean counts [s^{-1}]	21	1586
Signal/Background	87.7	2.8
Efficiency [%]	31	99

Last results

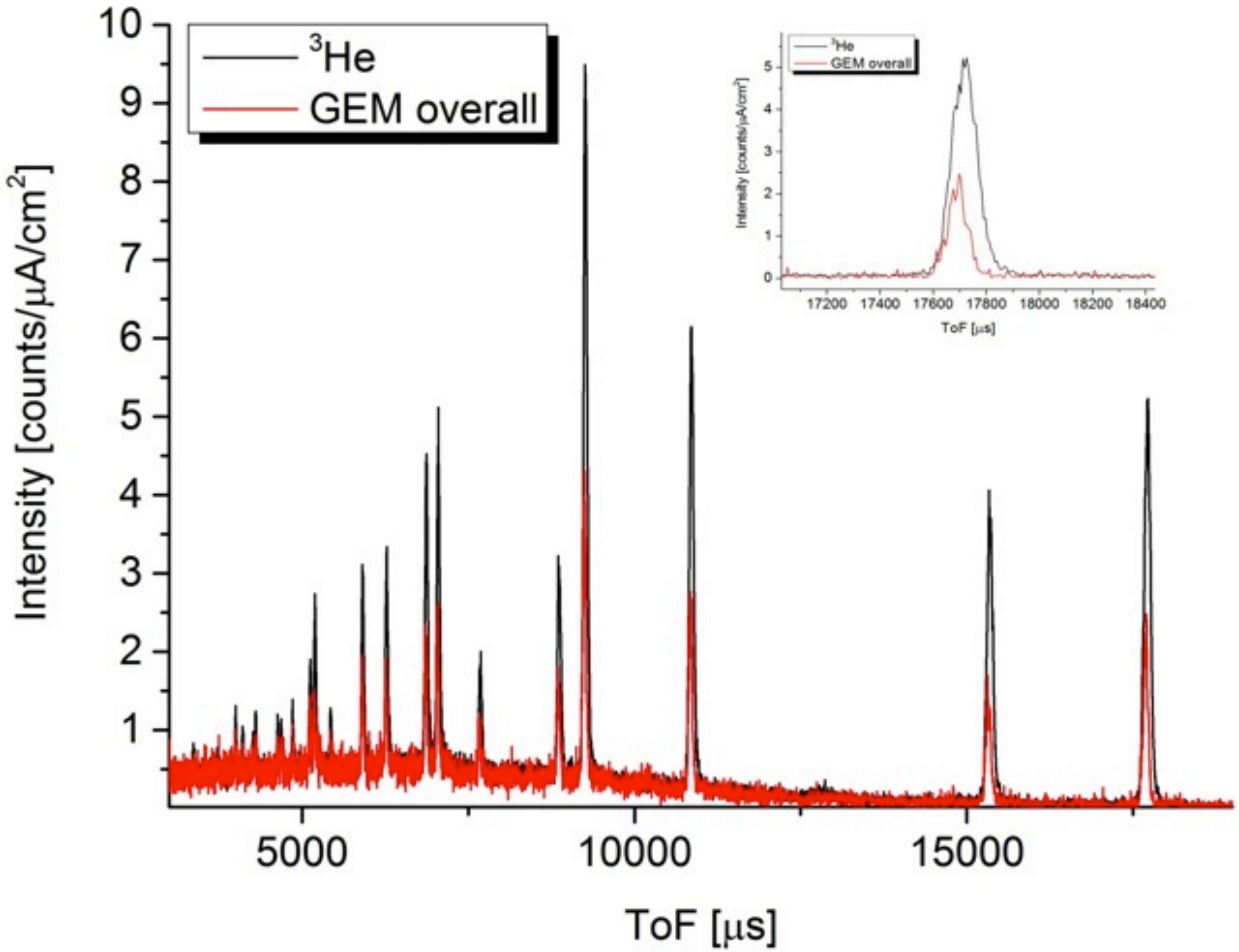

Useful references

- **F.G. Knoll,** Radiation Detection and measurements.
- **E.M. Schooneveld, A. Pietropaolo,** *et al*. Rep. Prog. Phys. **79** (2016) 094301
- **A. Pietropaolo and R. Senesi**, Physics Reports **508** (2011) 45.
- **N. Watanabe**, Rep. Prog. Phys. **66** (2003) 339.
- **J.M. carpenter and C.-K. Loong,** "Elements of slow-neutron scattering"
- **L. Squires**, Introduction to the theory of thermal neutron scattering